The behaviour of a flexible dolphin in the Port of Rotterdam.

TUDelft

Jur Peerden

The behaviour of a flexible dolphin in the Port of Rotterdam

By

Jur Peerden

MSc Student Geotechnical Engineering
Faculty of Civil Engineering and Geosciences
Delft University of technology

To be defended publicly on June 26th, 2023

Student number:	465387	
Supervisors:	Prof. Dr. Kenneth Gavin	Tu Delft
	Dr. Ir. Alfred Roubos	Tu Delft & Port of Rotterdam
	Ir. Dirk Jan Jaspers Focks	Witteveen+Bos
	DR. Ir. Evangelos Kementzetzidis	Tu Delft

Cover image by De Klerk (De Klerk, 2022)

Preface

This thesis serves as the concluding component of my study towards the degree of Master of Science in Geo-engineering at Delft University of Technology. I am sincerely grateful for the opportunity to work with the measurements of a full-scale test, which provided me with a unique experience being present at such a significant test.

Firstly, I would like to express my gratitude to Witteveen+Bos for granting me the opportunity to conduct this research for my graduation. I am particularly grateful to Dirk-Jan Jaspers-Focks for consistently offering valuable advice whenever I sought it and for sharing his expert insights on the topic. Additionally, I extend my gratitude to my colleagues at the office for their continued interest in my research and for providing a pleasant working environment.

I would also like to thank my University supervisors, Ken Gavin and Evangelos Kementzetzidis, for sharing their knowledge on the subject matter and for engaging in insightful discussions during our meetings. Furthermore, I express my gratitude to Alfred Roubos and the Port of Rotterdam for granting me access to the data from this extensive test and for sharing their expertise on flexible dolphins throughout the entirety of this thesis.

I am also deeply indebted to my family for their unwavering support not only during the completion of this thesis but throughout my entire study time. Finally, I wish to extend my gratitude to my friends for their support, both in terms of inspiration and providing occasional distractions.

<div align="right">
Jur Peerden
Delft, June 2023
</div>

Summary

The objective of this thesis is to enhance understanding of the behaviour of a flexible dolphin and its interaction with the surrounding soil in order to determine the optimal embedded depth. A comprehensive field test is conducted to gain deeper insights into the behaviour of the flexible dolphin and the soil surrounding the pile. The test measurements are then analysed to assess the pile's behaviour. Additionally, calculation models are employed to predict the pile's behaviour, and a comparison is made between the measurements and predictions.

Four different calculation models, namely Blum, Brinch Hansen, P-y curves, and Plaxis are utilized to predict the pile's behaviour during the test. The pile behaviour is compared across these models. While most models do not account for repetitive loading, the best available inputs are employed to simulate the test as accurately as possible. The majority of the models exhibit similar top displacements of 0.9 meters, except for the drained Plaxis model, which calculates displacements of 1.05 meter, and Blum's model, which calculates a displacement of only 0.8 meters.

During the test, multiple instruments are employed to measure various parameters of the pile, including load, displacement, water pressures, and strains at different depths and time intervals. The total station measurements indicate a maximum displacement of nearly 0.7 meters, which differs by 0.2 meters from the predictions.

The deviation between the predictions and measurements can largely be attributed to inaccuracies in the hydraulic jack load measurements. The pile load was back-calculated using the strain data obtained from the pile. The loads estimated based on the strain measurements were found to be hundreds of kilonewtons lower than the hydraulic jack load measurements. As the strain measurements were considered more reliable, the actual load during the test differed from the prescribed load scheme. Consequently, the load inputs in the models need to be adjusted to align with the loads derived from the strain data.

The displacement measurements are analysed and compared with each other. The Saaf and optical fibre measurements exhibit similar curvatures, enhancing the reliability of the optical fibre strain measurements during load analysis. However, the total displacement measured by the Saaf and the total station do not match due to the incorrect assumption of zero movement at the pile tip. Determining the exact displacement of the entire pile is impossible due to the inadequate number of boundary conditions available to translate the Saafs curvature measurements into displacement.

The calculation models utilize the loads derived from the strain measurements to make predictions, and their results align comparably with the measurements. Plaxis is the only model capable of simulating different load cycles, which improves the comparability of the Plaxis results with the test.

Load-displacement graphs obtained from the Plaxis results and the optical fibre measurements display hysteresis in load cycles, consistent with findings in existing literature. The initial load exhibits less stiffness compared to the repetitive loads in both datasets. The amount of energy absorption by the soil is determined from the areas of the loadcycles. When considering the most complete load cycles, Plaxis conservatively estimates the absorbed energy.

Reducing the length of a pile results in larger displacements of the pile, while concurrently enhancing its capacity for energy absorption. However, it is crucial to strike a balance between these two parameters, while paying close attention to the permanent soil displacements.

Contents

Table of Figures

Table of tables

1 Introduction

1.1 Problem description

All the ports and waterways in the Netherland have implemented Flexible dolphins, primarily comprised of steel tubular piles with sizeable diameters. But the older and smaller ones are also made from wood. These dolphins are utilized as waiting or mooring facilities, as well as for ship-to-ship transhipment. Two types of dolphins exist: Breasting dolphins and mooring dolphins. Breasting dolphins have direct contact with a berthing vessel and absorb the energy of said vessel, whereas mooring dolphins connect vessels with ropes to ensure secure mooring.

In 2018, the CROW established new design guidelines for flexible dolphins to provide comprehensive direction for all involved parties on their construction and design. Despite the publication of these guidelines, discussions surrounding the fixity of the piles in the soil have persisted, as varying calculation methods yield significant disparities and create substantial uncertainty regarding the recommended pile length.

A full-scale field test has been conducted to gain a more deep understanding of flexible dolphin behaviour. This field test aims to bridge the gap between theory and practice, allowing for the review and modification of various design models to provide better predictions. The test focus on the repetitive loading on the dolphin. Repetitive loading differs from cyclic loading, since the time between two loadstep is larger for repetitive loading. No clear evidence is found about the effect of lateral repetitive loading on the pile. Therefore, this thesis will investigate the effect of lateral repetitive loading on flexible dolphins.

1.2 Objective

The main objective of this research is to close the gap between the theory and practice of the design of flexible dolphins. Which results to the research question: "How can the behaviour of a flexible dolphin subject to repetitive berthing loads be determined, using the data from a full-scale test?".

This is to be done by using the test results of the Calandkanaal test together with the calculations of different calculation models to reach the main objective, the following sub-objectives are formulated:

- To give an overview of the literature about flexible dolphins and lateral loaded piles.
- To make the test-results align with each other, to have a clear view of the behaviour of the pile during the test.
- To compare the test results with the calculation models to analyse the accuracy of the models.
- To formulate design recommendations for the analysed models.

1.3 Outline of the master thesis

The report contains 7 chapters. Chapter 2 is the literature review of the thesis. The chapter starts with a review of lateral loaded piles. Afterwards, the different calculation models that are most used are explained. Finally, the repetitive behaviour of the soil is reviewed.

In chapter 3 the test setup is explained, and the predictions of the calculation models are made. The test setup consists of the soil and pile characteristics and the load scheme. The predictions of the pile test are made with the calculation models Blum, P-y curves, Brinch Hansen and Plaxis.

In Chapter 4 the test results are written down. The behaviour of the soil and pile is measured using 6 measurement instruments: Hydraulic Jack, Optical fibre, Total station, Saaf, Inclinometer and Piezometer. The results of those measurements are explained in this chapter.

In Chapter 5 the load analysis of the test is done. The applied load of the test was measured with the hydraulic jack, but the load is checked with the strain-measurements of the optical fibre.

In chapter 6 the displacement analysis of the test is done. The displacement measurements are compared with each other. The predictions of the calculation models are done with the loads from the strain measurement. The calculations of the models are compared with the measurements during the test.

In chapter 7 the repetitive behaviour is analysed. The repetitive behaviour of the test is analysed with load-displacements graphs of the results. Those graphs help with the explanation of the repetitive behaviour of the pile. The difference between the initial and repetitive loadcycles are explained and the hysteretic behaviour of the loadcycle is analysed. This is done for the measurements, but also for the Plaxis-results.

Finally, chapter 8 is the conclusion of the Thesis. In this chapter the final conclusions are written down. Also, some recommendations are done regarding the calculation models. Some recommendations are done for further research regarding flexible dolphins and the Calandkanaal test.

2   Literature review

2.1   Lateral loaded piles

Flexible dolphins are subjected to lateral loads. The lateral loads ensure displacements of the pile. The soil resistance prevents the displacement of the pile. The back pressure of the soil leads to bending moments and shear stresses in the pile and lateral stresses in the soil. A lateral loaded pile is a soil-structure interaction problem. The amount of displacement depends on the soil type and the pile specifications.
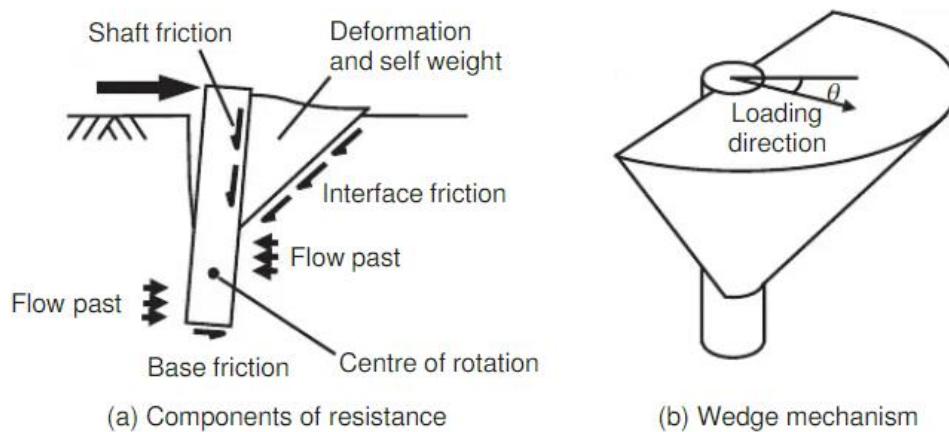
Figure 2.1 Collapse mechanism of soil layer under lateral loading (Fleming, 1985)

The normal stress in front of the pile will increase due to the lateral load on the pile and decreases behind the pile. The loaded pile pushes a soil wedge away in front of the pile and creates a gap behind the pile, as shown in Figure 2.1.

The soil resistance along a lateral loaded pile difference between long and short piles. Short piles or stiff piles rotates as a rigid body, with a centre of rotation point. Above the centre of rotation, the pile moves in the same direction as the load. Below the centre of rotation, the pile moves in the opposite direction as the load. This ensures passive and active pressures in the soil around the pile. Long and more flexible piles behaves more flexible, with curvature in the pile. The long pile has a plastic hinge at some depth, instead of the centre of rotation for shorter piles. The pile has only significant displacements above the plastic hinge, below the hinge the pile does not have significant displacements. There are stresses in the soil below the plastic hinge, but those stresses are not necessary for the determination of the soil resistance capacity (Fleming, 1985).

Differential equation

The pile can be modelled as a beam-column. The differential equation for the beam-column is derived by Hetenyi (Hetenyi, 1946). The differential equation consists of three components: a pile behaviour component, an axial load component and a soil behaviour component. The differential equation for a beam column that is laterally loaded is:

$$E_p I_p \frac{d^4 y}{dx^4} + P_x \frac{d^2 y}{dx^2} + E_{py} y = 0$$

In which:

-   E_p = elastic modulus of the pile [kN/m³]

1

- I_p = moment of inertia of the pile [m⁴]
- P_x = axial load on the pile [kN]
- E_{py} = elastic modulus of the soil [kN/m³]
- y = lateral deflection of the pile [m]

A few assumptions are made to get a more simplified formula. The three assumptions are:

- There is no axial load.
- $E_p I_p$ is constant over depth.
- E_{py} is constant and equal to α.

The solution of the simplified differential equation is shown in Figure 2.2. The behaviour of the pile is explained with the use of the differential equation. The formulas for different parameters can be used to derive those parameters, using other parameters. The assumptions and the static derivations ensure some limitations of the theory. The theory is only applicable for static loads. The assumptions are not satisfied in all cases. The cross section of the pile can differ over the pile, which result in changing moment of inertia of the pile. Next to that, the soil resistance needs to be uniform over depth. That is almost never the case in practice. Axial loads are limited at flexible dolphins.

The beam-column theory is used as starting point of the p-y curves. The solutions of the differential equations and the subsequent p-y curves are explained by Reese (Reese, 2011). The p-y curves are researched in many studies afterwards. The method that is used nowadays in practice and in calculation programs as D-pile group is the API method (API, 2000) derived by the American Petroleum Institute. This method is further explained in chapter 2.2.2.
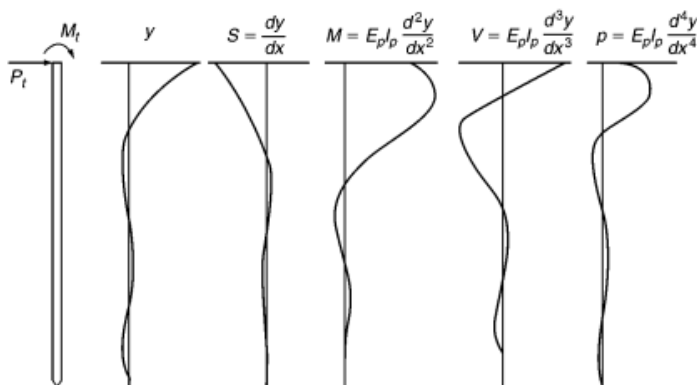
Figure 2.2. The solution of the simplified differential equation (Reese, 2011)

2.2   Design models

Different models are available to determine the behaviour of a flexible dolphin. The models that are frequently used in the industry are explained in this chapter. Every section explains how a model calculates the capacity of the soil. The models that are discussed are:

- Brinch Hansen method
- P-Y curves
- Blum
- Plaxis

2.2.1   Brinch Hansen

This method is made by Brinch Hansen (Brinch Hansen, 1961). It is assumed that the pile rotates as a rigid body around a specific point below the ground surface. The model only calculates the ultimate soil resistance. The model does not calculate working loads but is able to calculate layered and cohesive soils.

The general resistance of the soil is described by the formula:

$$e^D = qK_q^D + cK_c^D$$

$$q = p + \gamma D_d + \gamma' D_s$$

In which:

e^D = resultant horizontal pressure[kN/m²]

q = effective vertical overburden pressure [kN/m²]

c = cohesion[kN/m²]

K_q^D = resultant earth pressure coefficient caused by overburden pressure [-]

K_c^D = resultant earth pressure coefficient caused by cohesion [-]

p = surcharge load [kN/m²]

D_d = depth above groundwater level [m]

D_s = depth below groundwater level [m]

Brinch Hansen determined the earth pressure coefficient for three different depths. First the resistance for the ground level is determined. Second, for moderate depths. And third for great depths. After that the formulas are combined, where the soil resistances can be found more easily for every depth.

Ground level

At ground level, the K_q^0 coefficient insert the passive and active earthpressure, while the K_c^0 coefficient only takes the passive earth pressure into account. It is conservative to neglect the active earth pressure because it might lead to negative active earth pressures.

$$e^0 = qK_q^0 + cK_c^0$$

$$K_q^0 = e^{\left(\frac{\pi}{2}+\varphi\right)\tan(\varphi)} \cos(\varphi) \tan\left(\frac{\pi}{4}+\frac{\varphi}{2}\right) - e^{\left(-\frac{\pi}{2}+\varphi\right)\tan(\varphi)} \cos(\varphi) \tan\left(\frac{\pi}{4}+\frac{\varphi}{2}\right)$$

$$K_c^0 = \left(e^{\left(\frac{\pi}{2}+\varphi\right)\tan(\varphi)} \cos(\varphi) \tan\left(\frac{\pi}{4}+\frac{\varphi}{2}\right) - 1\right) \cot(\varphi)$$

At great depth the slip planes become horizontal around the pile.

$$K_c^\infty = N_c d_c^\infty$$

$$K_q^\infty = K_0 K_c^\infty \tan(\varphi)$$

$$K_0 = 1 - \sin(\varphi)$$

$$N_c = \left(\exp^{\pi \tan(\varphi)} \tan^2 \left(\frac{\pi}{4} + \frac{\varphi}{2} \right) - 1 \right) \cot(\varphi)$$

$$d_c^\infty = 1.58 + 4.09 \tan^4(\varphi)$$

 At arbitrary depth, two formulas for the earth pressure resistance are needed, one for K_q^D and one for K_c^D. The formula has two requirements, this requirement ensures that the formulas coupled with the formulas for ground level and great depth.

- If D->0, K^D ->K^0
- If D->∞, K^D ->K^∞

The equations that fulfil these requirements are:

$$K_q^D = \frac{K_q^0 + \frac{K_q^\infty \alpha_q D}{B}}{1 + \frac{\alpha_q D}{B}}$$

$$\alpha_q = \frac{K_q^0}{K_q^\infty - K_q^0} * \frac{K_0 \sin(\varphi)}{\sin\left(\frac{\pi}{4} + \frac{\varphi}{2}\right)}$$

$$K_c^D = \frac{K_c^0 + \frac{K_c^\infty \alpha_q D}{B}}{1 + \frac{\alpha_c D}{B}}$$

$$\alpha_c = \frac{2K_c^0}{K_c^\infty - K_c^0} * \sin\left(\frac{\pi}{4} + \frac{\varphi}{2}\right)$$

With those formulas for the earth pressure coefficient, the horizontal pressures on the pile can be easily calculated using the general formula.

The Brinch Hansen method is often combined with the Ménard method to model the bilinear soil behaviour. The subgrade reaction modulus can be calculated with the equation:

$$\frac{1}{K_h} = \frac{1}{3E_m} \left(1.3 R_0 \left(2.65 * \frac{R}{R_0} \right)^\alpha + \alpha R \right) \qquad \text{(For } R \geq R_0\text{)}$$

$$\frac{1}{K_h} = \frac{2R}{E_m} * \frac{4 * 2.65^\alpha + 3\alpha}{18} \qquad \text{(For } R < R_0\text{)}$$

In which:

E_m = pressiometer modulus [kN/m^2]

R_0 = constant = 0.3 [m]

R = half pile diameter [m]

α = rheological coefficient [-]

K_h = modulus of horizontal subgrade reaction [kN/m^3]

q_c = cone resistance from CPT [kN/m^2]

The values for the pressiometer modulus and the rheological coefficient are listed in Table 2.1Table 2.1for different soil types and consolidation ratios.

Table 2.1: Rheological coefficient determination per soil

		Rheological coefficients α [-]		
Soil	E_m [kN/m²]	Over consolidated	Normally consolidated	Decompensated
Peat	(3 to 4) * q_c	-	1	-
Clay	(2 to 3) * q_c	1	2/3	1/2
Loam	(1 to 2) * q_c	2/3	1/2	1/2
Sand	(0.7 to 1) * q_c	1/2	1/3	1/3
Gravel	(0.5 to 0.7) * q_c	1/3	1/4	1/4

The Brinch Hansen method with the Menard method can be used in the D-Sheet Piling software to calculate the ultimate lateral soil resistance. D-sheet Piling is a software from Deltares that can design horizontally loaded piles, sheet piles and Diaphragm walls (Deltares, 2021).

Limitations

The limitations of the Brinch Hansen method in D-sheetpiling:

- The model is only capable to calculate the ultimate soil resistance.
- The method cannot calculate cyclic loading.
- D-sheetpiling only calculates the passive earth pressure ones every soil layer.

2.2.2   P-Y curves

The p-y curves differ between cohesive and cohesionless soils. Both models start by determining the ultimate soil resistance. The ultimate soil resistance is used to determine a formula that connect the current pressure with the corresponding displacement. The cohesionless method is explain below since the research is about a sandy soil.

The ultimate soil resistance near the ground surface can be approached with:

$$p_{u1} = \gamma z \left[\frac{K_0 z tan(\varphi) \sin(\beta)}{\tan(\beta - \varphi) \cos(\alpha_s)} + \frac{\tan(\beta)}{\tan(\beta - \varphi)} (b + z * \tan(\beta) \tan(\alpha_s)) \right] + \gamma z [K_0 z tan(\beta)(tan(\varphi) \sin(\beta) - \tan(\alpha_s)) - K_a b]$$

- K_0 = coefficient of earth pressure at rest
- K_a = minimum coefficient of active earth pressure
- α_s = angle of the wedge
- φ = friction angle of the soil
- β = angle of inclined plane with vertical [°]
   - $\beta = 45 + \frac{\varphi}{2}$

The ultimate soil resistance for horizontal movement of the soil is.

$$p_{u2} = K_a b \gamma z (\tan^8(\beta) - 1) + K_0 b \gamma z tan(\varphi) \tan^4(\beta)$$

API-method

The API (American petroleum institute) (API, 2000) made design guidelines for to determine p-y-curves in sand. The guidelines consist of the ultimate resistance from (Reese, 2011) and a resistance-deflection curve that depends on the ultimate resistance.

The ultimate lateral resistance for sand is described as:

$$p_u = \min\{C_1 * z + C_2 * D)\,\gamma'z;\ C_3 * D * \gamma' * z\}$$

The resistance-deflection relationship is:

$$p = A * p_u * \tanh\left(\frac{k * z}{A * p_u} * y\right)$$

$$A = 3 - 0.8 * \frac{z}{D} \geq 0.9$$

In which

- For cyclic loading: A = 0.9
- p_u = soil pressure at failure
- γ' = volumetric weight at depth
- C_1, C_2 and C_3: coefficient
  - $C_1 = \frac{(\tan^2(\beta)\tan(\alpha))}{\tan(\beta - \varphi')} + K_0\left[\frac{tan(\varphi)\sin(\beta)}{\tan(\beta - \varphi)\cos(\alpha)} + tan(\beta)(tan(\varphi)\sin(\beta) - \tan(\alpha))\right]$
  - $C_2 = \frac{\tan(\beta)}{\tan(\beta - \varphi)} - K_a$
  - $C_3 = K_a(\tan^8(\beta) - 1) + K_0 tan(\varphi)\tan^4(\beta)$
- K = soil stiffness
- Z = depth below surface
- D = diameter pile

The constant value of 0.9 for cyclic loading is verified by literature up to 100 cycles (EA-Pfähle, 2012).

P-y curves can be modelled using the software D-Pile Group or Geocalcs.

Limitations

The limitations of the p-y curves in D-pile group are:

- The model has a limited amount of pile sections.
- The load can only be applied on the top of the pile.
- Only one load can be calculated in the model.
- Cyclic loading gives only the ultimate cyclic loading effect, so not with working loads.

2.2.3 Blum

The Blum model is a model to calculate the ultimate soil resistance and is developed by Blum (Blum, 1932). It is a simple and fast model, which makes it an attractive model compared to the advanced models. The model can be done by hand and there is no computer program necessary to make the calculations.
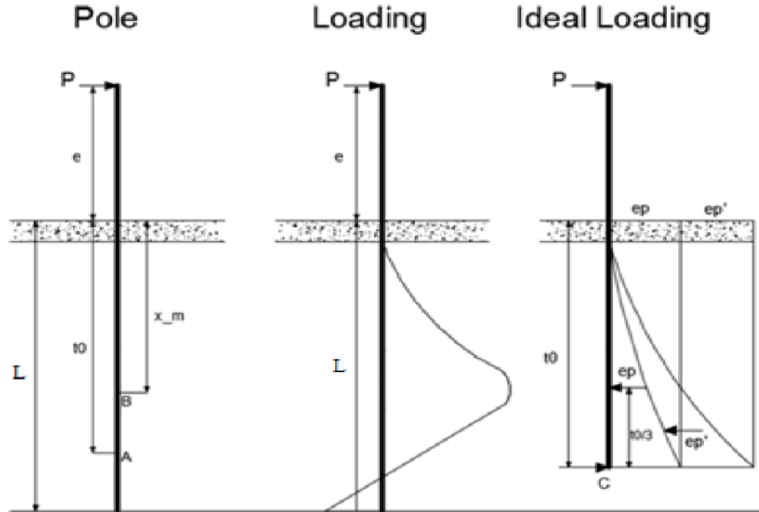
Figure 2.3: Load distribution in the soil according Blum (Blum, 1932)

The method only calculates the ultimate situation. The Blum model have different formulas for calculating the theoretical minimum penetration depth, point A, and the location of the maximum momentum. Each formula depends on the added lateral load on the pile. In the calculation the model assumed an ideal loading situation, in which the bending moment and the deflection at the toe of the pile are both zero. Relationships between the theoretical penetration depth and the pressure that is applied is:

$$\frac{24P}{f_w} = t_0^3 \frac{(t_0 + 4b)}{h + t_0}$$

This equation is derived from the formula of the bending moment at the theoretical penetration depth. The forces that act on the pile are shown in Figure 2.3 'ideal loading' and are 2 earth pressures and the applied load. A side view is shown in Figure 2.4, P stand for applied pressure and EP for earth pressure and G for unit load. The earth pressure is divided in two parts: part 1 is the part soil wedge at the width of the pile, part 2 is the 3d part of the soil wedge next to the width of the pile. The load of the soil wedge is rewritten to an earth pressure by multiplying it with the tangent of the angle of the soil wedge. The earth pressures are determined with the formula:

$$E_p = G * \tan\left(45 + \frac{\varphi}{2}\right) = \gamma * V * \tan\left(45 + \frac{\varphi}{2}\right)$$

$$E_{p1} = \gamma * \frac{b * t_0 * t_0 \tan\left(45 + \frac{\varphi}{2}\right)}{2} * \tan\left(45 + \frac{\varphi}{2}\right) = \frac{b * t_0^2}{2}\gamma * \lambda_p = \frac{b * t_0^2}{2} * f_w$$

$$E_{p2} = \gamma * \frac{2 * \frac{t_0}{2} * t_0 * t_0 \tan\left(45 + \frac{\varphi}{2}\right)}{6} * \tan\left(45 + \frac{\varphi}{2}\right) = \frac{t_0^3}{6}\gamma\lambda_p = \frac{t_0^3}{6} * f_w$$

The moment at the theoretical penetration depth, point A, is described below. Point A is chosen that the bending moment is zero. The formula can be rewritten as the relationship between the applied pressure and the penetration depth mentioned above.

$$M_a = P(h + t_0) - E_{p1} * \frac{t_0}{3} - E_{p2} * \frac{t_0}{4} = P(h + t_0) - \frac{b * t_0^2}{2} * f_w * \frac{t_0}{3} - \frac{t_0^3}{6} * f_w * \frac{t_0}{4} = 0$$

7

$$M_a = P(h + t_0) - f_w \left(\frac{b * t_0^3}{6} - \frac{t_0^4}{24} \right) = 0$$
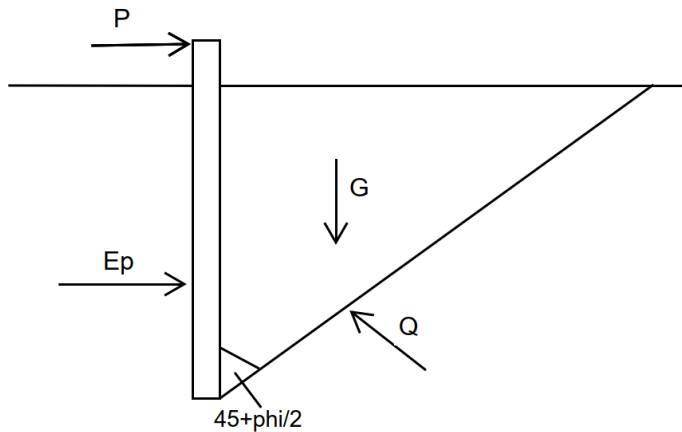
Figure 2.4: The equilibrium of the forces in the pile and soil (Ruigrok, 2010)

The formula for the bending moment can be rewritten to a general formula for the bending moment over depth, since there is no load at point A. The general formula for the bending moment over depth is:

$$M_x = P(h + x) - f_w \left(\frac{bx^3}{6} - \frac{x^4}{24} \right)$$

The depth of the maximum bending moment is at the location where the derivative of the bending moment over depth is equal to zero. The derivative of the bending moment is:

$$\frac{dM_x}{dx} = P - f_w \left(\frac{bx^2}{2} - \frac{x^3}{6} \right) = 0$$

The depth of the maximum bending moment, x_m, can now be related to the applied pressure. Besides the maximum bending moment can be calculated by enter the depth of the maximum depth in the general formula for the bending moment.

$$\frac{24P}{f_w} = 4x_m^2 (x_m + 3b)$$

In which:

- P = lateral load [kN]
- f_w = soil resistance [kN/m³]
  - $f_w = \gamma \lambda_p$
- γ = volumetric weight soil [kN/m³]
- $\lambda_p = \tan^2 (45 + \frac{\varphi}{2})$
- φ = angle of internal soilfriction [°]
- t_0 = Theoretical minimum penetration depth [m]
- b = width of the pile [m]
- h = height where load P is applied [m]
- x_m = location maximum moment below surface [m]

The Theoretical minimum penetration height is the location in the ground where the bending moment is zero. The real penetration depth is 20% larger than the theoretical penetration depth.

The deflection of the pile tip can also be calculated with the Blum model. The formula for the calculation of the pile tip is:

$$d = \frac{P(h + t_0)^3}{3EI} - \frac{f_w * t_0^4}{360EI}(2.5t_0^2 + t_0(3h + 12D) + 15Dh)$$

In which:

- E = Elastic modulus [kN/m^2]
- I = moment of inertia [m^4]
  - For piles: $I = \frac{\pi}{64} * (D^4 - D_{inner}^4)$
- D_{inner} = Inner diameter of the pile [m]
  - $D_{inner} = D - 2 * t$
- t = pile thickness [m]

The passive earth pressure without wall friction is:

$$\lambda_p = \tan^2(45 + \frac{\varphi}{2})$$

The model is updated a few times. The wall friction of the pile is added in the model, which resulted in different active and passive earth pressure. This was shown in "spudhand handbuch berechnung" (Krupp, 2007).

Limitations

The limitations of the Blum model are:

- Only calculates the ultimate soil resistance.
- No repetitive loading possible.
- Needs an adaptation for layered soil.
- Only one pile cross-section possible.

2.2.4 Plaxis

Plaxis 3D is a three-dimensional finite element model program (Plaxis, 2021). The program is made specifically for geotechnical calculations. Plaxis 3D can simulate soil behaviour with different material models. Those models differ in complexity, linearity and applicability for different soil/rock types and constructions. The appendix of the manual contains tables with the applicability of material models for different material types, applications and loading types. This report is about flexible dolphins in a sandy environment. Those dolphins have small deformations around the pile-tip and large deformations around the top. The Hardening soil model with small strain stiffness, also known as HSsmall, is the preferred model according to the appendix. The HSsmall model is an extension of the hardening soil model, with a better representation of the non-linear soil stiffness for small strains.

2.2.4.1 Hardening soil model

The model gives a hyperbolic relationship between the vertical strain and the deviatoric stress in primary triaxial test. The restriction is that the model assumes triaxial loading conditions with $\sigma'_2 = \sigma'_3$. The relationship can be described by the formula:

$$-\varepsilon_1 = \frac{2 - R_f}{2 * E_{50}} * \frac{q}{1 - q/q_a} \ for \ q < q_f$$

In which:

q_a = asymptotic value of the shear strength: $q_a = \frac{q_f}{R_f}$

R_f = failure ratio [-]

E_{50} = stiffness modulus at 50% of the maximum shear strength

The ultimate deviatoric stress is defined as:

$$q_f = \frac{2 * \sin(\varphi)}{1 - \sin(\varphi)} \left(\sigma'_3 - c * \cot(\varphi)\right)$$

The stiffnesses that are used in the models are derived from a reference stiffness modulus corresponding to the reference confining pressure, σ^{ref}. The default input parameter of E_{ur} is three times E_{50}. The unloading and reloading stiffness, E_{ur}, and the E_{50} are derived as:

$$E_{ur} = E_{ur}^{ref} \left(\frac{\sigma_3 + c * \cot(\varphi)}{\sigma^{ref} + c * \cot(\varphi)}\right)^m$$

$$E_{50} = E_{50}^{ref} \left(\frac{\sigma_3 + c * \cot(\varphi)}{\sigma^{ref} + c * \cot(\varphi)}\right)^m$$

In which:

m = stress dependency coefficient [-]

σ_3 = minor principal stress [kN/m^2]

E^{ref} = reference stiffness modulus [kN/m^2]

The yield surfaces that can be found using a triaxial test are:

$$f = \frac{2 - R_f}{2E_{50}} * \frac{q}{1 - \frac{q}{q_a}} - \frac{2q}{E_{ur}} - \gamma^p$$

$$\gamma^p = (2\varepsilon_1^p - \varepsilon_v^p)$$

In which:

γ^p = function of plastic strain

ε_1^p = axial plastic strain

ε_v^p = volumetric plastic strain

Next to the plastic strains, the model also accounts for elastic strains. For drained triaxial test the elastic Young's modulus E_{ur} remains constant. The elastic strains can be calculated with the equations:

$$-\varepsilon_1^e = \frac{q}{E_{ur}}$$

$$-\varepsilon_2^e = -\varepsilon_3^e = -v_{ur} \frac{q}{E_{ur}}$$

In which v_{ur} is the poisson's ratio for unloading and reloading. The total strain is the combination of the plastic strain and the elastic strain.

The plastic volumetric strain can be described with a relationship between the plastic volumetric strain and the function of plastic strain γ^p. The shear hardening flow rule is linear with the function:

$$\varepsilon_v^p = \sin(\Psi_m)\,\gamma^p$$

$$\sin(\Psi_m) = \frac{\sin(\varphi_m) - \sin(\varphi_{cv})}{1 - \sin(\varphi_m)\sin(\varphi_{cv})}$$

In the equation is Ψ_m the mobilized dilatancy angle, φ_{cv} the critical friction angle and φ_m the mobilized friction angle.

HSsmall

In HSsmall model uses the same functions and input parameters as the normal hardening soil model. There are only 2 additional parameters: initial or very small-strain shear modulus, G_0, and the shear strain level, $\gamma_{0.7}$. $\gamma_{0.7}$ is the shear strain level at which the secant shear modulus, G_s, is reduced to about 72.2% of G_0. Those two additional parameters ensures that the unloading and reloading phase is not linear anymore but hysteretic. Besides the initial shear modulus ensures a better prediction of initial soil stiffness. The relationship between the shear modulus and the small strains is (Hardin, 1972):

$$\frac{G_s}{G_0} = \frac{1}{1 + \frac{0.385\gamma}{\gamma_{0.7}}}$$

A factor 0.385 is used in the formula. Because of this factor, a shear strain equal to $\gamma_{0.7}$ gives $\frac{G_s}{G_0} = 0.722$. Which makes the $\gamma_{0.7}$ not exact of 70% but more accurate on 72.2%.

The stiffness reduction curve reaches the plastic domain. Therefor the curve is bound by a lower limit. The lower limit is determined by lab tests. This shear strain limit, G_t, and the shear strain limit, $\gamma_{cut-off}$ can be determined by the following formula:

$$G_{ur} = \frac{E_{ur}}{2(1 + v_{ur})}$$

$$\gamma_{cut-off} = \frac{1}{0.385}\left(\sqrt{\frac{G_0}{G_{ur}}} - 1\right)\gamma_{0.7}$$

The Hysteretic behaviour of materials is described by (Masing, 1926). The formula's that are used above with $\gamma_{0.7}$ are valid for unloading and reloading. But virgin loading happens twice as fast. For the calculation of virgin loading the shear strain must be multiplied by 2.

$$\gamma_{0.7\,virgin-loading} = 2\gamma_{0.7re-loading}$$

Figure 2.5 shows the hysteretic behaviour of materials according Masing's rule. The hysteretic soil behaviour is occurs during a loadcycle when the soil experienced a cyclic load.
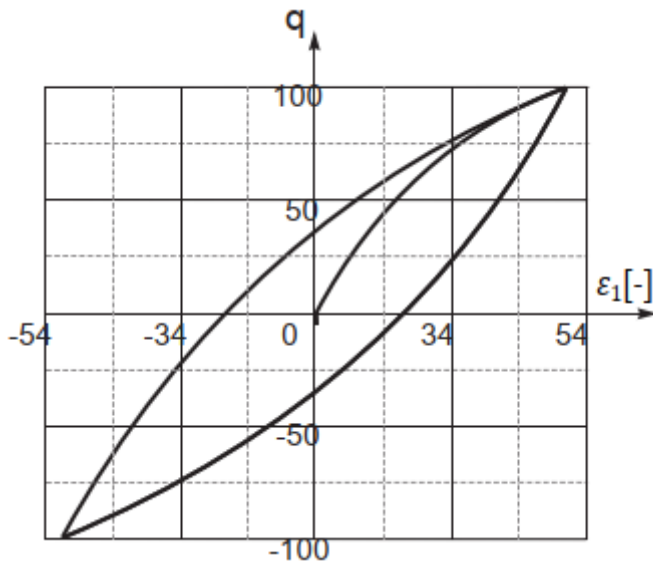
Figure 2.5: Hysteretic soil behaviour.

The limitations of the Plaxis model:

- The model needs a lot of soil input parameters, which are not always available.
- The calculation time is long.

2.3   Repetitive loading

2.3.1   Stress-strain behaviour

This research is partly done to improve the knowledge about repetitive loading for flexible dolphins. Repetitive loading means that the loads are applied multiple times, but not in a constant rhythm like in cyclic loading. The loading type during the using phase of the pile is also repetitive loading. Ships come berth, which caused the load on the pile, and after a certain time, the ship leave again. When the next ship will berth varies.

The pile transfers the load to the soil. The load on the soil will have an influence on the soil characteristics. Especially the soil stiffness will change. Figure 2.6 gives the stress-strain curve of a material. In the figure three stiffness parameters are introduced: E_i^{ref}, E_{50}^{ref} and E_{ur}^{ref}. In which E_i^{ref} is the initial reference stiffness at the start of the first time the soil is loaded. The stiffness at 50% of the maximum strength is quantified as E_{50}^{ref}. The stiffness of the soil during unloading and reloading is called E_{ur}^{ref}.

The diagram starts at point A, which is the steady state situation. The first load cycle follows the course from A to B, at point B, the desired load height is reached. The first loadstep is done and the pile will be unloaded and reaches point C. The soil is not fully elastic, so after the first load the soil characteristics does not go back to their original state. The stiffness of the soil is increased, and the soil have some plastic strains. The second loadstep is applied and the stress-strain course goes back from point C back to point B. When the load in the second loadstep is larger than in the loadstep before, the soil behaviour follows the line from B to D.

The soil behaviour can be used to determine the differences between the initial load and repetitive loads on the soil. The initial stress-strain behaviour of the soil is less stiff, compared to the repetitive stress-strain behaviour. The model does not give a difference between the repetitive loads.
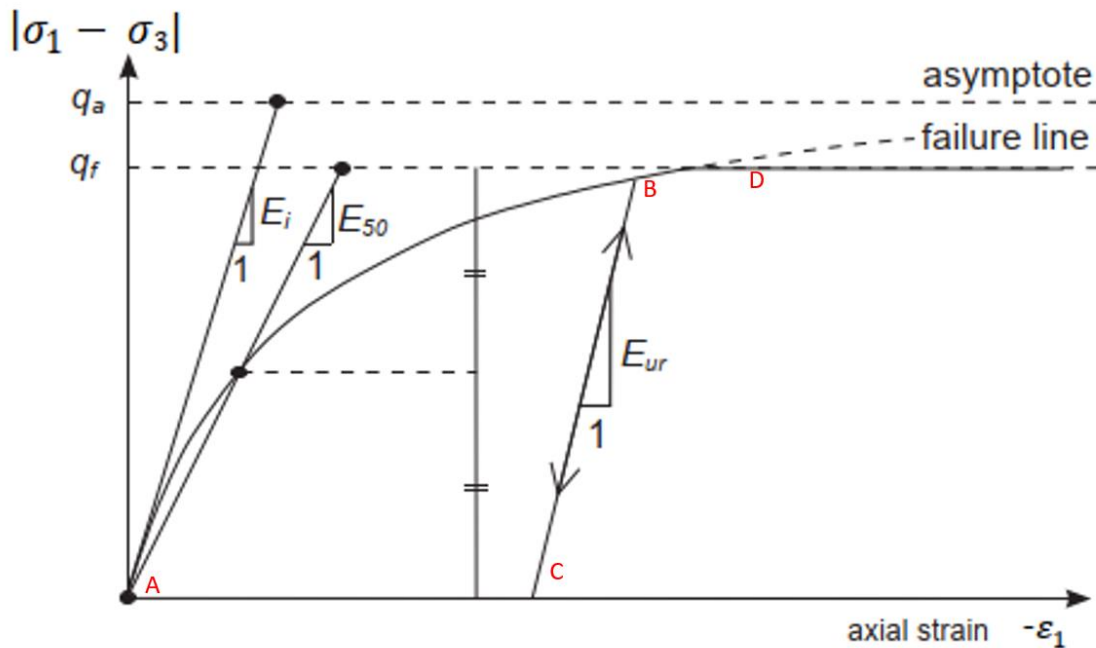
Figure 2.6: Stress strain diagram with unloading and reloading (Plaxis, 2021)

Figure 2.7 shows a visualized stress-strain behaviour from literature (Anderson, 2015). The cyclic trend in the figure shows the differences between the initial cycle and a random cycle. The initial cycle behaves stiffer compared to the random cycle. The loadcycle is more vertical. The loadcycles behaves as a real cycle during unloading and reloading. This unloading and reloading behaviour is the hysteretic behaviour of the soil. The unloading trend differ from the reloading trend and is not identic line as in Figure 2.6. The displacement during unloading is larger than the reloading displacement at the same load. The displacement consists of a permanent load and a cyclic load. The permanent load increases with the increasing amount of loadsteps. The cyclic displacement is dependent on the load on the pile.
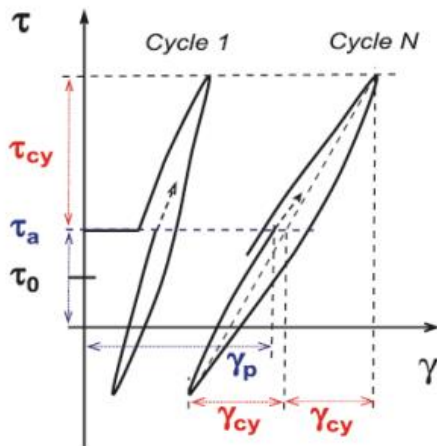
Figure 2.7: stress strain behavior of a lateral loaded soil (Anderson, 2015)

2.3.2 Cyclic models

There are several methods who describes the influence of cyclic loading on flexible dolphin. EA-Pfähle (EA-Pfähle, 2012), the German society of geo-engineering, has listed three methods for this. The scale test for piles in sand of Duhrkopf and Grabe is used to determine the methods. The test is verified with many load cycles (SBRCURnet, 2018). The test was a cyclic load test, to determine the behaviour of a wind turbines. A conclusion of the test was that the displacement of the test increases with an increasing number of load cycles.

The first two methods have an equation that determines the displacement using the amount of load cycles. The first equation is a natural logarithmic approach and the second is an exponential approach:

Natural logarithmic approach:

$$y_{zyk} = y_{N=1} * (1 + t * \ln(N))$$

Exponential approach:

$$y_{zyk} = y_{N=1} * N^m$$

where:

N = Number of load cycles [-]

y_{zyk} = horizontal deformation pile after N load cycles [m]

$y_{N=1}$ = horizontal deformation pile after first load cycle (N = 1) [m]

t = factor for system behaviour under cyclic loading [-]

- The factor t depends on the relative pile stiffness, the installation method, and the type of loading. For piles in sand the value of t varies between 0.16 and 0.22.

m = factor for system behaviour under cyclic loading [-]

- short, stiff pile in sand: m = α
- long, flexible pile: pure horizontal load: m = 0.6 α
- pure bending: m = 0.4 α

α = factor depending on the installation method, type of loading and sand density. This factor varies between 0.10 and 0.25 [-]

The two models mentioned above are single load magnitude models. If the pile is tested with different load magnitudes, an adapted model is available. The multiple loads model is an enlargement of the logarithmic model. The approach mentioned above stays the same, only the number of loadcycles (N) changes. An equivalent number of load cycles is determined relative to a made load magnitude. The equivalent number of loadcycles is derived by comparing the static horizontal pile deformations of the load with the baseloads. The equation of the equivalent number of cycles is:

$$N_{eq} = N_1 + \sum N_k^*$$

In which the equation for the total equivalent number of cycles for load is:

$$N_k^* = e^{\frac{1}{t}\left(\frac{y_{1,k}}{y_{1,1}}\right)*(1+t*\ln(N_k)-1)}$$

Where:

N_{eq} = total equivalent number of cycles

N_1 = number of cycles for base load

N_k = number of cycles of load k

N_k^* = equivalent number of cycles of load k relative to baseload

$y_{1,k}$= static horizontal pile deformation under load k

$y_{1,1}$= static horizontal pile deformation under base load

3   Test predictions

This chapter consists of two parts. The first part, section 3.1, describes the test. The pile and soil properties are shown in this section and the prescribed load scheme is written down. The second part, section 3.2, consist of predictions of different calculation models. P-Y curves, Brinch Hansen, Blum and Plaxis have made predictions of the soil-pile behaviour.

3.1   Test setup

The full-scale test that is used in this study was performed at the Calandkanaal, a canal located within the Port of Rotterdam. In the Calandkanaal, new flexible dolphins were installed. Two of those piles are used for the full scale test. The piles examined are part of berth location 81 and identified as 81-D01 and 81-D04.

The test procedure involved utilizing a hydraulic jack to bring load on the two piles. The jack was situated on pile D04, with a fixed installation placed on pile D01. The two structures were connected with two bars that are fixed into the installation at pile D01. The hydraulic jack has the ability to retract or push out the stroke, thereby bringing load on the piles. To facilitate this movement, a pump was connected to the hydraulic jack. A visual representation of this setup is provided in Figure 3.1.
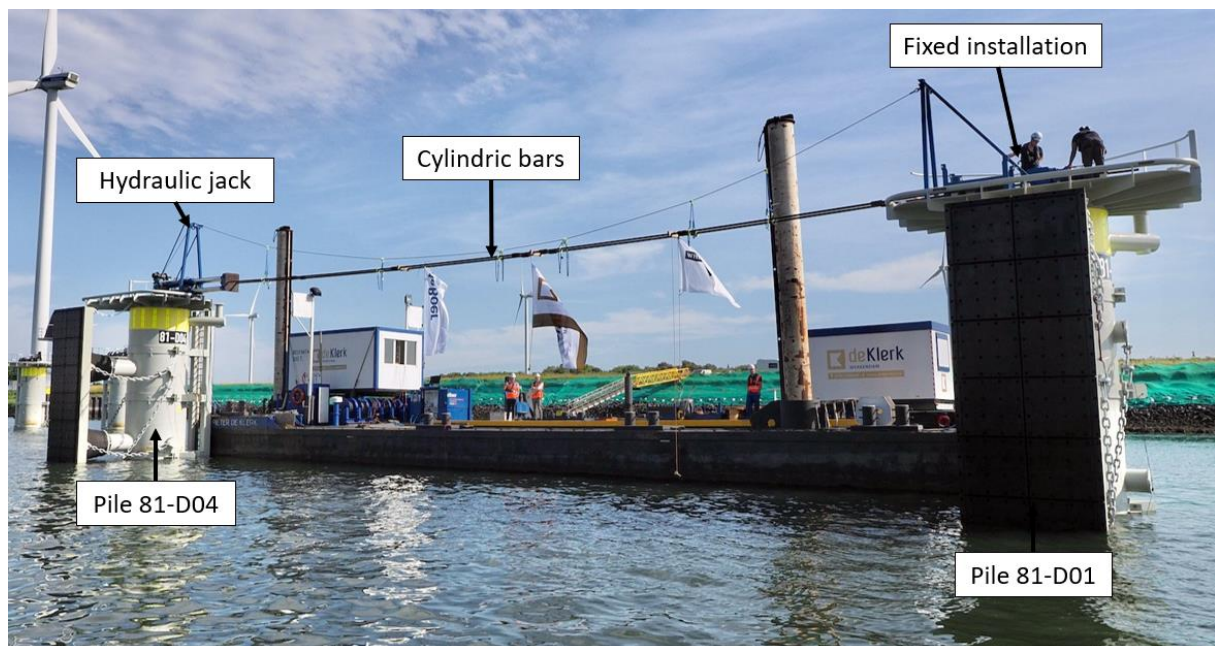
Figure 3.1: Test setup. (De Klerk, 2022)

The two flexible dolphins are open ended piles with equal dimensions. The pile consists of 9 pile sections, each with a consistent diameter but a different wall thickness. Table 3.1 displays the properties of the pile concerning the wall thickness, the steel quality and EI-factor. Table 3.2 show the properties of the steel, the steel properties are constant for the whole pile and are obtained from project documents (Griffioen, 2021). The moment of inertia of a ring is calculated with the formula:

$$I = \frac{\pi}{64}(D^4 - (D - 2 * t)^4)$$

In which:

I = Moment of inertia

D = outer diameter pile [D]

t = Wall thickness [m]

Table 3.1: Pile specification of the piles used during the test.

Pile section number	Steel quality	D	t	Top section	Bottom section	EI
		mm	mm	mNAP	mNAP	10^6 kNm^2
1	S355	2400	25	6,00	-0,75	27,6
2		2400	25	-0,75	-10,00	27,6
3		2400	30	-10,00	-12,75	32,9
4		2400	35	-12,75	-15,25	38,2
5	X70	2400	40	-15,25	-18,25	43,4
6		2400	50	-18,25	-22,50	53,5
7		2400	55	-22,50	-34,00	58,5
8		2400	40	-34,00	-37,00	43,4
9		2400	30	-37,00	-42,00	32,9

Table 3.2: The steel properties of the pile

Parameter	unit	Value
γ	kN/m^2	78.5
ν	-	0.25
E	kN/m^2	$210*10^6$
G	kN/m^2	$84*10^6$
f_y	MPa	485

The soil parameters used in this study are obtained from the cone resistance recorded during a cone penetration test (CPT), the CPT is shown in Figure 3.2Figure 3.2: CPT measurements at the location of the tested pile. The parameters are derived for the hardenings Soil Small Strain Plaxis model, as it provides the most comprehensive set of parameters. If other parameters are required in a calculation method, the parameter are specified in the corresponding section. The soil parameters are taken from intern project documents (Griffioen, 2021).

The relationship between the cone resistance and relative density are derived. Brinkgreve derived empirical formulas to derive the soil parameters for the hardening soil small strain model using the relative density (Brinkgreve, 2010). Previous research on the same location is used to derive R$_{inter}$. The empirical formulas provide an adequate first assessment of the soil parameters but is not a replacement of detailed soil investigation. As no further soil investigation was done at the test location, the empirical relationship are used. However, this inaccuracy must be considered in the further research.

Parameter	Unit		Empirical formula	Loam	Sand2	Sand3	Sand4
q_c	[MPa]	Cone resistance	CPT-measurement	9.6	40.4	16.6	11.6
Top of Layer	[mNAP]		CPT-measurement	-24.6	-31.0	-38.0	-44.0
γ_{unsat}	[kN/m³]	Unsaturated unit weight	$= 15 + 4 * RD/100$	17.6	18.8	17.8	18.2
γ_{sat}	[kN/m³]	Saturated unit weight	$= 19 + 1.6 * RD/100$	20	20.5	20.3	20.1
ϕ	[°]	Internal friction angle	$= 28 + 12.5 * RD/100$	36	39.9	38	36.6
c'	[kN/m²]	Cohesion	0	0	0	0	0
ψ	[°]	Dilatancy	$= -2 + 12.5 * RD/100$	6	9.9	8.1	6.6
$E'_{50}{}^{ref}$	[kN/m²]	Secant stiffness	$= 60000 * RD/100$	38.5*10^3	70*10^3	48.3*10^3	41.4*10^3
$e3E'_{oed}{}^{ref}$	[kN/m²]	Tangent stiffness	$= 60000 * RD/100$	38.5*10^3	70*10^3	48.3*10^3	41.4*10^3
$E'_{ur}{}^{ref}$	[kN/m²]	unloading/reloading stiffness	$= 180000 * RD/100$	115.5*10^3	210*10^3	144.9*10^3	124.2*10^3
$\gamma_{0.7}$	[-]	Shear strain threshold	$= \left(2 - \frac{RD}{100}\right)*10^{-4}$	1.35*10^-4	1.05*10^-4	1.2*10^-4	1.31*10^-4
m	[-]	power of stress-level dependency	$= 0.7 - RD/100$	0.5	0.4	0.45	0.48
POP	[kN/m²]	Pre-overburden pressure		0	0	0	0
OCR	[-]	Over consolidation ratio		1.0	1.0	1.0	1.0
$G_0{}^{ref}$	[kN/m²]	Shear modulus at very small strains	$= \frac{60000 + 68000RD}{100}$	103.7 E3	124.6 *10^3	114.7 *10^3	106.9 *10^3
R_{inter}	[-]	Strength reduction factor interfaces	Earlier research	0.67	0.67	0.67	0.67

Table 3.3: Soil properties of the test location
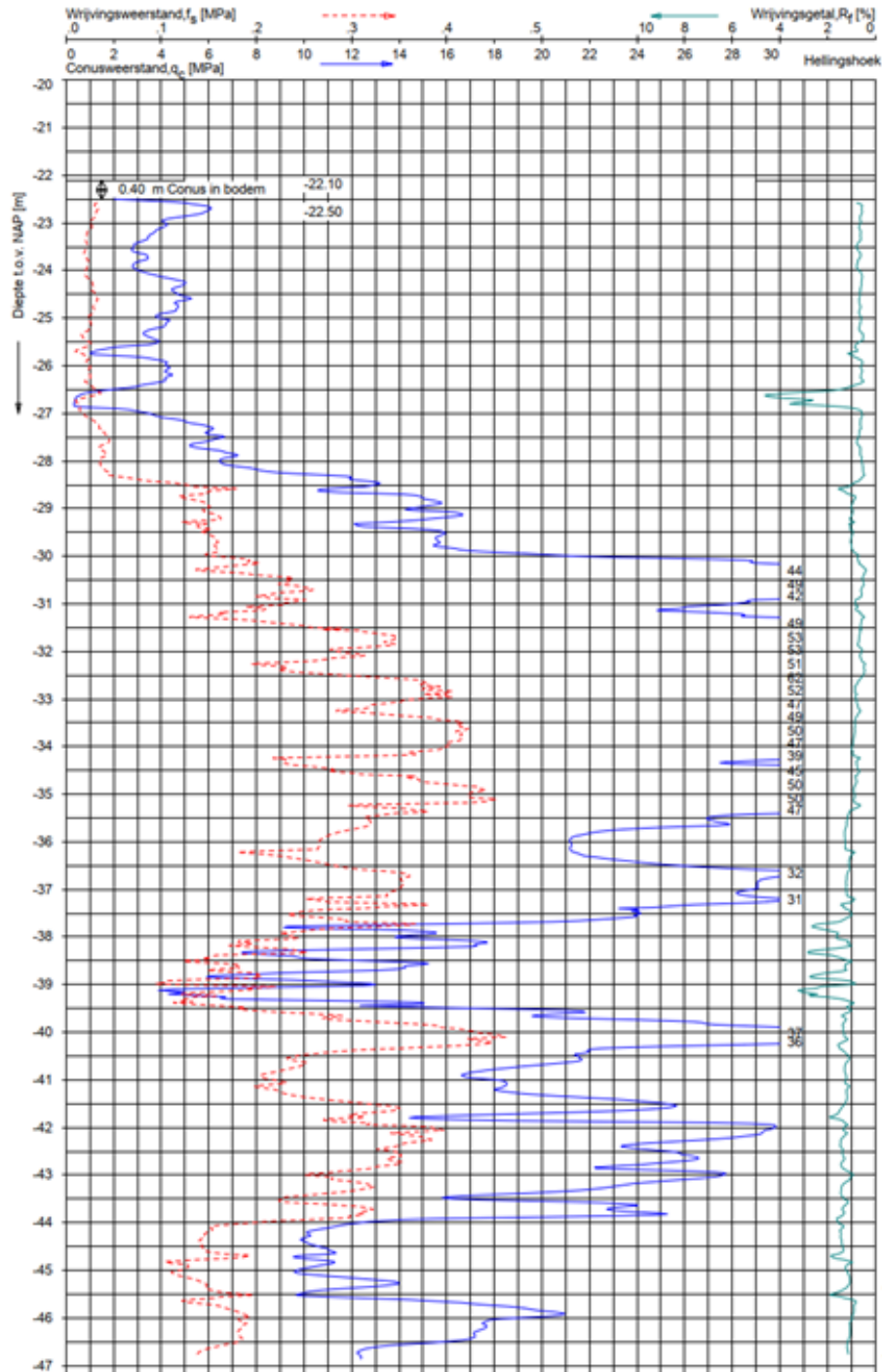
Figure 3.2: CPT measurements at the location of the tested pile

During the test procedure, the hydraulic jack applies the load on the piles according the prescribed load scheme. The test is done using a load-controlled test, so the load on the pile is controlled instead of the amount of displacement. The ultimate limit state, ULS, load of the piles is calculated before the test. The ULS load of the piles is 2025 kN (Griffioen, 2021). During the test, the pile is loaded until 90% of the calculated ULS load to maintain a margin of safety before the pile fails. The load is applied at a height of +6.5m NAP, the pile is 6 meter above NAP and the load application height of the hydraulic jack is 0.5 meter above the pile top. To keep the piles and strokes stable, the hydraulic jack installation is under a rest load of 10 kN during unloading.

The loading scheme contains 9 loadstep, each loadstep has its own maximum load. Every loadstep consists of 3 phases:

- Load built up phase: The load is slowly applied on the pile until it reached its the maximum load.
- Constant load phase: The maximum load is kept constant in this phase for about 15 minutes.
- Unloading phase: The load is phased out to the minimum 10 kN and kept unloaded briefly.

Table 3.4 shown the loadcycles with its corresponding maximum load. The load is gradually and steadily increased. Although the unloading may occur faster than loading, some patience is still required. The maximum load is kept constant until the displacements remain constant.

Table 3.4: Load scheme of the test

Loadcycles	Load percentage of ULS	Maximum load [kN]
1	40%	810
2	55%	1114
3	70%	1418
4	80%	1620
5	90%	1823
6	90%	1823
7	90%	1823
8	90%	1823
9	90%	1823

Various measuring instruments are utilized during the test to obtain information about the behaviour of the pile. Each parameter is measured by multiple instruments to ensure the accuracy of the results. Table 3.5 provides an overview of the measuring instruments employed during the test, along with the corresponding parameter each instrument measures. Some parameters are measured directly, while others are measured indirectly. Figure 3.3 depicts the setup of the measuring instruments during the test.

Table 3.5: Measurement instrument and what the instruments measures

Measurement instruments	Load	Hor. Displacement	Ver. Displacement	Total displacement	Strains	Time	Depth	Water-pressure
Hydraulic jack	x			x		x	x	
Optical fibre	x	x	x	x	x	x	x	
Total station		x	x	x		x	x	
Saaf		x	x	x		x	x	
Piezometer						x	x	x

- ■ - Optical fibre (over the bottom 40 meter of the pile)
- ■ - Saaf (over a large part of the pile)
- ➡ - Lateral Load direction
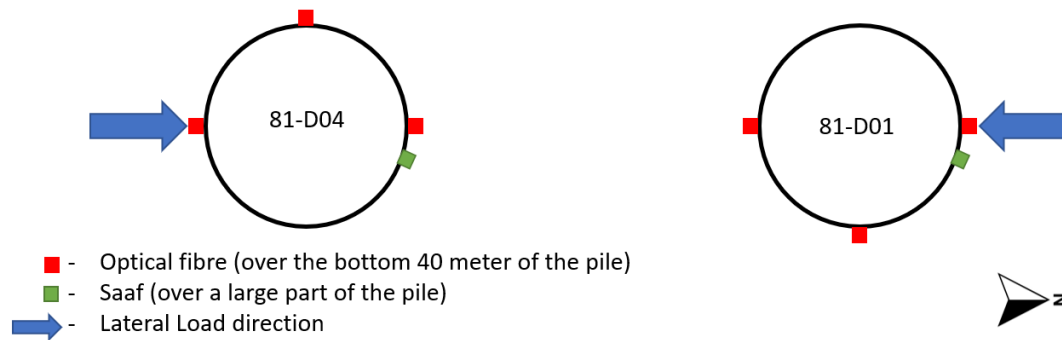
Figure 3.3: Visualization of the measurement instrument during the test

3.2 Test Predictions

3.2.1 Brinch Hansen

D-sheetpiling uses the Brinch Hansen model to calculate the lateral soil resistance. D-sheetpiling is develop by Deltares. The flexible dolphin is best modelled with the single pile model. The calculation is an elastic calculation. The pile is loaded by force some explained in chapter 3.1. The pile is modelled with the 9 sections, each section has its own wall thickness and elastic stiffness. The top section is extended by 0.5 meter to enable the load to be applied at the same height as during as during the test. The soil layers have a maximum thickness of 1 meter since the passive earth pressure (K_p) is calculated only ones every soil layer, which is performed in the middle of a layer (Peters, 2017). When the layers become too large, the average K_p is not representative for the entire layers. The smaller layers ensure more representative K_p determination in the soil. The soil has 4 different soil types, as described in chapter 3.1. The soil types are spread along more layers in the model.

The single pile model uses the Brinch Hansen method with the Menard modulus of subgrade reaction. Both methods are used in the calculation, the input parameters for the model are shown Table 3.6. The input values, except the pressure meter modulus (E_m), the general input parameters of the soil. The E_m value is calculated using a correlation with the cone resistance of the soil and a correction factor for the soil type (Deltares, 2021). In this model the cone resistance and the average correction factor for sand is chosen, the correction factor of sand varies between 0.7 and 1, so 0.85 is chosen. The water level is at 0 mNAP.

Table 3.6: input data of D-sheetpiling model

Input section	Input parameters	Sand1	Sand2	Sand3	Sand4
General	γ_{dry} [kN/m^3]	17.6	18.8	18.2	17.8
	γ_{wet} [kN/m^3]	20	20.5	20.3	20.1
	c'	0	0	0	0
	φ [°]	36	39.9	38	36.6
Menard	E_m Menard	8160	34340	14110	9860
	Soil type Menard	Sand	Sand	Sand	Sand

It is not possible to implement a time effect in this model, so only one loadstep can be modelled. The maximum load, 1823 kN, is applied on a height of +6.5 mNAP on the pile.

The results of the bending moment and displacement are shown in Figure 3.4 and Figure 3.5. The maximum displacement at the top of the pile is 933 mm. The tip displacement is -17.61 mm. The maximum bending moment is 61570 kNm, which is on a height of -28.6 mNAP.
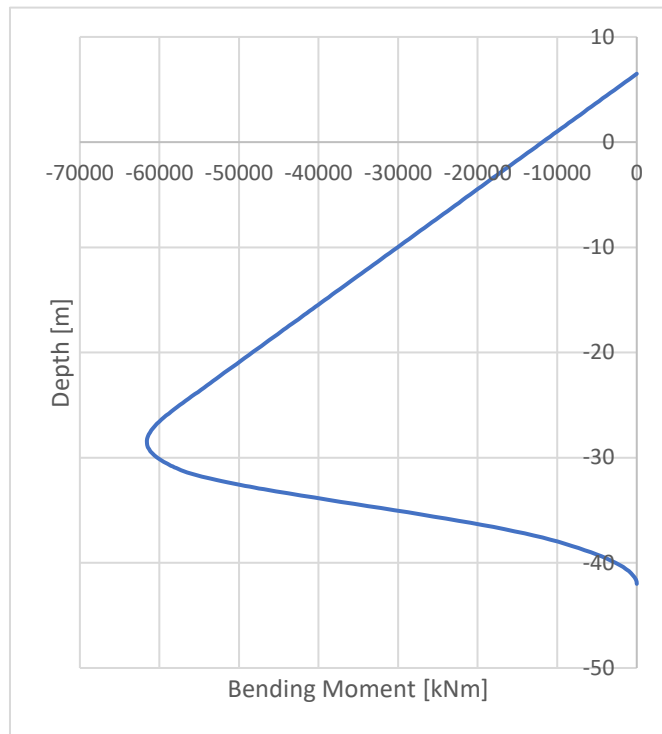
Figure 3.5: Bending moment in pile of D-sheetpiling model
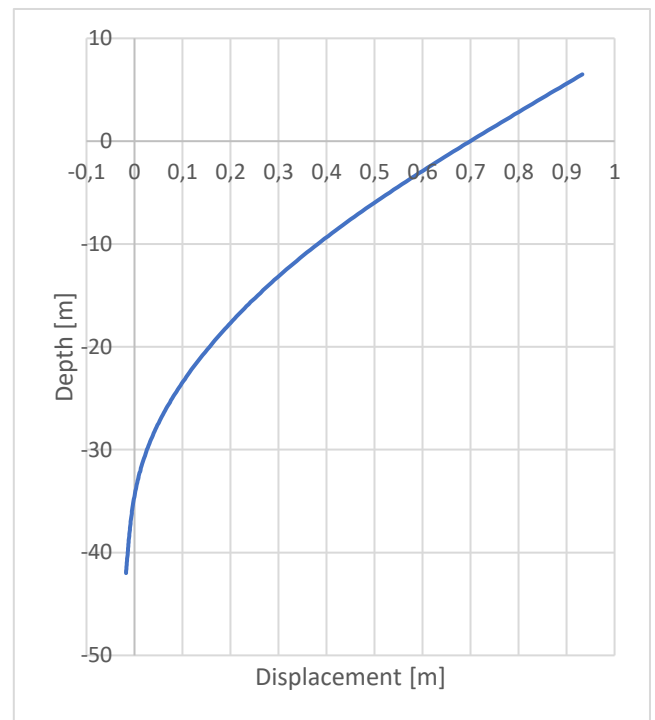
Figure 3.4: Pile displacement of D-sheetpiling model

3.2.2 P-y curves

3.2.2.1 D-pile group

D-pile group uses p-y curves to calculate the behaviour of the soil. D-pile group is a program developed by Deltares. The Cap (Cap interaction) method is chosen as calculation method, this method is the best applicable to calculate a flexible dolphin. The soil profile is modelled as mentioned in chapter 3.1, with four different sand layers and a water level on 0 mNAP. The four different soil layers are created in the soil layer menu. The parameters and corresponding input values for this model are shown in Table 3.7. The OCR value in the model is estimated as 1, like in Table 3.3. The K0 value can be calculated using the equation: $K_0 = 1 - sin\ (\varphi)$, *(Verruijt, 2001)*. The API cyclic loading model is used, because during the test the flexible dolphin is loaded repetitive. The API rule is chosen as axial friction rule, but the axial friction data for the API rule are unknown, just like the axial parameters. The influence of the axial parameters can be neglected, since only lateral loads are applied. The friction at the top and bottom of the pile is chosen as the half of the friction angle, which was suggested in the manual *(Deltares, 2020)*.

The pile is modelled as a user defined pile, which gives the possibility to add 5 pile sections. This is still not sufficient for the 9 sections of the pile. Every two pile sections are combined to one section in the model, only section 7 (the section with the highest wall thickness) has its own section. The

weighted average wall thickness is used, considering both section lengths. The input parameter of the pile sections are the length, diameter, EI and EA. The two section lengths are combined, and the diameter is constant, 2.4 m. The elastic modulus is constant for steel and the moment of inertia and area can be calculated using the wall-thickness of each section. The pile tip curve is an unknown parameter. The curve is manually changes to investigate the influence, but the influence of the pile tip curve is neglectable in the lateral loading situation.

Table 3.7:Input data of D-pile group model

Parameters		Sand1	Sand2	Sand3	Sand4
Soil type		Sand	Sand	Sand	Sand
	γ_{dry} [kN/m³]	17.6	18.8	18.2	17.8
	γ_{wet} [kN/m³]	20	20.5	20.3	20.1
	φ [°]	36	39.9	38	36.6
	K_0 [-]	0.41	0.36	0.38	0.40
Lateral rule		API Cyclic	API Cyclic	API Cyclic	API Cyclic
Axial friction rule		API	API	API	API
	dz at 100% [m]	0.002	0.002	0.002	0.002
	Friction at top [°]	18	20	19	18
	Friction at bottom [°]	18	20	19	18

The results of the bending moment and displacement are shown in Figure 3.5 and Figure 3.6. The maximum displacement is 938 mm at the top and the tip displacement is -2.5 mm. The maximum bending moment is 62675 kNm at a depth of -29.1 mNAP.
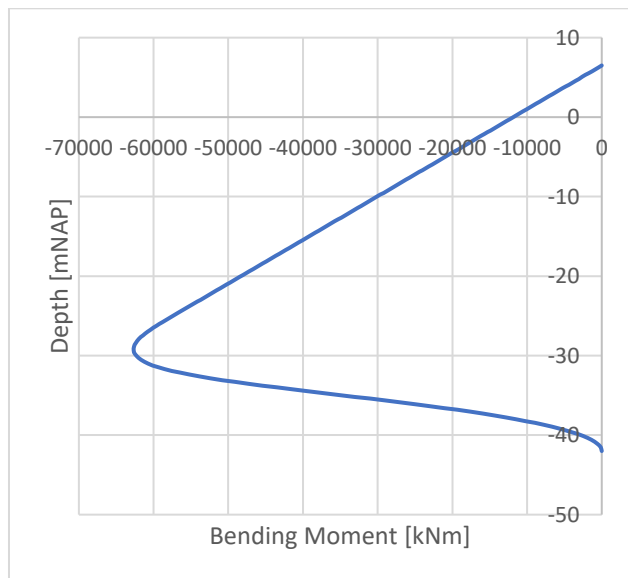
Figure 3.7: Bending Moment in pile of D-pile group model
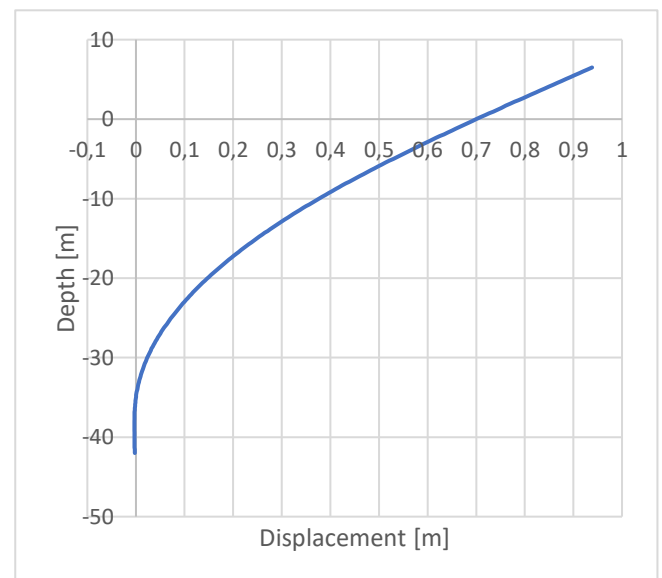
Figure 3.6 :Bending Moment in pile of D-pile group model

3.2.2.2   Geocalcs

Geocalcs is an online calculation program with different application tools. The LAP (Lateral analysis of Piles) model is used on Geocalcs. The lateral loaded piles can be calculated with different soil models (Doherty, 2020). The available models for sandy soils are: Sand API and CPT Sand (Suryasentana,

2014). The API model is the same model as used in D-pile group. The CPT sand model is a model based on the CPT data.

The API method uses the soil layers as mentioned in chapter 3.1. The CPT-based method uses the cone resistance of the CPT-data from figure 3.2 and is not divided in different soil layers. The cone resistance at certain depths is shown in Table 3.8. The pile can be divided in 5 sections in the program. 2 pile section needs to be combined with a weighted average wall thickness and corresponding moment of inertia. The load is applied on +6.5 mNAP. Only one load can be applied during the calculation, the maximum load of 1823 kN is applied on the pile.

The results of the calculation are the bending moment, displacement, rotation, and the soil pressures. The displacement of the pile is shown in Figure 3.8 and Figure 3.9. The maximum displacement of the CPT-model calculation is 927 mm, and the top displacement of the API-model is 897 mm. The tip displacement of the CPT-model is -28mm, while the API model has a tip displacement of only -2 mm. The bending moment of the CPT-model is also smaller in the soil. The calculation models determine the stresses in the soil, in the water the pressures are not considered. The bending moment above the soilbed is equal for the different models.

Table 3.8: soil input values CPT-based model

Depth [m]	q_c [MPa]	Depth[m]	q_c [MPa]
-24,6	5	-34,5	43
-25	5	-35,5	47
-26	6	-36,5	44
-27	7	-37,5	42
-28	2	-38,5	33
-29	14	-39,5	39
-30	16	-40,5	28
-31	20	-41,5	27
-31,5	65	-42,5	16,5
-32,5	61	-43,5	17
-33,5	50		
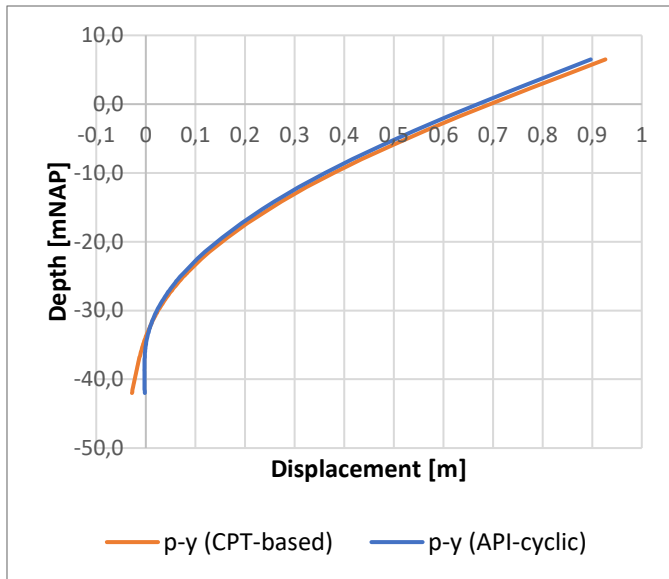
Figure 3.9: Pile displacement of Geocalcs model
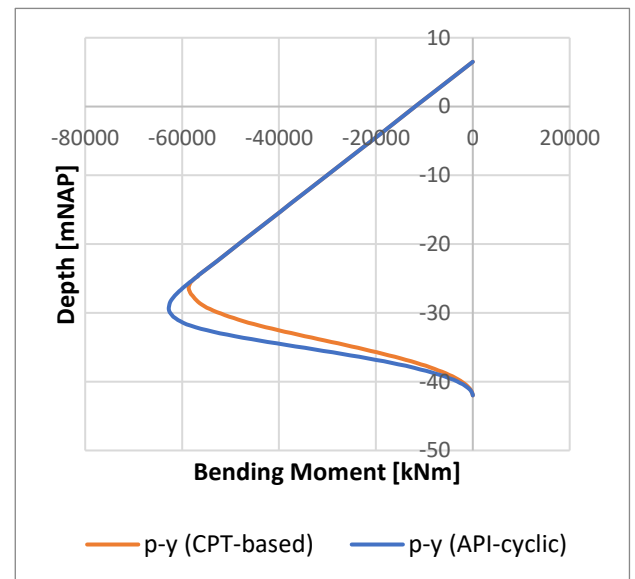
Figure 3.8: Bending moment in pile of Geocalcs model

3.2.3   Blum

A Python script calculates the Blum model. The original Blum model is used together with the wall friction of the Spudhand Handbuch Berechnung. The input parameters of the soil are the internal friction angle, and the volumetric weight of the soil. The original formulas cannot include layered soils., but the formulas are adapted to be able to calculate two different soil layers in the model. The Blum model calculates the ultimate soil resistance and uses a single load. The pile parameters that are used in the model are the Elastic modulus of steel, the wall thickness, and the length of the pile. The wall-thickness influences the moment of inertia. The weighted average moment of inertia is calculated, that moment of inertia is used to determine the input wall thickness. The upper 3 soil layers are used in the calculation. The bottom soil layer is below the pile and doesn't have influence on the soil resistance in this model. Table 3.9 shows the input parameters of the soil.

The model determines the displacement on 3 depths: the tip of the pile, the top of the pile and at the soilbed. The displacement of the pile is shown in Figure 3.10.

Table 3.9: Soil input parameters Blum

	Sand1	Sand2	Sand3
φ [°]	36	39,9	38
γ [kN/m³]	17,6	18,8	18,2
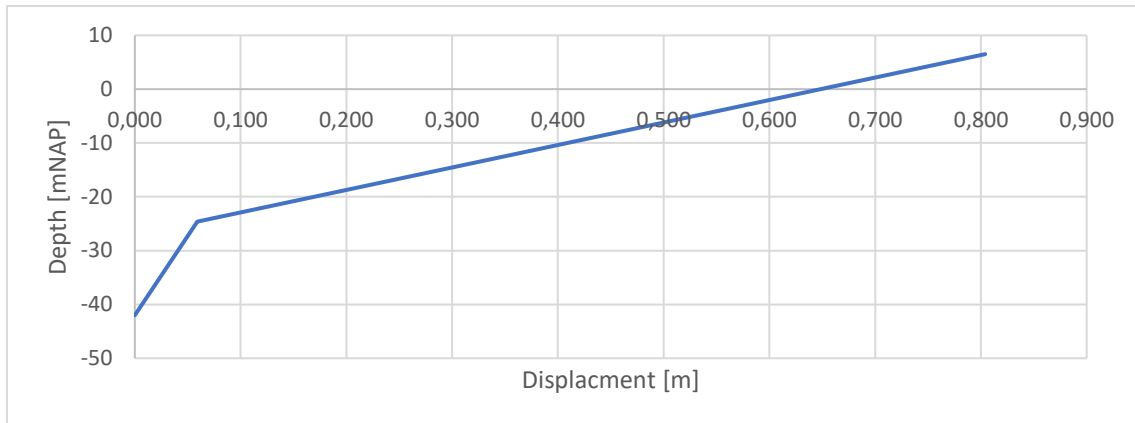
Figure 3.10: Pile displacement of Blum model

3.2.4 Plaxis

Plaxis 3D is a three-dimensional finite element model program (Plaxis, 2021). The program is specifically made for geotechnical calculations. Plaxis 3D can simulate soil behaviour with different material models. Those models differ in complexity, linearity and applicability for different soil/rock types and constructions. The appendix of the manual contains tables with the applicability of material models for different material types, applications and loading types. This report is about flexible dolphins in a sandy environment. Those dolphins have small deformations around the pile-tip and large deformations around the top. The Hardening soil model with small strain stiffness, also known as HSsmall, is the preferred model according to the appendix. The HSsmall model is an extension of the hardening soil model, with a better representation of the non-linear soil stiffness for small strains.

The flexible dolphin is modelled as a plate-pile, since the plate marches best with the pile tube. Since the slope in the subsoil must been considered, it is not possible to make half of the model. Otherwise, when the model is symmetric it is more user-friendly to use a half model to reduce the runtime. The pile is divided in 9 sectors, with each sector their corresponding wall thickness. The diameter of the circle is chosen at the outside of the pile wall, so for every sector the diameter is chosen at 2.4 meter. The plate does not have a specific thickness in the model. Since the outer diameter has more influence on the behaviour of the pile than the inside, the outside diameter is chosen as the diameter of the plate. A positive and a negative interface is created around the pile. The interface ensures that the soil and the plate are not directly connected to each other, but a transition area is created.

The load is applied on the pile as a surface load. To get the surface load on the top of the pile, a pile head is modelled at a height of 6.5 mNAP, using a horizontal plate. The load is applied as a surface load on the pile head. The area of pile head is equal to the area of the pile cross section. The total load of the loadstep is divided by the area of the pile head to create a surface load in kN/mm^2. The model has 9 pile sections, each section has their own wall thickness. One model is made with drained soil layers and another model uses undrained soil layers. The soil behaviour is not fully known on this point, so both models are calculated to have them both to analyse.

The slope of the soilbed is considered. The soilbed is designed predefined using drawings and dredging. The soilbed after dredging is drawn with the blue line in Figure 3.11, the cross-section is at the location of the pile. The soilbed is approached as good as possible in the model, which is close to the prescribed dredging depth, red line.
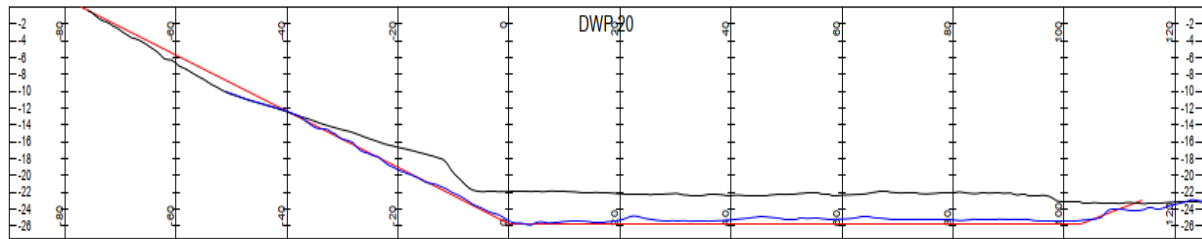
Figure 3.11: Soilbed course in the canal

 The phase explorer in Plaxis gives the possibility to model all the stages of the test on their own. The separate phases in Plaxis ensure that the test can be modelled as accurate as possible. The input phases of model are shown in Table 3.10.

Table 3.10: input of load phases in Plaxis model

Stage	Load [kN]	Calculation type	Specification
Initial stage	-	Initial stress generation	K0 procedure
Loading stage 1	810	PLASTIC	Staged construction
Unloading stage 1	-	PLASTIC	Staged construction
Loading stage 2	1114	PLASTIC	Staged construction
Unloading stage 2	-	PLASTIC	Staged construction
Loading stage 3	1418	PLASTIC	Staged construction
Unloading stage 3	-	PLASTIC	Staged construction
Loading stage 4	1620	PLASTIC	Staged construction
Unloading stage 4	-	PLASTIC	Staged construction
Loading stage 5	1823	PLASTIC	Staged construction
Unloading stage 5	-	PLASTIC	Staged construction
Loading stage 6	1823	PLASTIC	Staged construction
Unloading stage 6	-	PLASTIC	Staged construction
Loading stage 7	1823	PLASTIC	Staged construction
Unloading stage 7	-	PLASTIC	Staged construction
Loading stage 8	1823	PLASTIC	Staged construction
Unloading stage 8	-	PLASTIC	Staged construction
Loading stage 9	1823	PLASTIC	Staged construction
Unloading stage 9	-	PLASTIC	Staged construction

The corresponding input values are assigned to each of the separate phases. The input of phase loading stage 2 is shown in Figure 3.12, this phase is representative for the other phases except for phase loading stage 1. Loading stage 1 is the first calculation phase, the deformation control parameters form the initial stage are reset in this phase and the start values are set to zero. The parameters for which the reset is checked include displacements, small strains, and the pore pressure calculation type, which is set to phreatic. The time interval has no influence on the model since the soil model is not time dependent, a time interval of 0.01 day is chosen as constant time interval. Since it is a continues test, the pore pressures of each loadstep are taken to the next loadstep.

3. Test predictions

Name	Value
General	
ID	unload1 [Phase_2]
Start from phase	Load1
Calculation type	Plastic
Loading type	Staged construction
ΣM_{stage}	1,000
ΣM_{weight}	1,000
Pore pressure calculation ty	Use pressures from p
Time interval	0,01000 day
First step	10
Last step	18
Special option	0
Deformation control parameters	
Ignore undr. behaviour (A,	☐
Reset displacements to zer	☐
Reset small strain	☐
Reset state variables	☐
Reset time	☐
Updated mesh	☐
Ignore suction	☑
Cavitation cut-off	☐
Cavitation stress	100,0 kN/m²

Figure 3.12:input phase menu of Plaxis model

The computation for both the drained and undrained models has been conducted, and the outcomes of these calculations at three distinct depths are presented in Table 3.11, respectively. The chosen depths are: the top of the pile (+6.5 mNAP), the tip of the pile (-42 mNAP) and the soilbed (-24.6 mNAP).

Table 3.11: Plaxis lateral displacement of the drained and undrained model.

Displacement of Plaxis models [m]						
Drained model			Undrained model			
Load [kN]	+6.5 mNAP	-24.6 mNAP	-42 mNAP	+6.5 mNAP	-24.6 mNAP	-42 mNAP
0	0,000	0,000	0,000	0,000	0,000	0,000
810	0,392	0,036	-0,003	0,390	0,034	-0,002
0	0,067	0,017	-0,003	0,067	0,017	-0,001
1114	0,561	0,055	-0,006	0,545	0,050	-0,003
0	0,112	0,030	-0,005	0,111	0,028	-0,003
1418	0,743	0,078	-0,011	0,700	0,067	-0,005
0	0,168	0,045	-0,010	0,159	0,041	-0,005
1620	0,876	0,096	-0,016	0,800	0,077	-0,007
0	0,216	0,058	-0,014	0,197	0,050	-0,006
1823	1,020	0,116	-0,021	0,901	0,088	-0,009
0	0,269	0,072	-0,019	0,234	0,060	-0,008
1823	1,030	0,120	-0,022	0,898	0,088	-0,009
0	0,286	0,077	-0,020	0,247	0,063	-0,008
1823	1,040	0,123	-0,022	0,896	0,088	-0,009
0	0,299	0,081	-0,021	0,254	0,064	-0,009
1823	1,040	0,125	-0,023	0,894	0,088	-0,009
0	0,310	0,084	-0,021	0,259	0,065	-0,009

1823	1,050	0,127	-0,024	0,893	0,088	-0,009
0	0,319	0,086	-0,022	0,262	0,066	-0,009

3.2.5   Overview prediction

Figure 3.13 illustrates the displacement results of the models. The majority of the lines exhibit a consistent trend, with maximum displacements around 0.9 m. However, two lines deviate from this pattern. Specifically, Blum's calculation estimates a lower displacement of approximately 0.8 m, whereas the drained Plaxis calculation yields a higher top displacement of 1.05 m. When evaluating the capacity of calculation models to handle repetitive loads, the models incorporate such capability in their calculations. In this regard, Plaxis employs the results of the 9th load step. The predictions of the test are made. It is noticed that the models predicted similar displacements, especially as top displacements. The tip displacements are relatively larger. The hypothesis is that the Plaxis drained model was able to determine the soil-pile behaviour best. Because of this, it is even more noticeable that the displacements of Plaxis drained are far from the rest. In chapter 4, the measurements of the test are analysed. The actual displacement will be compared with the calculations of this chapter.
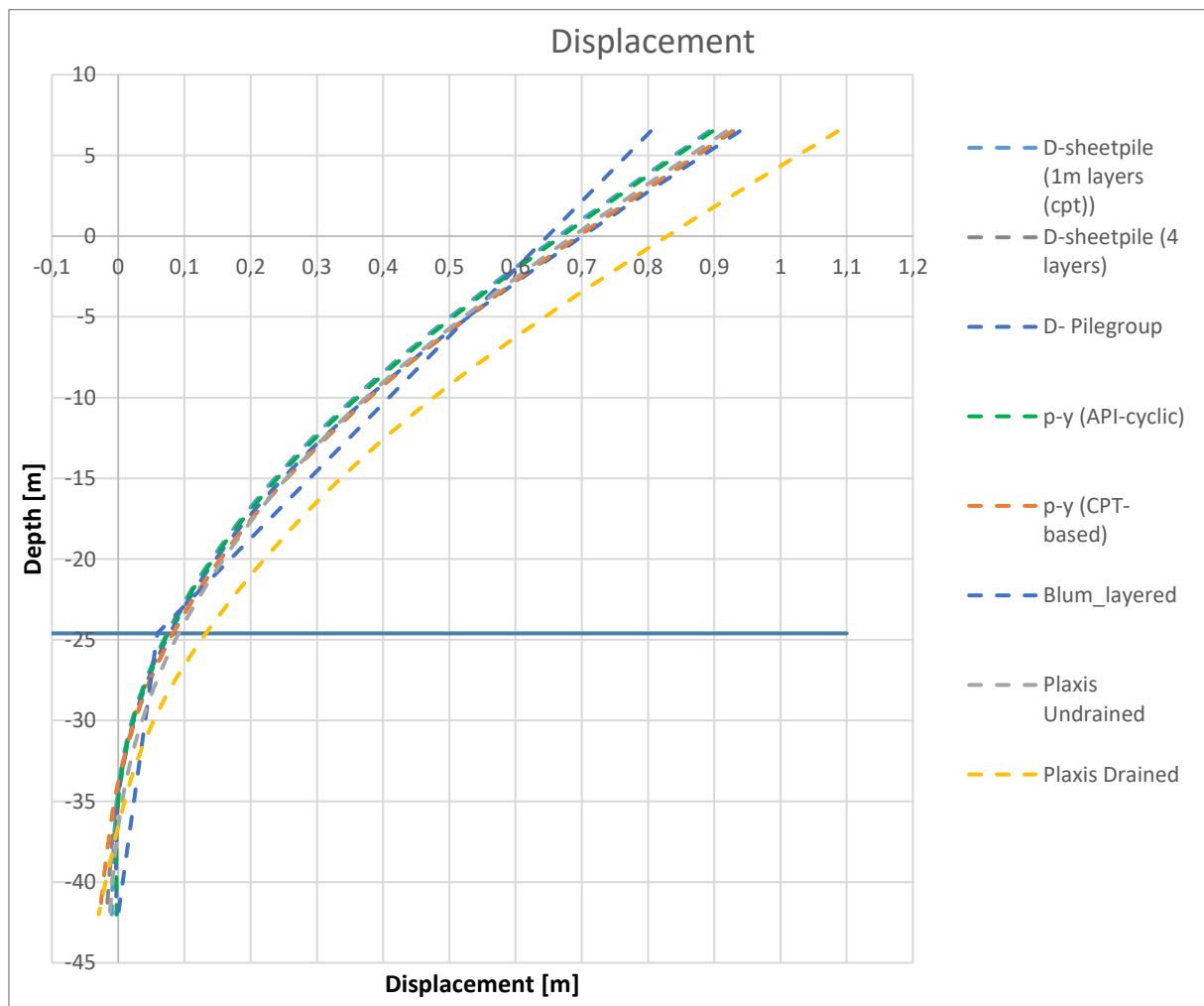
Figure 3.13:Predictions of pile displacement according to multiple models

4 Test results

In this chapter the measurement results of the test are shown. The result of the different measurement instrument is shown and analysed. The instruments that are used during the test are:

- Hydraulic Jack
- Optical fibre
- Total station
- Saaf
- Inclinometer
- Piezometer

The results of those instruments are analysed in this chapter. Each instrument has its own section. The inclinometer isn't used in the analysed and the measurements are listed in the appendix. The measurements of the inclinometer had problems with a narrowing in the tube, so that not the whole pile could be measured but only half.

The instruments start measuring at various times. To synchronize the measurements, a uniform starting time is chosen as base-measurement. At the starting time, the displacement is set to zero. With the equal starting time, the different instruments can be compared with each other. The start time is chosen at 9:00 AM. At this time, all the instruments have started measuring and the pile was still not loaded.

4.1 Hydraulic Jack

The hydraulic jack put the load on the piles. The hydraulic jack measures the oil pressure in the jack, this oil pressure is translated to the load that the jack creates. The load output is the amount of load that is applied on the pile during the test, which makes it a useful tool during the test. The prescribed load scheme is executed with the data from the load measurements of the hydraulic jack. Next to the load, the shortening of the cylinder is measured. The piles are pulled towards each other, while the bar must stay under tension, therefor the cylinder becomes shorter between the point of loading by the hydraulic jack and the other side. The shortening of the cylinder is the total displacement of both piles.

The measurement results of the load and displacement of the hydraulic jack are shown in Figure 4.1. The green line represents the load, while the yellow line indicates the shortening of the cylinder. The nine loadsteps are clearly shown in the figure. Once the maximum load is reached the load is kept constant. A little bit of noise is visible due to the manual control of the load. The collected data can be employed to determine the timing of load application. The total displacements will be compared with the other displacement measurements. The displacement and load are calculated every second, so a lot of data is available from the hydraulic jack. The displacement of the hydraulic jack is the combined displacement of both piles at a height of +6.5 mNAP.
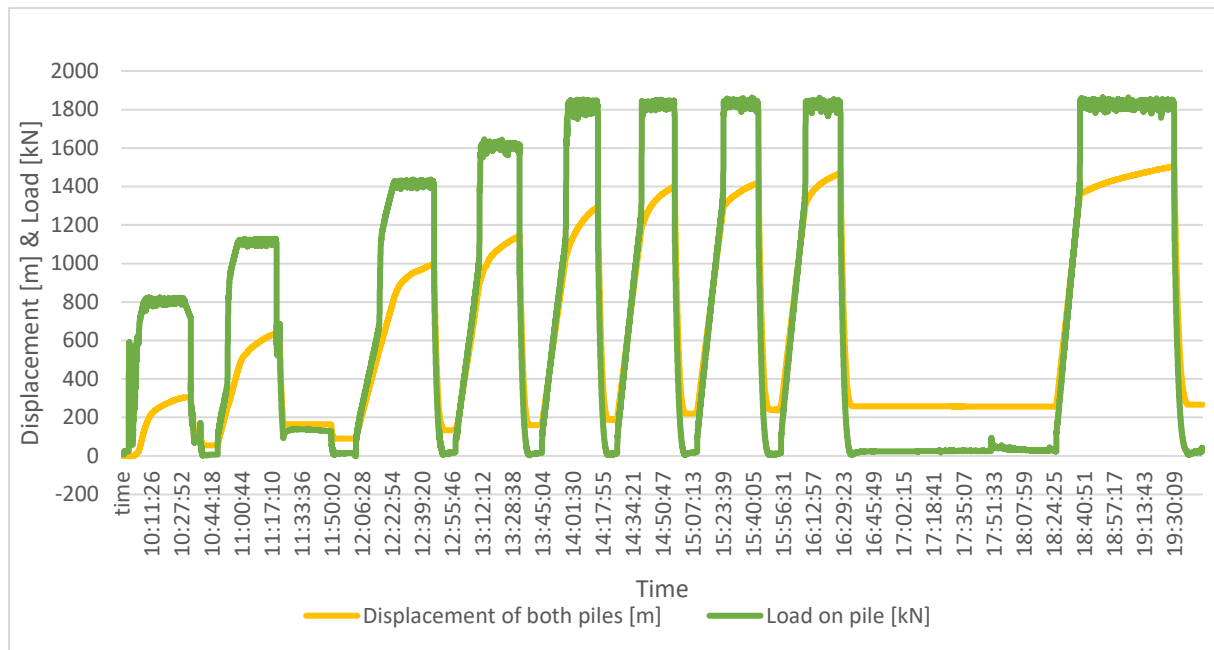
Figure 4.1: Load and displacement of Hydraulic Jack

4.2 Optical fibre

Optical fibre cables are connected to the pile and measure the strains. The optical fibre method employed for the testday is BOTDA (Brillouin Optical Time Domain Analysis). Initially, a BOTDR (Brillouin Optical Time Domain Reflectometry) sensor configuration is used, but all sensors are later changed to a BOTDA configuration during test preparation. The BOTDA technic has a strain accuracy of 20 με (OZ-optics, 2015). The inaccuracies have the most significant impact on the smallest strains, but their influence diminishes as the strain differences increase due to larger strains.

Light is sent through the cable during an optical fibre measurement. If the cable deforms, the light transmission in the cable changes. This changes in light transmission are detected by the system. The system converts the changes in the light transmission into a strain in the cable. The two parameters that affect this transition are the frequency of the light and the temperature. The company responsible for the optical fibre measurements has already determined the strains from the data they collected.

Four optical fibres are installed on the pile, the cables measure the data every +- 4 minutes. The output parameters are: the location on the cable, frequency, strain, gain and width. The location on the cable and the strain are used in this chapter. The location on the cable can be transferred towards the location on the pile, using the tip of the cable. The tip of the cable is indicated in the data by a jump in the strain-data. The cables measure the bottom 40 meter of the pile twice, once during the descent and once during the ascent. The assumption is made that the tip of the cable is at the tip of the pile. Due to the double measurement, the data from the cables can be cross-validated.

The strain data measurements are the raw data. The difference between the raw data and the base-measurement data reflect the additional strain, caused by the load. The additional strain is utilized in the calculations. The base measurement for the four cables is taken around 9:00 AM on the testing day, when the pile was not loaded.

The data of the optical fibres can be used to calculate the bending moment and the shear force exerted on the pile. The bending moment is particularly useful for determining the additional load imposed on the pile, as discussed in chapter 5.

Four cables were installed on the piles during the test. The location of the cables is schematized in Figure 4.2. At both piles, three sides of the pile are measured with the optical fibres. On both piles the "Noord" and "Zuid" sides are measured, which are the sides in the load-direction. And one side perpendicular on the pull-direction on both piles is measured. Due to the extensive number of measurements performed during the test, this chapter focuses on the results obtained at the end of the eighth load step. The eighth loadstep is the last loadstep where the saaf also have measured the curvature of the pile. The later loadsteps consist of larger strains. The assumption is made that the largest displacement ensures the best measurement with the least amount of influence of the noise and inaccuracies. Two cables consist of the measurements of one side of the pile and the two other cables contain the measurements of 2 sides of the pile. The sides of the pile that are measured with the cable are listed in the name of the cable. The four cables used are as follows:

- D01_Zuid
- D01_Noord-Oost
- D04_Noord
- D04_West-Zuid
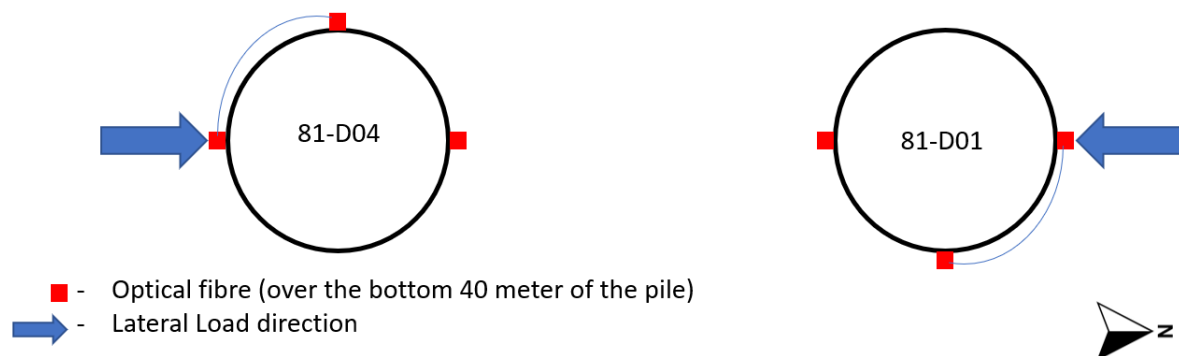
Figure 4.2: Optical fibre cable distribution on pile

This chapter shows the strain data of cable D01_Noord-Oost (North-East). The additional strain of all four cables is analysed. The strain-data from this cable gives the clearest trend of the strain and has the least amount of noise or outliers. The measurements of stain cable D01-NO is used in the report. The other three strain cables are shown in the Appendix.

The strain data that is shown in the graph, is the strain data of the cable that was connected to the north and east part of pile D01. The useable strain measurements are shown in Figure 4.3. The grey line represents the base-measurement, which is taken before the load is applied on the pile, at 09:03 on the testday. The orange line represents the strain at the end of the eighth loadstep. The green line represents the difference in strain between the blue and grey line, which is the additional strain due to the load.

The first 100 meter of the cable is extra cable length that is not connected to the pile, so this data can be filtered out. The middle part, between roughly 100 and 220 meters, shows a clear trend with two bows. This part is connected to the North side of the pile. The last +-100 meter is connected to the east part of the pile. The last part has a lot of noise and there is no trend visible in the data, which makes this data unusable. The middle part, shown in figure 4.3, shows a clear trend, with a sharp

peak. The peak in the middle of the trend means the tip of the cable. Preceding the peak, the cable descends along the North side of the pile for 40 meters, while following the peak, it ascends again for another 40 meters. These two parts are expected to be symmetric since it measures the strain two times on the same height on the pile. The strains are positive, which means that the cable length increases. This outcome aligns with expectations as the North side of the pile experiences tension when subjected to the current loading conditions.

Only the north part of the data will be used in the continuation of this research since the other data is unusable due to the noise. The "oost" side was the only measurement perpendicular to the pull direction on pile D01.
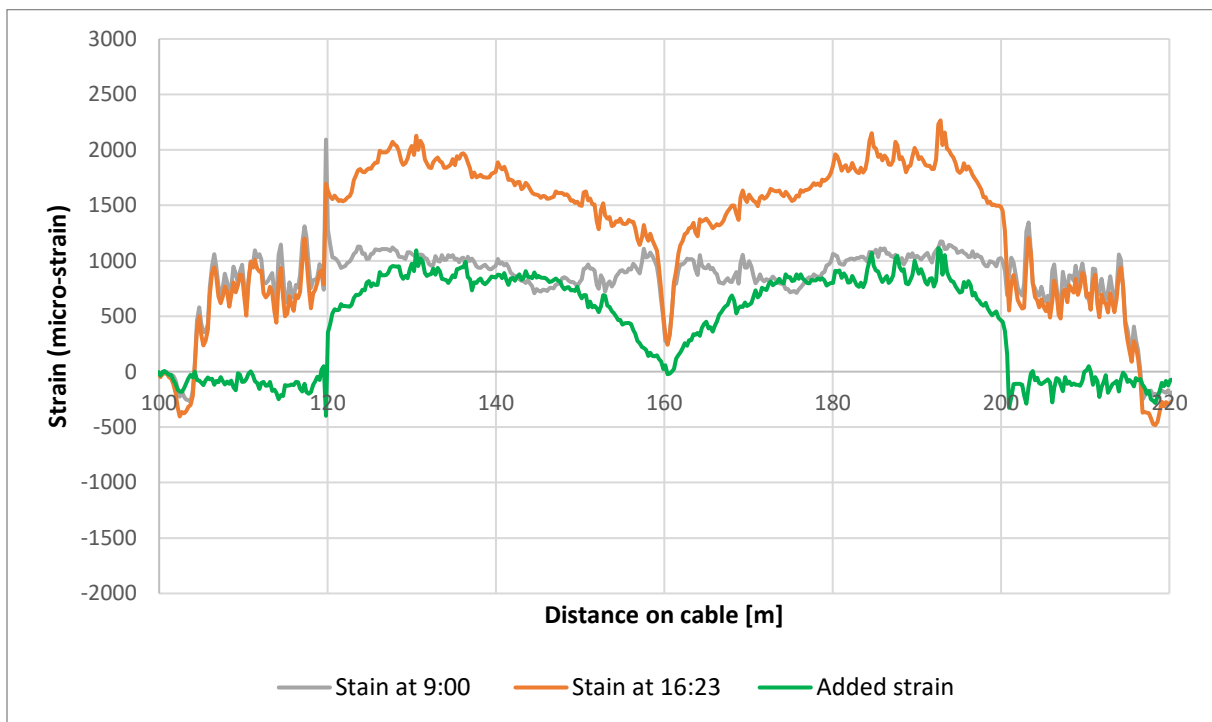
Figure 4.3: Strain-measurement of optical fibre cable D01-NO

4.3   Total station

A total station measures the displacement of a point and is used during the test. The total station measures angles and distances. With the use of the angles and the distances, the instrument determines the coordinates of a point relative to another known coordinate point. A total station has an accuracy of 2 mm and can measure the angle with an accuracy of 3 arcseconds (Meetconsult, sd).

The total station measures the displacements of 8 specific points on the pile in three directions. The measurement points are marked with stickers on the pile. The points have three measurements per loadstep: when the maximum load is reached, at the end of the applied load and after unloading. The displacement of the pile is also measured a few days after the test, this measurement is the last point in the figure. The data can be used to check and compare the displacement data of the different instruments. The measurements of the total station have a high accuracy. The data can be used as actual displacement course but also as boundary conditions for the curvature measurements of the saaf and strain-measurements. Figure 4.4 shows the displacement measurements during loading, left figure, and unloading, right figure. The measurement point are on both piles and on different locations on the pile. So small differences can be seen between point on the same height.
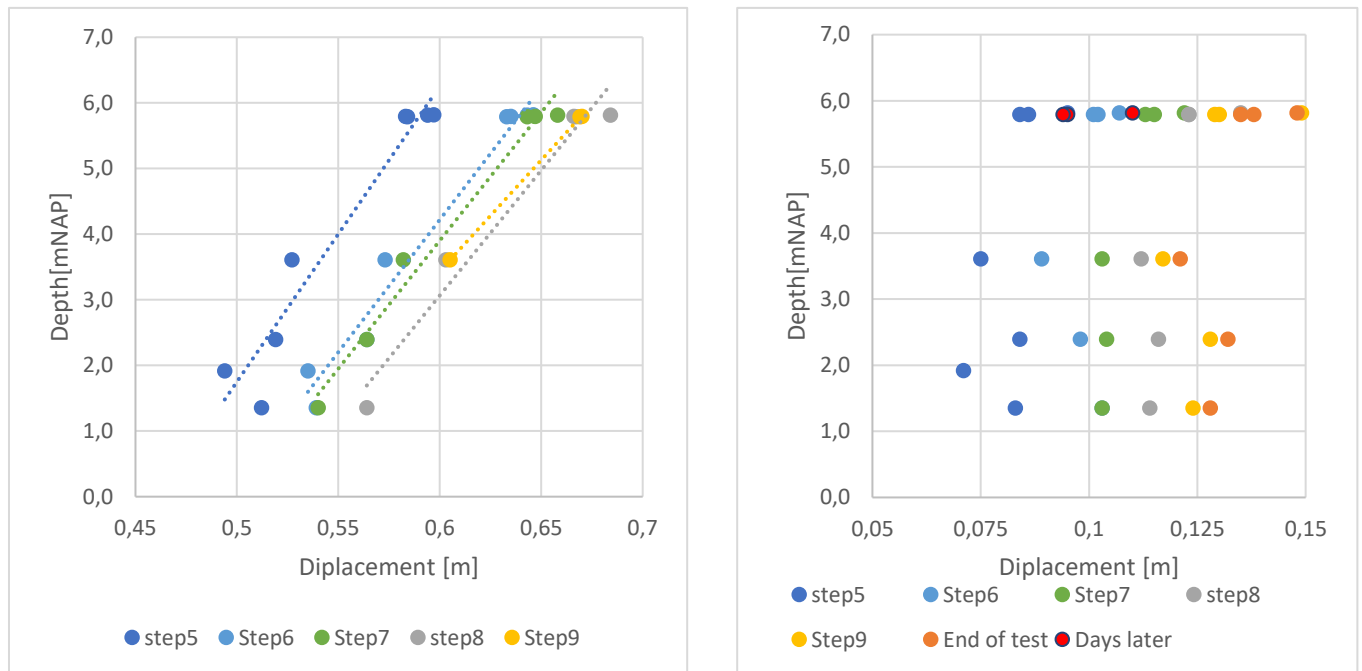
Figure 4.4: Horizontal displacement of total station during loading (left) and unloading (right)

4.4 Saaf

A saaf, Shape Accel Array Field, is a tube which measures the horizontal curvature of the pile. The saaf tube is installed in a pipe that is welded on the pile. The saaf-tube is a concatenation of hinges with sensor elements. The sensors measure every 50 cm the curvature of the pile in two horizontal directions. The accuracy of the saaf is +/- 1.5 mm over 32 meters (Inventec, s.d.), within 20 degrees inclination. The longest saaf of the two is 44.5 meter and the inclination is within the 20 degrees, which result in an accuracy of +/- 2.1 mm.

The curvature is the second derivative of the displacement, two boundary conditions are necessary to derive the displacement with the measured curvature. In the current data, it is expected that the saaf does not have any displacement neither angular displacement at the tip of the saaf. The saaf measurements are done during the first 8 loadsteps, during the 9th loadstep the saaf is replaced by the inclinometer to get a validation measurement. The data can be used to determine the curvature of the pile and to have a better insight into the displacement of the pile.

Saaf D01

The saafdata of pile D01 has a reach from 3.85 mNAP to -34.65 mNAP and a period between "29-06-2022 07:34:37" and "30-06-2022 16:38:56". The curvatures are measured approximately every minute. The base-measurement is taken at the same time as the base-measurement of the total station, which is at 9:00 during the testday. The boundary conditions that are used as first estimation is a displacement and the angular displacement of zero both at the bottom of the saaf. The assumption is made since it is expected that the bottom of the pile does not move during the test. The first assumption can be modified later, because the total station can be one of the boundary conditions. The saaf on pile D01 has a maximum depth of -34.65, which is more than 7 meter above the pile tip. The assumption that the bottom of the pile does not move during the loadsteps, is in this case not completely the same as the assumption that the tip of the saaf does not move.

The data of the top of the saaf, +3.75 mNAP, are shown in Figure 4.5. The results have the same trend as the hydraulic jack data. It looks like there is a small disruption in the data between loadstep 5 and 6, but the rest of the data is usable with a minimum amount of noise.
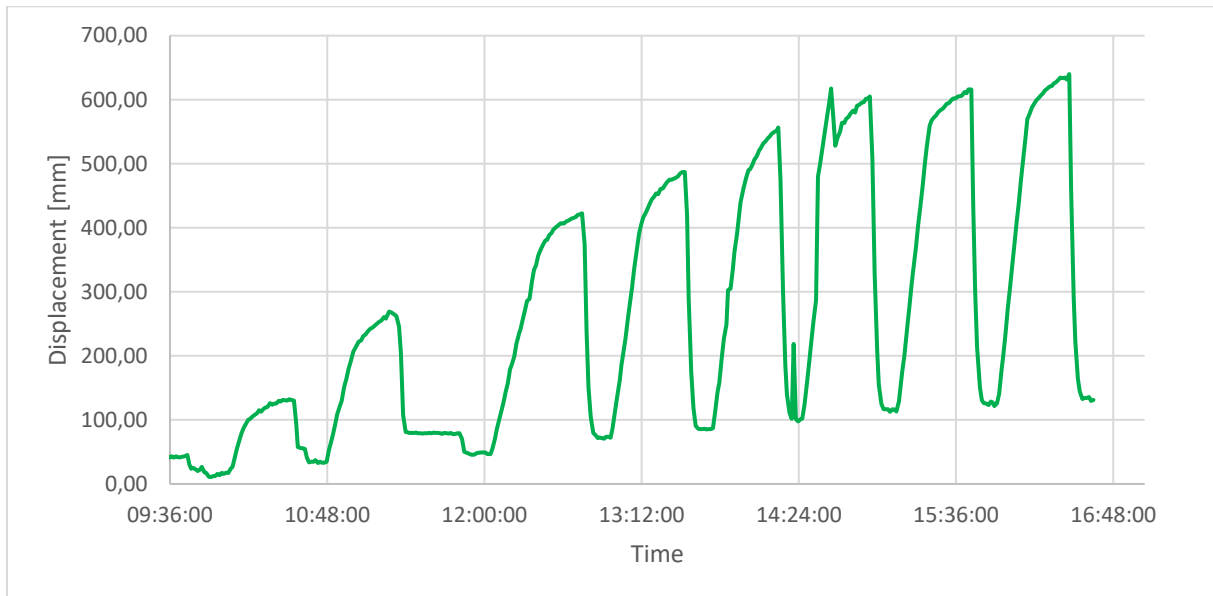
Figure 4.5: Horizontal displacement of saaf D01 over time

Next to the displacement of a point over time is it also possible to plot the entire pile at a certain moment. The maximum displacement of the pile for each loadstep is shown in Figure 4.6The displacements become larger and larger each loadstep, which is also expected. In this figure the maximum displacements per loadstep are taken.
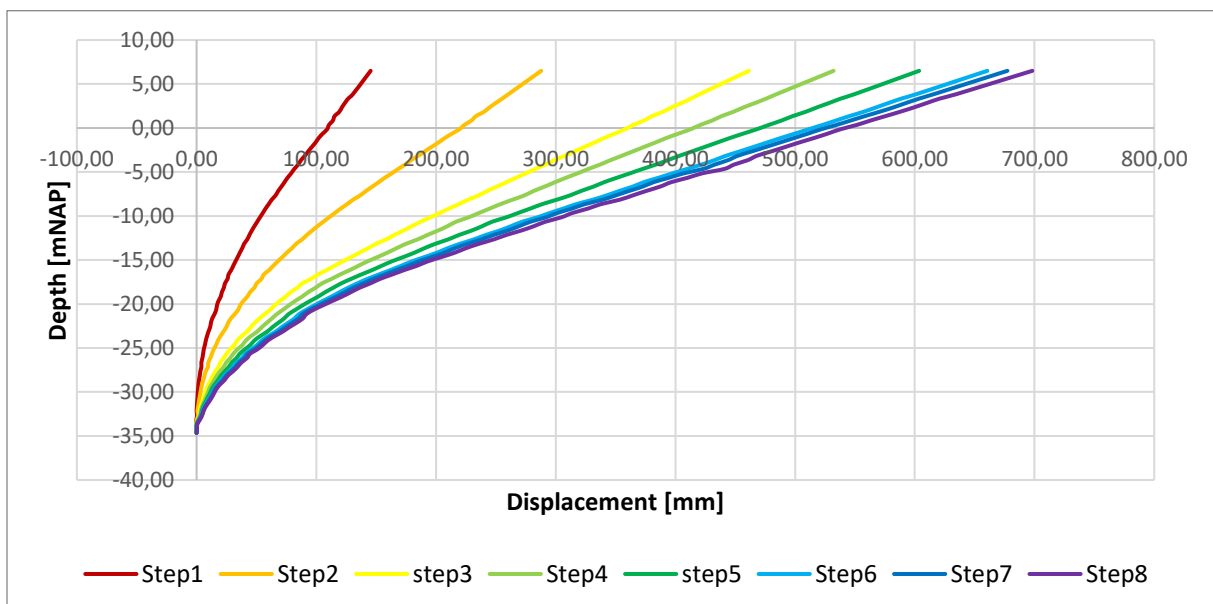
Figure 4.6: maximum pile displacement of 8 loadsteps of Saaf-D01

Saaf D04

The saafdata of pile D01 has a reach from +2.75 mNAP to -41.75 mNAP and a period between 29-06-2022 07:34:35 and 30-06-2022 16:38:54. The curvatures are measured almost every minute. The

zero measurement is taken at the same time as the first measurement of the total station, which is around 9:00 during the testday. The boundary conditions that are used as first estimation is a displacement and the angular displacement of both zero at the bottom of the saaf. This assumption is done since it is expected that the bottom of the pile does not move during the test. This first assumption can be modified later with the help of the total station measurements. The displacements are negative since they use the same coordinate system for both piles.

The bottom of the saaf is 0.25 meter above the tip of the pile. Which assumes of zero displacement at the tip of the saaf more reliable since it is more in line with the assumption of the fixed pile tip. Next to that, this saaf gives the curvature of a major part of the pile.

The data of the top of the saaf over time is shown in Figure 4.7. The data has the same shape as the other saaf, but the maximum displacement of the loadcycles is nearly 100 mm lower for this saaf, than for the saaf at pile D01. The expectation is that both piles have equal displacements. The total station has measured almost equal displacements for both piles, which suggest that something must be changed in the assumption of the saaf data. These differences can be assigned to the difference in the height of the boundary conditions. In Figure 4.8. the evolution of the pile over time is shown, with each maximum displacement per loadstep. The top of the saaf shows vibrations in the line, these vibrations are not expected in the pile, which tends to inaccuracies in the data. The expectation is that the displacement becomes steeper, higher on the pile. But after the vibration around X81, the line becomes flatter again. The vibrations/noise in the data can cause some inaccuracies in the data. This must be considered in the further analysis of this data.
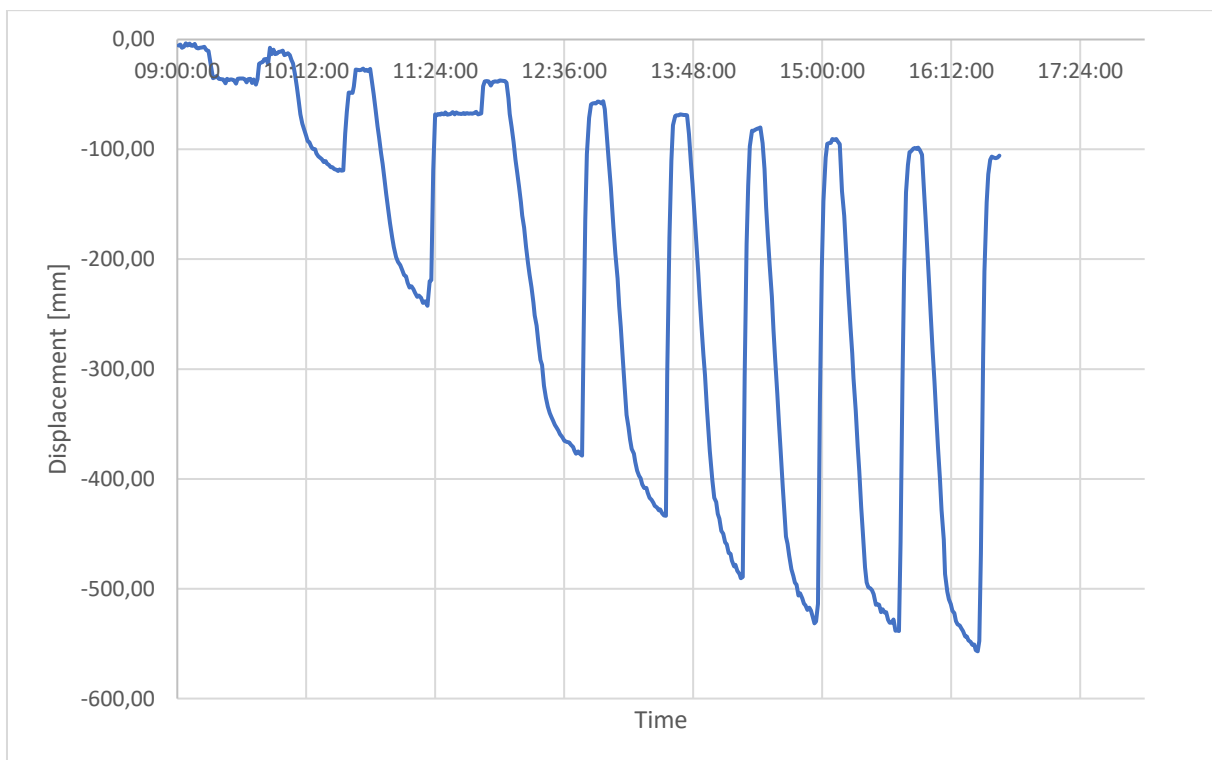
Figure 4.7: Horizontal displacement of saaf D04 over time
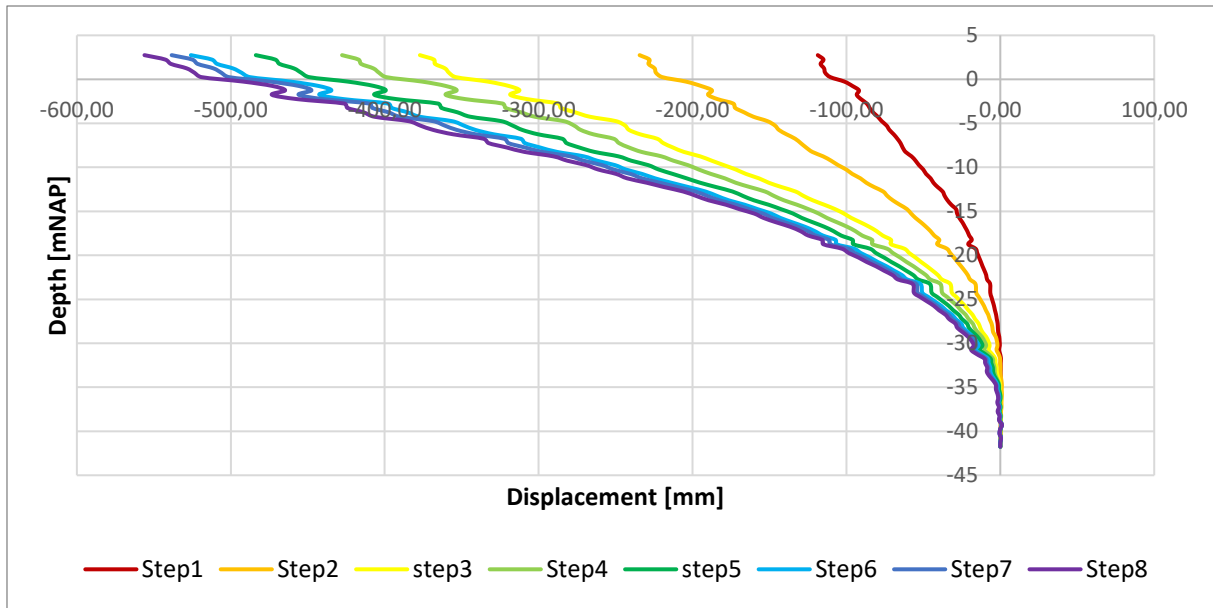
Figure 4.8: Maximum pile displacement of 8 loadsteps of Saaf-D04

Combined Saaf data

The two saaf are installed up to different depths. Saaf-D04 nearly reaches the piletip, while saaf-D01 has its tip 7 meter above it. The assumption that both saaf has no displacement nor angular displacement at the tip differs for both piles. Saaf-D04 shows displacement at the height of the saaf-D01 tip, which indicates that the assumption for saaf-D01 is incorrect. The assumption of saaf-D01 can be changed to the shape of saaf-D04. The new assumption for the boundary condition of saaf-D01 is a tip displacement equal to the displacement of saaf-D04 at that depth, 34.65 mNAP. The second boundary condition is received from try and error of the angular displacement at the tip of saaf-D01. The saaf line is turned until both saaf lines are closest together. Figure 4.9 shows the original saaf-D04 displacement and the adapted saaf-D01 line at the end of loadstep 8, 16:26 hour. The saaf-D04 has now a tip-displacement of -3.2 mm and an angular displacement close to the angular displacement of Saaf-D01 at the same depth.
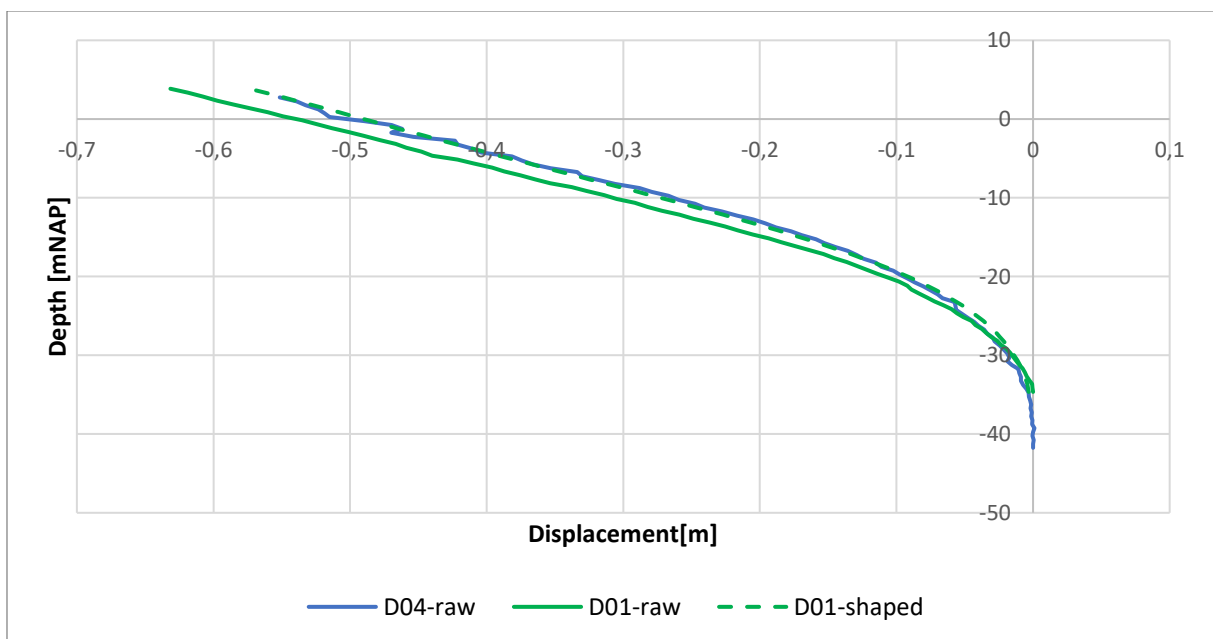
Figure 4.9: Saaf-displacement of both piles

4.5   Piezometer

The piezometer is utilized to gauge the excess water pressure within the soil. Measurements of water pressure are taken at six different locations, with three measurements conducted at varying depths for both piles. These measurements are performed at 5 meters difference from the centre of each pile. The instruments measure the excess water pressures in the soil, the base measurement of the excess water pressure is manually chosen after each loadstep. During the base measurement, the water pressure is set to zero. The water pressures are measured every second during the test. Before the water pressures are set to zero, a high peak occurs. This peak is not considered in the further analyse of the data but are seen as inaccuracies by the manually intervention in the data.

The results of the 6 piezometer measurements are shown in Figure 4.10. The measurements of 5 of the 6 gauges follow the same trend, only water pressure meter 5 shows a moderate trend during the entire test. The pore pressure during the first 4 loadsteps varies within the 1 kPa from the base-measurements. During loadstep 5 till 7, the pore pressures rise linearly during the whole loadstep. The excess pore water pressures during the 8th loadstep flattens out at the end of the loadstep, to a maximum of 4 kPa. The end of load step 8 marks a significant turning point in the behaviour of excess pore water pressure. Prior to this point, there was a consistent increase in the excess pore water pressure, while following load step 8, a decrease in excess pore water pressure is observed. When examining the relationship between the excess pore water pressures and applied load on the pile, one would expect a clear trend to emerge, displaying a relationship between loading and an increase in pore pressures. However, such a load-related trend is not apparent in the data. Since the last loadstep shows a decrease in excess pore pressure during loading.

Instead, it appears that the excess pore water pressures are influenced by tidal effects. Tidal effects result in variations in water levels over time, causing an increase in pore water pressures for a few hours, followed by a subsequent decrease in pore water pressures for a few hours. The measured data from the piezometer aligns with these tidal effects. Specifically, the pore pressures exhibit an increase of approximately 13 kPa over the first 8 loadsteps, corresponding to a water level change of around 1.3 meters. Those water level changes can be expected according to the tidal effects in the port of Rotterdam (Port of Rotterdam, sd). Therefore, it is assumed that the sand layers are drained, with no pore pressure build-up during the loading process.
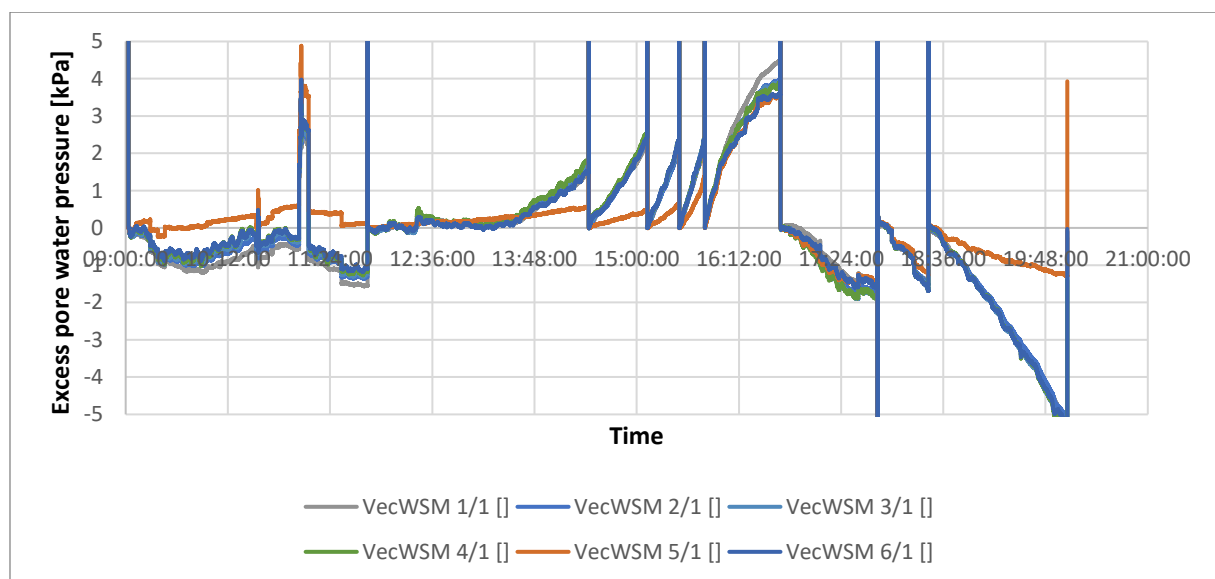
Figure 4.10: piezometer measurements during the test

4.6   Comparison test-measurement with predictions

This section compares the measurements of the test with the predictions of the calculation models. The total station and saaf displacement at the end of loadstep 8 are shown in Figure 4.11, together with the predictions of the calculation models. The solid lines are the measured displacement of the saaf and the total station displacement. The difference in displacement between the saaf and the total station are discussed in chapter 6. For now, the total station measurements are being relied upon. The dashed lines represent the predictions. The measurements and the predictions have a clear difference. Most of the predictions have a maximum displacement of around 0.9 meter. The two outliers are the Plaxis-drained model and the Blum model. Blum predicted the lowest displacement, but is still 0,1 meter higher than the measured displacement. The difference between the Plaxis-drained model and the measurement is about 0,4 meter, which is huge. The total station measured a maximum displacement of nearly 0.7 m. There is a difference of roughly 0.2 meter between the measurement and the prediction. This difference needs a declaration. The expectation is that those differences cannot only be dedicated by the inaccuracies in the calculation models. A more thorough examination needs to be conducted to all the input parameters in the models and the test procedure.
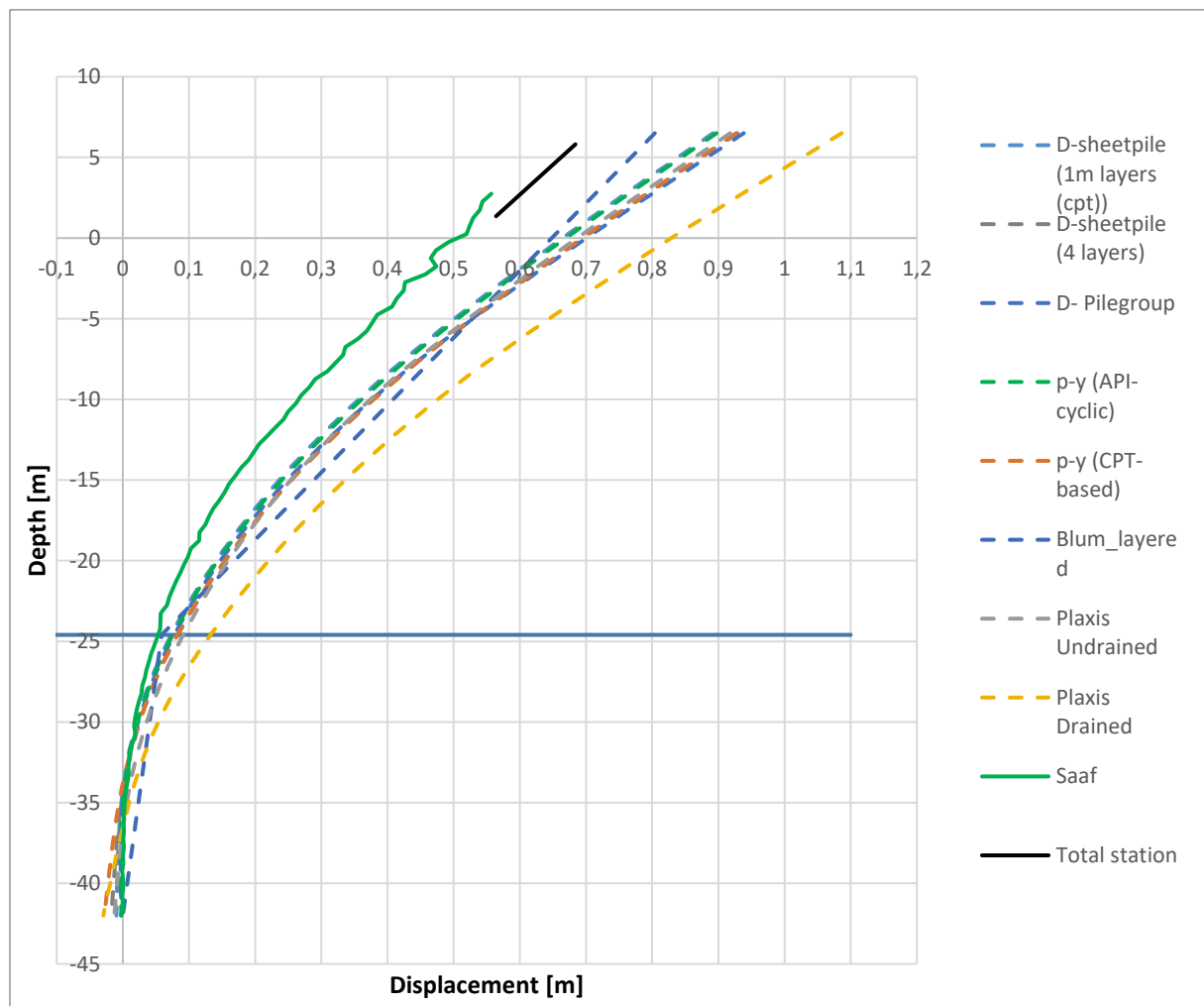
Figure 4.11: Predicted displacement and measured displacements of the test

5   Load analyse

In chapter 4, a gap was found between the measurements and the predictions. The gap was too large to dedicate it to model inaccuracies. A more general inaccuracy needs to be found to close the gap.

The test involved the application of load on the piles using a hydraulic jack. The magnitude of the load on the pile is determined by a control panel that regulates the load supplied by the hydraulic jack based on its load measurement. This hydraulic jack load provision is employed to align with the designated load scheme during the test. The hydraulic jack derives the load from the oil pressure within the jack. However, it is important to note that this method may contain inherent inaccuracies.

Typically, the load during a test is cross-verified or measured using a load cell. A load cell is specifically designed to accurately measure loads with a higher degree of precision. However, in this test, a load cell is not utilized, necessitating the adoption of an alternative method for load verification. One such approach involves determining the load using strain data. It should be noted that the strain data is only available after the completion of the test and did not influence the applied load during the test itself. In this chapter, the optical fibre strain measurements are converted into an estimation of the applied load on the pile

5.1   Comparison bending moment

The optical fibre cables measure the strain along the pile. The strain of the pile is used to calculate the applied load. The optical fibre cables attached to the pile are used in this analyse. The tip of the cable is detected in the data, with which the useable cable data is found. The data from cable D01 Noord-Oost, particularly the Noord part, is used to determine the load on the pile, and those results are shown in this chapter. The data from cable D01-Noord has the least amount of noise and shows the clearest trend in the data, therefor this dataset is used.

The data between 120 and 200.5 meter on cable D01-Noord-Oost is the part of the cable attached to the pile. The cable is attached 40 meters on the pile from the tip of the pile upwards to -2mNAP. The extra 0.5 meter is the turning loop at the tip of the cable. A tuning loop of 0.5 meter is chosen since this gives a decent symmetric output. Figure 5.1 shows the strain on the y-axis and the depth on the x-axis, the data is from the test at the end of loadstep 8 . The two lines follow the same trend and have little deviations, which confirmed that the peak is well-chosen. The small peaks between 20 and 35 meters from the tip are on the same location. The peaks are most likely due to the changes in wall thickness. The transitions in wall thickness are on the same depths as the peaks in the graph.
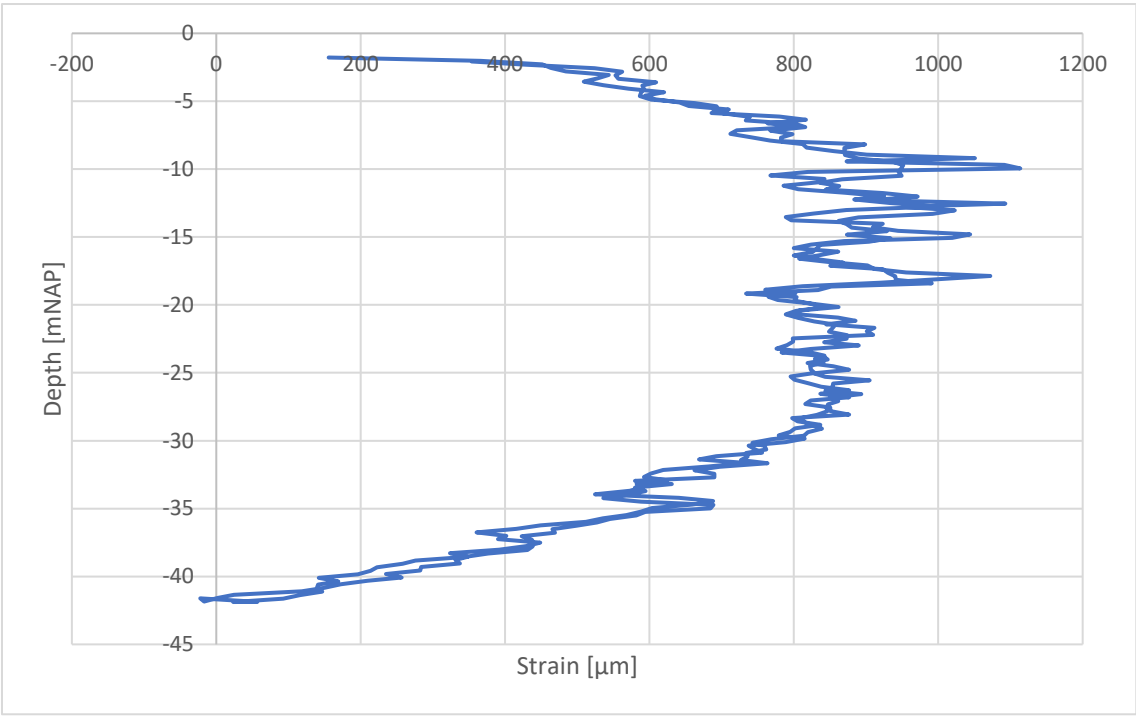
Figure 5.1: Strain-measurement versus at certain depth of strain cable D01-NO

The load on the pile causes the added strains. The pile has a compression and a tension side in the pile. On the compression side, the steel is compressed to each other, and the strains are negative. On the tension side, the steel is extended, and the strains are positive. The strains from Figure 5.1 are from the tension side of the pile.

The applied load is the only load on the pile that has influence on the bending moment above the water table. The assumption is made that the water does not have influence on the bending moment, since the water forces are insignificant compared to the added load and are equal on both sides of the pile. The strain of the pile is dependent of the bending moment on the pile. The stain-measurement can be converted into the bending moments of the pile. The strain and the bending moment are combined in one equation using Hooke's Law and the bending moment equation.

Hooke's law:

$$\sigma = E * \varepsilon$$

Bending moment equation:

$$M = \frac{\sigma * I}{z}$$

4 parameters have influence on the strain of the pile. The first parameter is the bending moment, M [kNm]. The second parameter is the moment of inertia, I [m^4]. The moment of inertia is: "In general, when an object is in angular motion, the mass elements in the body are located at different distances from the centre of rotation. The total moment of inertia is the sum of the moments of inertia of the mass elements in the body." (Davidovits, 2013). The third parameter is the distance to the neutral axis, z [m]. And fourth the elastic modulus of the material, E [kN/m]. The elastic modulus is a material property and indicates the elasticity of a material.

The elastic modulus is material specific and known for the steel that is used (210 MPa). The moment of inertia is depending on the cross-section on the pile. Those two parameters of the pile are known.

The neutral axis of the pile is in the middle of the pile, perpendicular on the load-direction, so the distance to the neutral line is equal to the radius of the pile since the optical fibre cable is installed on the outside of the pile. The cross-section of the pile changes with height, so the moment of inertia changes over the pile. The strains are measured with the optical fibre cables. The Bending moment follows from the strains data and the above-mentioned formulas and parameters. Figure 5.2 shows the bending moment during loadstep 8 in blue. The soil bottom is at -24.6 mNAP.
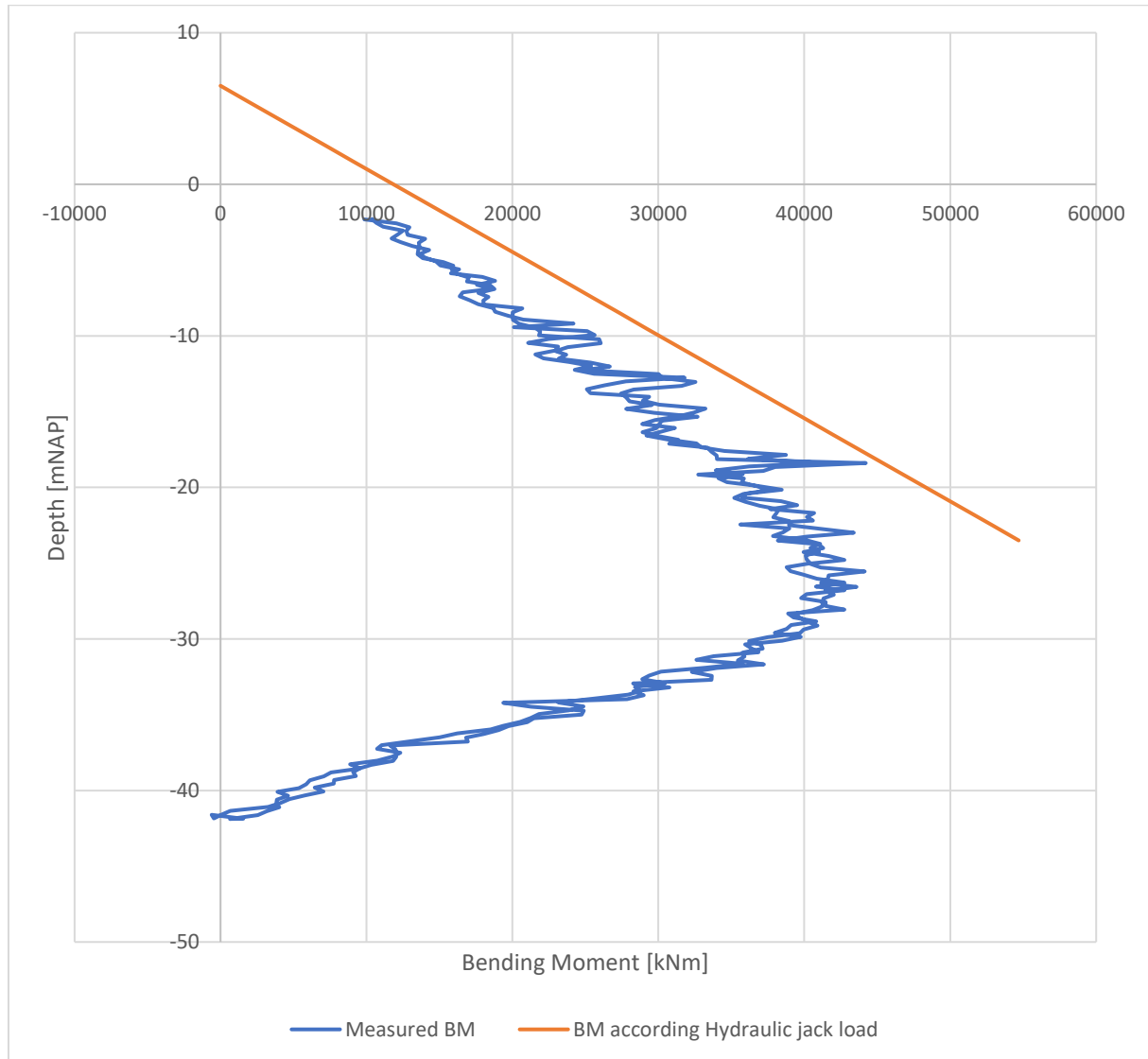
Figure 5.2:Bending moment of pile determined with the strain-measurement.

The bending moment is the summation of the forces times the length to a chosen point. The only load that influences the bending moment above the soilbed is the applied load from the hydraulic jack. The load is applied on +6.5 mNAP. The bending moment above the soil bed is expected be linear, with a slope equal to the applied load. The load according the hydraulic jack during the 8th loadstep is 1823 kN. The expected bending moment above the soilbed is drawn in orange in Figure 5.2. The hypothesis that the calculated bending moment and the measured bending moment are equal is incorrect. The calculated bending moment line is much steeper than the measured line and gives too high values. Since the slope of the line depends on the load, the load measured by the hydraulic jack are not equal to the real load that was applied on the pile. Throughout all the load steps, a disparity between the measured bending moment and the calculated bending moment based on the hydraulic jack load was consistently observed.

5.2 Adapted load determination.

Since the loads according the hydraulic jack doesn't correspond to the strain measurements, new expected loads needs to be found using the strain data.

The expected load according to the strain-measurements is equal to the slope of the bending moment above the soilbed, -24.6 mNAP. A linear trendline is drawn through the bending moment measurements above the soilbed. The drawn trendline in excel gives the equation of the trendline. This trendline gives the best matching slope of the bending moment data. The slope of this trendline and corresponding applied loads is 1500 kN, with a least square error of 0.95.

At the load application height, the bending moment should be zero. However, the trendlines drawn through the data, isn't zero at that point. The trendlines intersect the y-axis around 1.5 meter lower than expected, which indicates that the load is applied lower than expected. The applied load height is a reliable parameter which makes it unlikely that the differences between the measured height and the determined height are as large as determined. The trendline is adapted with the use of the applied load height. Minor differences in the slope of the line can ensure that the trendline goes through the application point, within the same order of accuracy. The noise in the data enables the possibility to have different trendlines with minor changes in accuracy.

The two principles of the determination of the new expected loads are.

- The bending moment is zero at the load application height.
- The bending moment according the expected load, needs to fit the bending moment data as good as possible.

The load determination consist of two phases.

The first phase draws line between the applied load height and all the data point above the soilbed. The slopes of all those lines are calculated. This is visualized in Figure 5.3, where a few of those lines are drawn. The average slope of those lines is calculated, which results in the average expected load according all the datapoints. The accuracy can be improved by using the least square error of the bending moment lines.
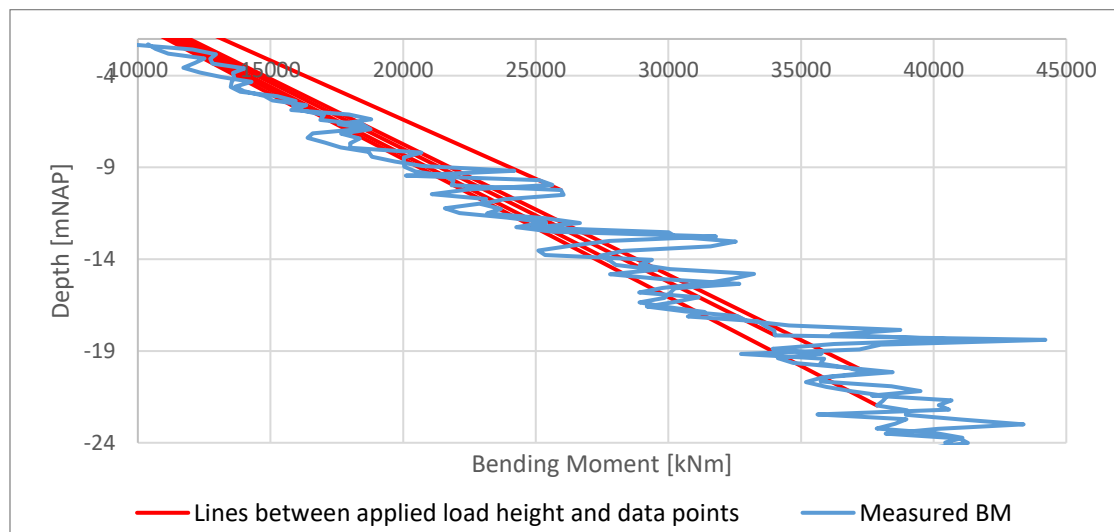
Figure 5.3 Slope in bending moment between measurement points and applied load height.

The second phase of the study builds upon the findings of the first phase. In this phase, the bending moment lines are determined for loads of ±50 kN from the expected load obtained in the first phase.

The least square error (LSE) is then calculated for these loads. The bending moment for all loads falling within this range is determined at the same height as the measurements taken on the strain-cables.

To assess the accuracy of the calculated data, the LSE is computed by comparing the measured data points with the corresponding calculated data points at the same heights. The load that yields the most favorable least squared error is selected as the expected load for this measurement. The bending moment resulting from this expected load is depicted in Figure 5.4.

By taking into account the known boundary conditions, such as the application height, this approach ensures a comprehensive consideration of relevant factors. The LSE analysis aids in achieving the best possible fit of the data, thereby reducing uncertainty. This combination of techniques provides a realistic estimation of the expected applied load on the pile.
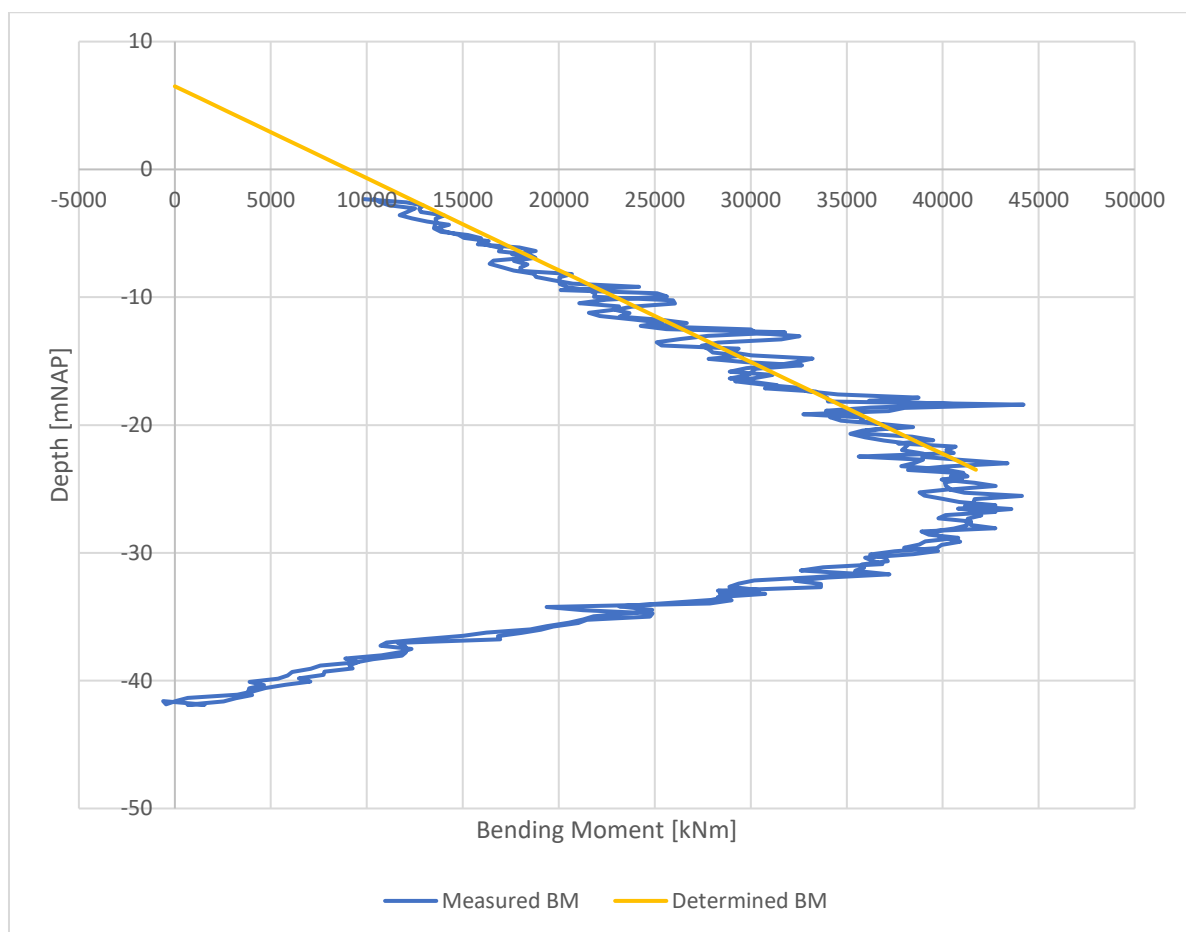
Figure 5.4 Bending moment measurement and calculated bending moment using the expected load.

This method determines the applied load according to the optical fibre measurement. The applied load is determined every time the specific optical fibre cable (D01-NO) had a measurement, which was about every 3 minutes. Figure 5.5 shows the measured load course during loadstep 9 according to the optical fibre measurements. The whole load course is determined to have a better inside in the load-coarse during a loadcycle and to choose which load is representative for the loadcycle. Next to that, the load coarse is used to make a load-displacement analyses of the test in chapter 7.

The maximum load was kept constant for multiple minutes according to the hydraulic jack measurements. The optical fibre load course shows a load build up during the first 5 measurements,

has a kink at the 6th measurement, after which the load becomes more constant between measurements 6 and 21. After measurement 21, the load is decreasing again to an unloaded stage. The load between measurement 6 and 21 is expected to be constant, which was also the case in the hydraulic jack measurement. But the optical fibre measurements show an increase in load during this phase. The load increment, during the constant load phase, is visible during all the loadstep. This can be caused by inaccuracies in the hydraulic jack or with an delay between the applied load and the movement of the pile.

A maximum value of the load course is chosen as representative maximum load of the loadcycle unless it is an outlier. It is assumed that the maximum load in the load course is the representative applied load on the pile during the loadstep. The soil and pile need some time to show the real curvature of the pile due to the load.
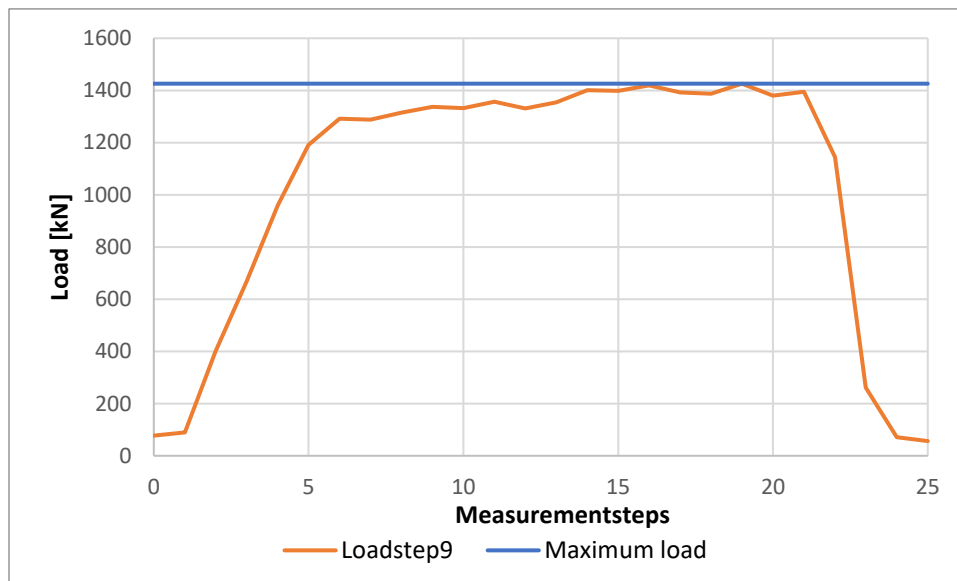
Figure 5.5: The applied load of loadcycle 9 determined with the strain measurements.

The expected load according to the strain-measurements is determined for all 9 loadsteps. The loads from the stain-data is hundreds of kilonewtons lower compared to the loads from the hydraulic jack. The measured maximum loads per loadstep of both measurements are shown in Table 5.1. The table includes both methods mentioned above: the strain-measurement and the original measured loads by the hydraulic jacks.

The hydraulic jack determined the load with the use of the oil pressures, this method can give larger deviations. The strain-measurement uses the slope of the bending moment, which contains noise and may therefor differ slightly. The model also uses the application height, which is a fixed height with a known bending moment of zero, which results in a best possible expected load determination using the strain-data. The strain-measurement are more reliable than the hydraulic jack measurements. The applied load on the pile differ from the preconceived loads. This could be the cause of the gap between the measurements and the predictions in chapter 4. The predictions with the different calculation models are redone in chapter 6, to determine if this closes the gap.

Table 5.1: Load measurement of the hydraulic jack and the optical fibre

	Applied height measurements [kN]	
Loadstep	Optical fibre	Hydraulic Jack
1	382	810
2	682	1114
3	960	1418
4	1109	1620
5	1252	1823
6	1357	1823
7	1348	1823
8	1391	1823
9	1426	1823

Table 5.1: Load measurement of the hydraulic jack and the optical fibre

6   Displacement analysis.

In this chapter, the displacement of the test and the calculation models are analysed. First the results of different measurement tools are compared with each other. After that, the measurements are compared with the calculation methods. The calculation methods are redone with the loads derived in chapter 5.

6.1   Optical fibre displacement

The strain of the pile during the test is measured with optical fibre cables. The strains can be used to calculate the curvature of the pile. The curvature of the pile is used to determine the displacement of the pile. The curvature and displacement of the pile is used to check the saaf measurements.

The curvature of the pile can be determined by using the two types of bending moment equations and Hooke's Law together:

$$M = E * I * \kappa \ = \frac{E * \varepsilon * I}{z}$$

$$\kappa = \frac{\varepsilon}{z}$$

In which the κ is the curvature [1/m], ε is the strain [-] and z is the distance to the neutral axis [z]. The equation calculates the curvature using two parameters: the strain-measurements and the distance from the neutral line of the pile to the stain cable (which is the radius of the pile). The curvature of pile D01 during loadstep 8 is shown in Figure 6.1. The curvature at the tip of the pile is equal to zero. The curvature line has a shape of an arc with the top op 0.00075 m/m², with an outlier of 0.0009 m/m².
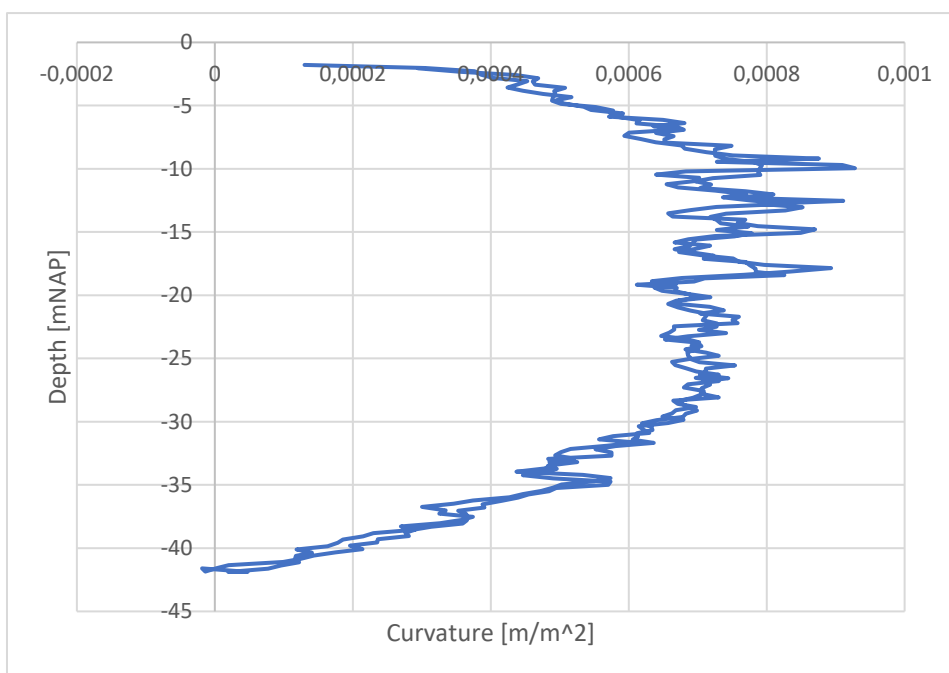
Figure 6.1: Curvature of pile D01 during loadstep 8

The goal is to convert the curvature into the displacement of the pile. The curvature is the second derivative of the displacement. Two boundary conditions are needed to make this conversion. The first assumption for the boundary conditions is that the pile tip has no displacement nor angular displacement, so u'_0 & u_0 are zero. This is the same assumption as made with the Saaf-measurement. The angular displacement is the primitive function of the curvature, and the displacement is the primitive function of the angular displacement.

The displacement of the pile is shown in Figure 6.2. The descending and rising cables are taken separately, so two lines are plotted of the same pile. The difference between the two lines is small, which was also expected with the matching curvature measurement. The displacements differ less than 1 cm at the top.
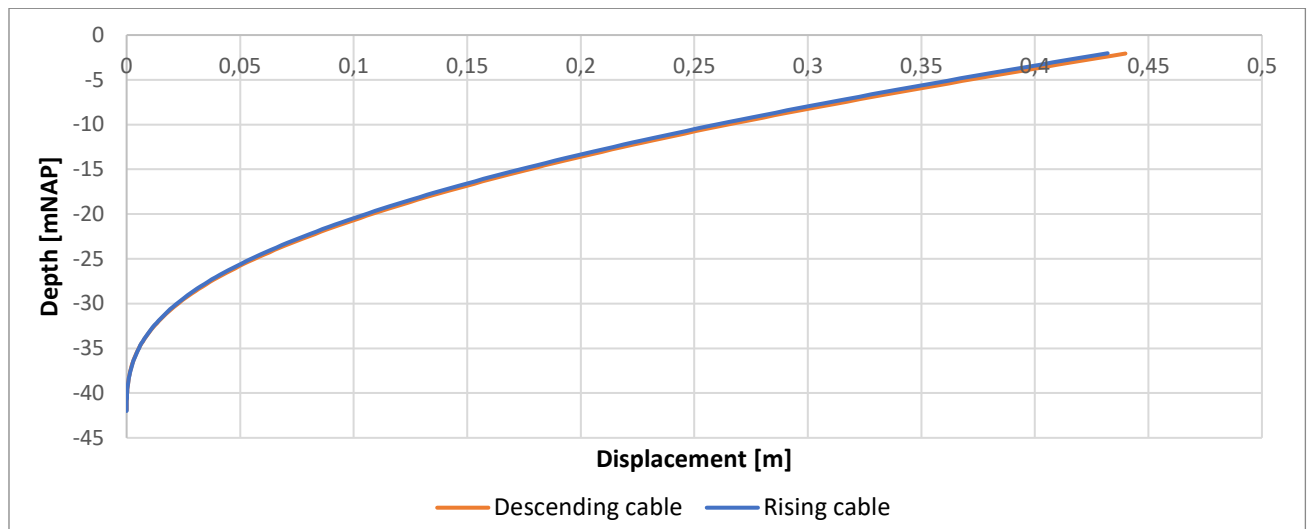
Figure 6.2: Displacement of the pile during loadstep 8 with the use of the strain-measurement

6.2   Compare measurements.
Compare curvature measurements

The displacements of the strain-cables can be compared with the displacement of the saaf. Both methods use the same assumption of zero displacement and zero angular displacement at the tip of the cable. The tip of saaf-D04 is on the same depth as the tip of the optical fibre, which is close to the tip of the pile (-42 mNAP). The tip of Saaf D01 is higher on the pile (-34 mNAP). The saaf-D01 results can be adapted to the displacement of saaf-D04. The adapted Saaf-D01 trend is more in line with the assumption of zero angular displacement and displacement at the tip of the pile. Which is the original assumption of the measurements.

Figure 6.3 shows the displacement of the saaf and the optical fibre at 16:27. The results of the optical fibre and the D04-saaf displacement matches well. The adapted saaf-D01 measurement is also close to the other measurements, but that is partly because it is adapted to the measurement of saaf-D04. The original Saaf-D01 measurement differ from the other measurements.

The curvature trend obtained from both curvature measurement tools provides a distinct representation of the pile's curvature. As these measurements are obtained using two different instruments, they serve to cross-validate the data. Consequently, the data from both instruments exhibits increased reliability. Given that the optical fibre measurements demonstrate high reliability, the load measurement derived from the optical fibre also benefits from enhanced reliability.
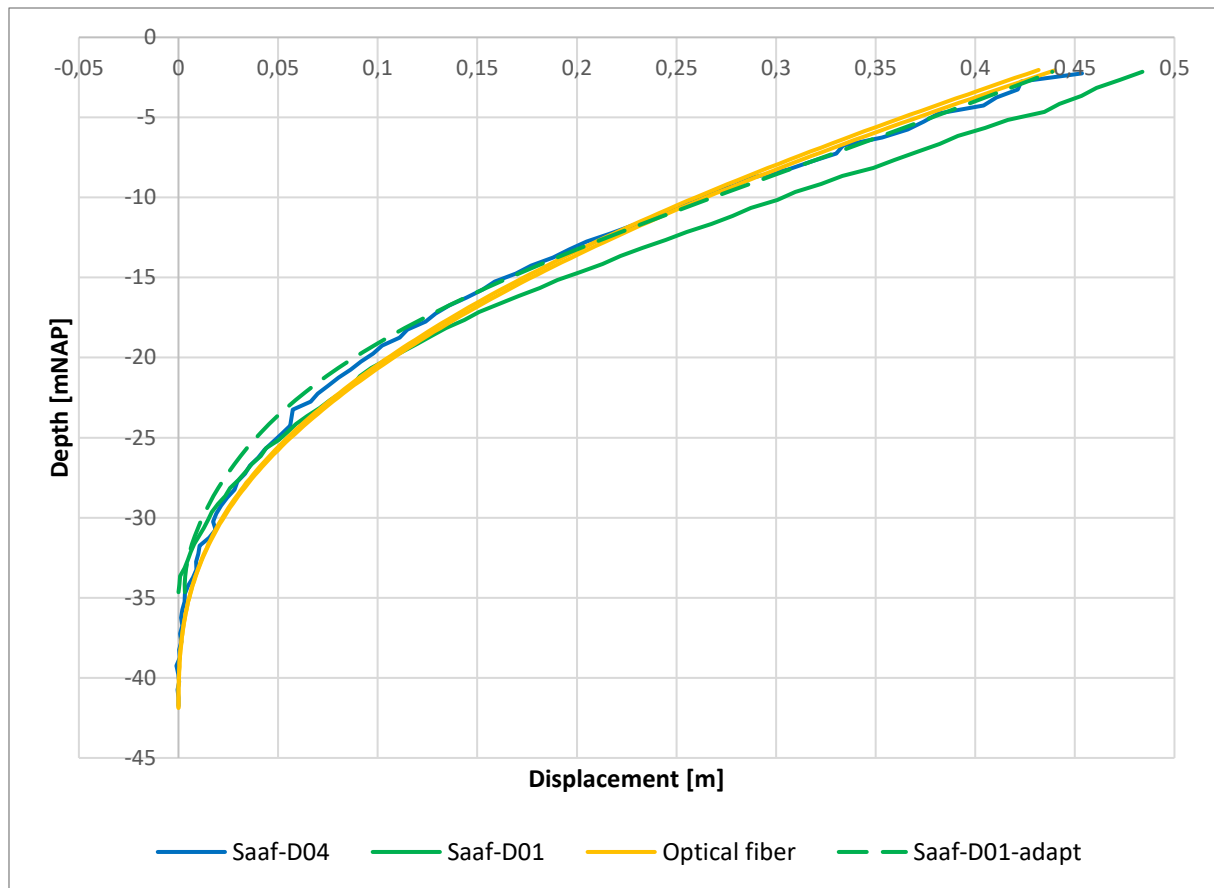
Figure 6.3: Displacement of the saaf compared with the optical fibre measurement.

Compare displacement measurements.

The results of the different displacement measurement tools are combined. The total station has accurate displacements, but only at 8 points above the water table. The saaf has curvature measurements along the entire pile, but the boundary conditions to transform the curvature into displacement are not known. The hydraulic jack only measures the combined displacement of both piles at 6.5 mNAP.

The Saaf and total station measure the displacement in x and y direction, while the hydraulic jack measures the total displacement. The displacements of the pile in the direction of the load are significantly larger than the displacements perpendicular on the load. The differences in displacement are sufficient large to disregard the displacement perpendicular to the load. The base-measurements are close to 9:00 AM during the testday, for all the measurement data. The total station measures the displacement at 5.8 meter mNAP, while the hydraulic jack measurement is on 6.5m NAP. The saaf measurements are linear extended to a height of 6.5m NAP, to be able to compare the different methods. The line is extended by using the average increase in the top 5 meter of the saaf and extend the displacement with this average increasement until 6.5 meter. The top 5 meter give a good representation of the trend, but this extended contains still some inaccuracies in the amount of displacement above 3.25 mNAP. The saaf-data from pile D04 is chosen, since that saaf goes almost to the tip of the pile, while saaf-D01 doesn't measure the lowest 7 meter. The total-station measurement of pile D04 is chosen to have measurements on the same pile as the saaf. The hydraulic jack measurements are halved to get the measurements of a single pile..

6. Displacement analysis.

The displacement of the three methods are shown in Figure 6.4 over time. Table 6.1 gives the displacement of the three-measurement instrument at the total station measurement times. The pile displacement of the saaf, hydraulic jack and the total station are shown over time. The total station has only three measurements point per loadstep, which results in a more angular trend line. The total station measurement points need to be analysed and not the line, since the lines are only a straight connection between the points.
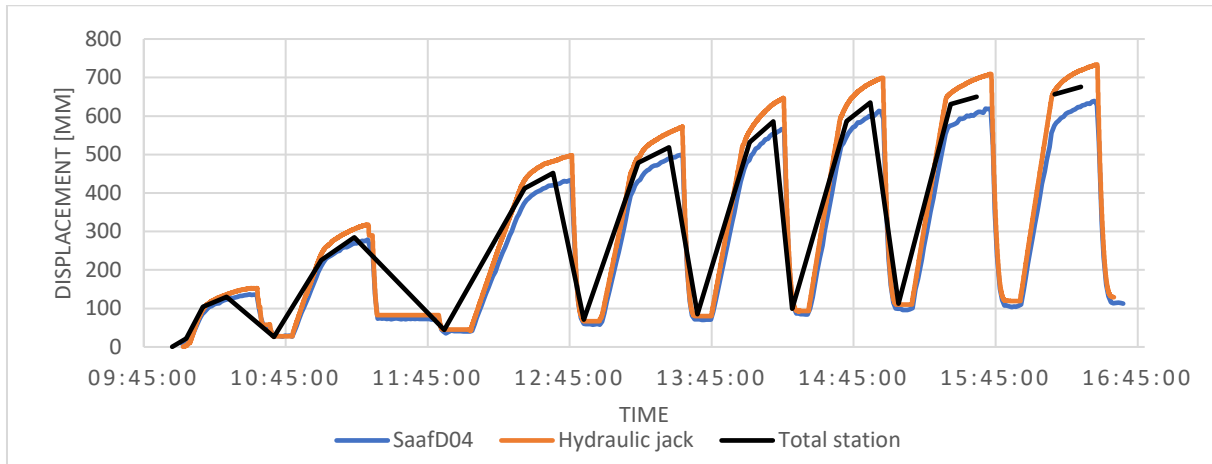
Figure 6.4: Comparison of Saaf, Hydraulic jack, and Total station

Throughout the entire test, the displacements recorded by the hydraulic jack are consistently larger than those measured by the other two instruments. The hydraulic jack and total station measurements provide direct measured values without any underlying assumptions. Although the hydraulic jack measurements are taken 0.7 meters higher than the total station measurements, resulting in slightly lower displacements for the total station, the observed differences are too significant to be solely attributed to the discrepancy in height. It is more probable that the differences between the total station and hydraulic jack measurements occur from uncertainties or inaccuracies in the measurement process. Hereby it is assumed that the total station measurements have an higher accuracy since the total station has a high level of accuracy and is specially used for accurate displacement measurements. The hydraulic jack has more inaccuracies and is primarily used for applying the load on the pile instead of measuring the displacement of the piles. The boundary condition

The assumption made for the saaf measurements is that the saaf tip remains unaffected by angular or horizontal displacements. However, this assumption may be incorrect, leading to disparities in the recorded displacements. The disparity in displacement between the saaf and total station measurements indicates that the boundary conditions assumed for the saaf are incorrect and need to be revised. The total station and hydraulic jack measurements can be utilized as alternative boundary conditions for the saaf measurements.

Table 6.1: Comparison of Saaf, Hydraulic jack, and Total station displacements

Time	Total station [mm]	Hydraulic jack [mm]	Saaf [mm]
Height	5.8 [m]	6.5 [m]	6.5 [m]
30-06-2022 10:03:00	22	4	11
30-06-2022 10:10:00	104	97	85
30-06-2022 10:20:00	130	136	122
30-06-2022 10:40:00	26	28	28
30-06-2022 11:00:00	226	241	209
30-06-2022 11:14:00	285	307	270
30-06-2022 11:52:00	44	45	40
30-06-2022 12:26:00	412	434	372
30-06-2022 12:38:00	452	482	419
30-06-2022 12:51:00	71	67	61
30-06-2022 13:14:00	479	491	430
30-06-2022 13:27:00	519	557	489
30-06-2022 13:39:00	85	80	71
30-06-2022 14:01:00	532	560	485
30-06-2022 14:11:00	586	631	553
30-06-2022 14:19:00	99	136	144
30-06-2022 14:42:00	587	628	542
30-06-2022 14:52:00	635	685	600
30-06-2022 15:04:00	113	110	99
30-06-2022 15:26:00	631	659	575
30-06-2022 15:37:00	650	697	608
30-06-2022 15:50:00	-	120	107

6.2.1   Determine pile tip displacement

The initial assumption regarding the boundary conditions of the saaf was that there would be no displacement or angular displacement at the pile's tip. However, this assumption was an initial estimate and not based on any actual measurements. In order to establish suitable boundary conditions for the saaf data, the total station measurements are employed. The total station is preferred over the hydraulic jack due to its higher accuracy in measuring displacement. The total station provides boundary condition with the displacement at a specific height.

To mitigate noise in the data, a trendline is generated from the saaf data. The trendline has a sixth-order polynomial fit. To convert curvature to displacement, two unknown parameters need to be defined based on the boundary conditions. The x-axis is placed at the height of the total station measurement point (+1.35 mNAP). The displacement at this point is known, and therefore, this parameter is incorporated into the formula. The equation of the trendline is presented below, where parameters a till e are known parameters obtained from the trendline, only the parameter f needs to be adjusted as a boundary condition and parameter g is already fill in by the total station measurement. The first boundary condition of the saaf is represented by y(0) in the formula.

$$y = ax^6 + bx^5 + cx^4 + dx^3 + ex^2 + f * x + y(0)$$

The second boundary conditions will be the rotation or a displacement of the pile on a specific height. The total station has measurements on multiple height. The second boundary condition is chosen at another measurement height of the total station. This height is above the saaf height and requires a manual increasement of the saaf-data. The height difference between the total station points is 4.6 meter. However, due to small inaccuracies between these two points, there is a propensity for larger errors in the pile tip displacements. The saaf data exhibit vibrations at the top, and when combined with the manually extended results, the reliability of using two boundary conditions from the total station becomes questionable. Consequently, the second set of boundary conditions cannot solely rely on the measurements obtained from the total station.

To find a suitable saaf line for the displacement, an alternative approach is adopted, involving trial and error by adjusting the rotation and observing the resulting displacement line. Although this method does not provide the actual displacement of the pile, it is utilized to combine the measurement data and derive the best possible approximation for the displacements along the entire length of the pile.

Figure 6.5 presents the original saaf trend (solid line), the total station measurements (black line), and two shaped saaf lines (blue striped). Both shaped lines can be accurate as they are fitted based on the total station measurements, yet they exhibit different angular displacements at the height of the total station measurement. Since there is no additional data available regarding the displacement of the pile, the angular displacement near the total station measurement remains unknown. A deliberate decision was made to refrain from employing calculation models that rely on assumptions about toe displacement. This approach ensures that when comparing measurements with calculations, they remain compatible. Further research is necessary to gain a more comprehensive understanding of the tip displacement of the pile.
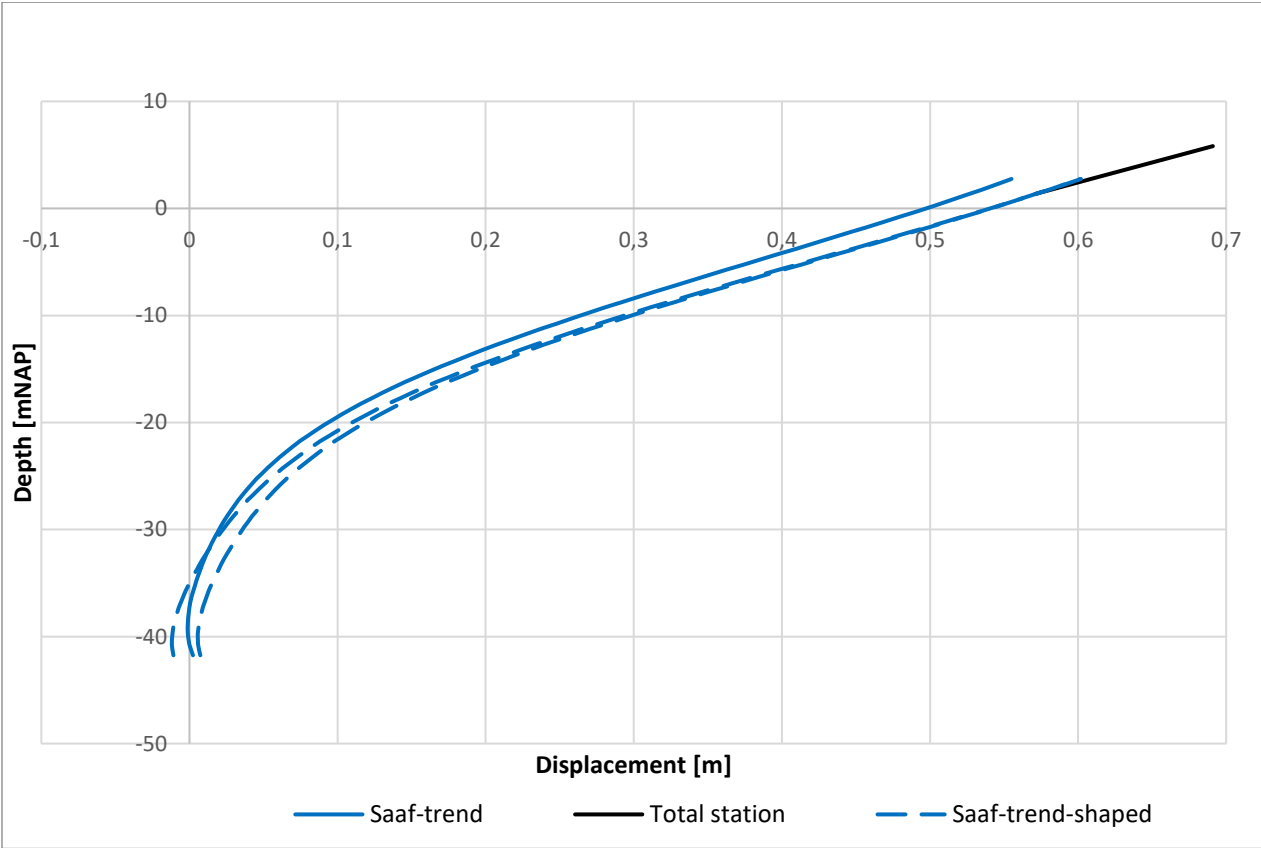
Figure 6.5: Saaf displacement fitted with the total station results during loadstep 8

6. Displacement analysis.

Another aspect of the data can be utilized to gain a better understanding of the magnitude of pile tip movement. A potential discrepancy between the saaf and total station data may arise due to the assumption of a rigid connection at the pile tip. The data indicates that the difference between the total station and saaf measurements increases with higher loads and fluctuates around a certain level during constant loads. As the differences become larger, greater corrections are required for the saaf data, deviating further from the original assumption. These significant corrections imply increased pile tip movement. Figure 6.6 illustrates the displacement differences between the saaf and total station at the same height, +1.3 mNAP. The figure displays the difference in displacement of the pile at the end of every loadstep.
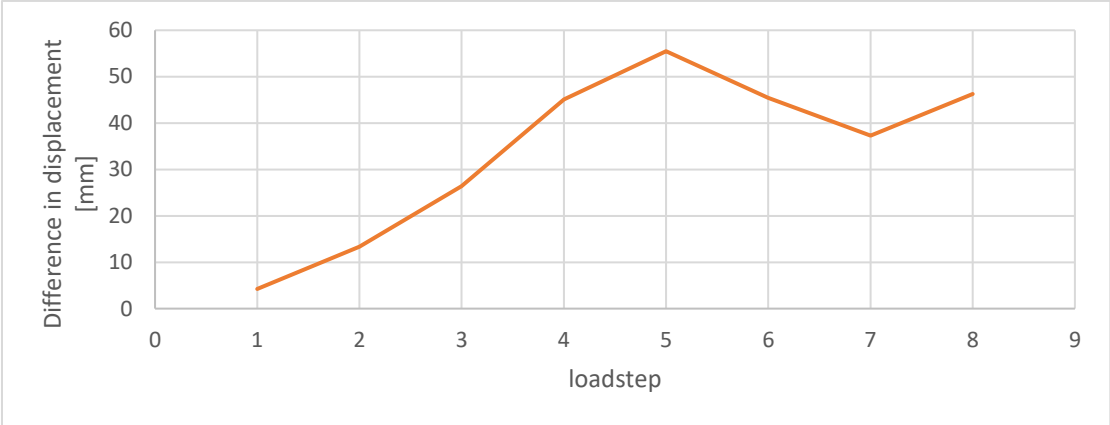
Figure 6.6: Difference between total station and saaf displacement during every loadstep.

6.3   Plaxis calculations

The loads obtained from the optical fibre measurements are used in Plaxis to calculate the displacement of the model with these loads. The rest of the model remained the same, only the old surface loads are changed into the adapted surface loads. The model is calculated only calculated with drained soil conditions, since the piezometer shows a drained soil behaviour without excess pore pressure due to the load. Figure 6.7 shows the behaviour of the pile during the different loadsteps.
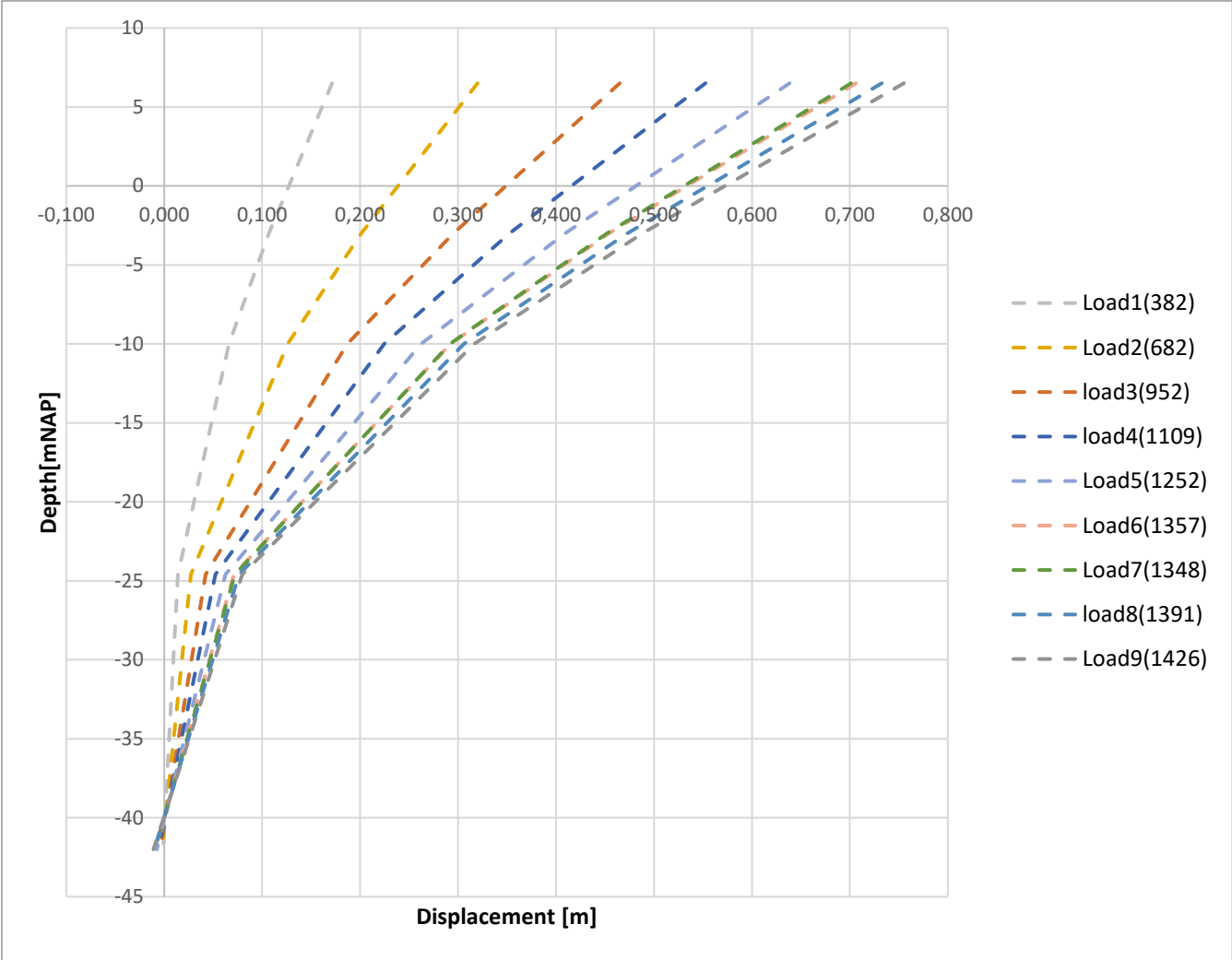
Figure 6.7: Plaxis drained calculation with 9 loadsteps

The order of magnitude of these calculations are more in line with the measured displacements during the test compared to the model with the old loads. The displacement of Plaxis can be compared with the saaf and total station measurements. The total station measurements are laying below the Plaxis calculation. Table 6.2 shows the Plaxis results and the total station on 5.8 mNAP and 1.3 mNAP. The total station measurements are from pile D04. Figure 6.8 shows the displacement at a 1.3 mNAP during the test. The total station measurement misses a measurement point, so the total station line stops during loadstep 9.

6. Displacement analysis.
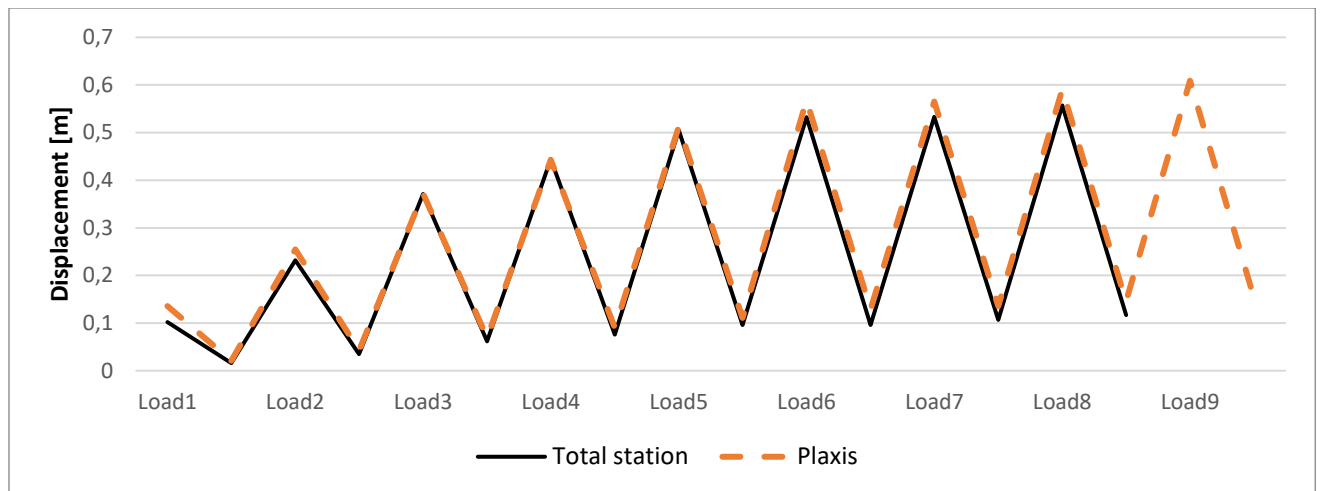
Figure 6.8: Comparison of Plaxis calculation with Total station measurements at +1.3mNAP

Table 6.2:Plaxis displacements and total station displacements at equal heights.

Loadstep	Load [kN]	Total station 1.3 mNAP	Total station 5.8 mNAP	Plaxis Drained 1.3 mNAP	Plaxis Drained 5.8 mNAP
Load1	382	0,102	0,131	0,136	0,167
Unload	10	0,016	0,027	0,021	0,023
Load2	682	0,232	0,286	0,255	0,312
Unload	10	0,035	0,045	0,042	0,047
load3	960	0,371	0,453	0,372	0,454
Unload	10	0,062	0,072	0,069	0,077
load4	1109	0,444	0,52	0,443	0,539
Unload	10	0,076	0,086	0,090	0,100
Load5	1252	0,505	0,587	0,513	0,623
Unload	10	0,096	0,100	0,111	0,124
Load6	1357	0,532	0,636	0,568	0,689
Unload	10	0,096	0,114	0,129	0,145
Load7	1348	0,533	0,651	0,565	0,684
Unload	10	0,107	-	0,136	0,152
load8	1391	0,557	0,677	0,591	0,715
Unload	10	0,117	-	0,145	0,162
Load9	1426	-	-	0,609	0,737
Unload	10	0,121	0,14	0,153	0,171

Table 6.2 shows the results from the Plaxis model and the total station measurement on the same height. The displacements have equal order of magnitudes. The Plaxis model gives too large displacement compared to the total station measurement. The total station displacements increases every next loadstep, during loading and unloading. Which means that the "plastic" displacement increases every loadcycles. 6 days after the test, the pile was measured again. The pile bounced back

and the displacement of the pile decreases. So, the unloading-displacement is not permanent displacement, and the soil has a healing effect.

The Plaxis results are more sensitive to load-decreases, which is visible between loadstep 6 and 7. Between these loadsteps the load decreases slightly and the Plaxis displacement also decreases, while the total station displacement increases. In the Plaxis prediction of chapter 4, the maximum load was constant for the last few loadsteps. The displacement of the pile becomes lower when the same amount of load was applied on the pile. It seems there is an inaccuracy in the Plaxis model. But with minor load increase, the inaccuracy is resolved.

The tip displacement of the pile increases slightly every loadstep and hardly bounces back during unloading. The maximum tip displacement is -0.011 meter. This means that the pile tip moves to the other side as the top of the pile.

The differences in displacement could be causes by uncertainties in the soil parameters, inaccuracies in the load determinations and other uncertainties in the Plaxis model.

6.4 D-pile group, D-sheetpiling and Blum

The D-pile group model is utilized with loads obtained from strain measurements. The D-pile group can only calculate one load step. However, it is possible to simulate cyclic loading by modifying an input parameter in the model. Three calculations are performed to compare the model output with the measurement results. The first calculation approximates load step 6, which is the initial maximum load, using the cyclic calculation in the D-pile group and the load of loadstep 6. The second model approximates load step 8, the final cyclic load step with results from the total station and SAAF, with the cyclic load calculation and the load of cycle 8. The third model approximates load step 6 using the single load calculation since this represents the first maximum load of the test. Loadstep 6 is neither a single load nor a cyclic load, both methods are used to have a look into the results and how those loadcycles can best be modelled. Figure 6.9 illustrates the three models alongside the total station measurement of load steps 6 and 8.

The displacements caused by cyclic loading in the D-pile group exhibit a good correlation with the measurements obtained from the total station. Specifically, the cyclic loading calculation for load step 6 aligns more closely with the results of load step 6 from the total station compared to the single load calculation. However, it should be noted that load step 6 does not involve cyclic loading itself.

The cyclic loading calculation used in the D-pile group incorporates a reduction factor that accounts for the decrease in soil strength, resulting in larger displacements. This calculation predicts displacements after a significant number of cyclic loads. In the test, load step 6 represents the initial maximum load. Furthermore, the flexible dolphin undergoes repetitive loading rather than cyclic loading. Repetitive loading involves longer intervals between unloading and reloading, leading to variations in soil behavior due to time-dependent soil properties, such as water pressures. Consequently, the cyclic load calculation is not suitable for determining displacements during the test. It may be employed to study the pile's behavior after a large number of loads, but the repetitive loading during the test differs from the cyclic loading assumption used in the model, which assumes a higher number of repetitions.

Load step 6 cannot be considered a virgin loading since both the pile and soil have already experienced load cycles with loads close to the newly reached load. The preceding load steps induce

permanent displacements in the pile and soil, resulting in a different starting position for the pile before load step 6 in the total station measurements compared to the single load calculation in the D-pile group. Additionally, the soil has already undergone forces that affect its stiffness. The single load calculation in the D-pile group does not accurately represent the repetitive load steps. Although it could be used to understand the behavior of the first load cycle, the determination of load step 1 is unreliable due to noisy data. Consequently, relying solely on an analysis based on load step 1 would yield unreliable results.
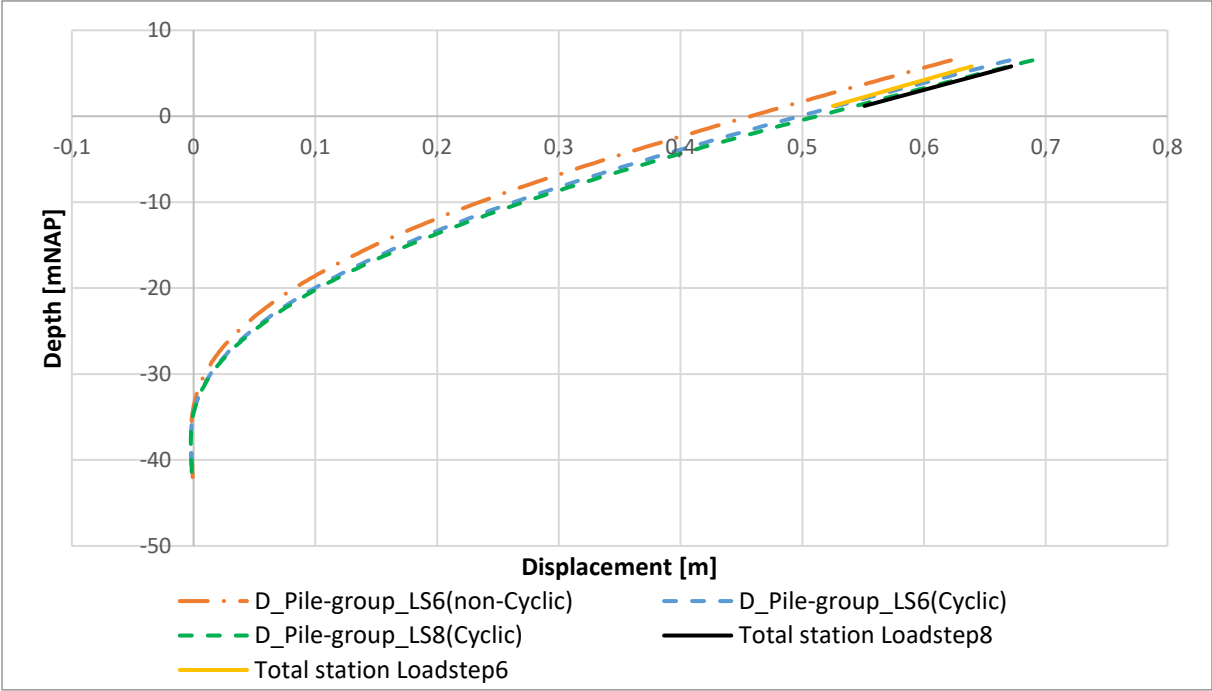
Figure 6.9: D-pile group calculated displacement compared with total station measurement.

The D-sheetpiling model is utilized with loads obtained from strain measurements. The Brinch Hansen model calculates the ultimate soil capacity. Two models are created to compare the model results with the measured results. One model represents the maximum load of load step 6 (1357 kN), and the other model represents the maximum load of load step 8 (1391 kN). The model doesn't take repetitive loading into account. The soil is already subjected to loads prior to the occurrence of load steps 6 and 8. These previous loads result in different soil strength and stiffness compared to the pre-test conditions when the soil parameters were determined. Since the repetitive behaviour is not considered in this analysis, this method is not suitable for application to flexible dolphins. Both models are depicted in Figure 6.10.

6. Displacement analysis.
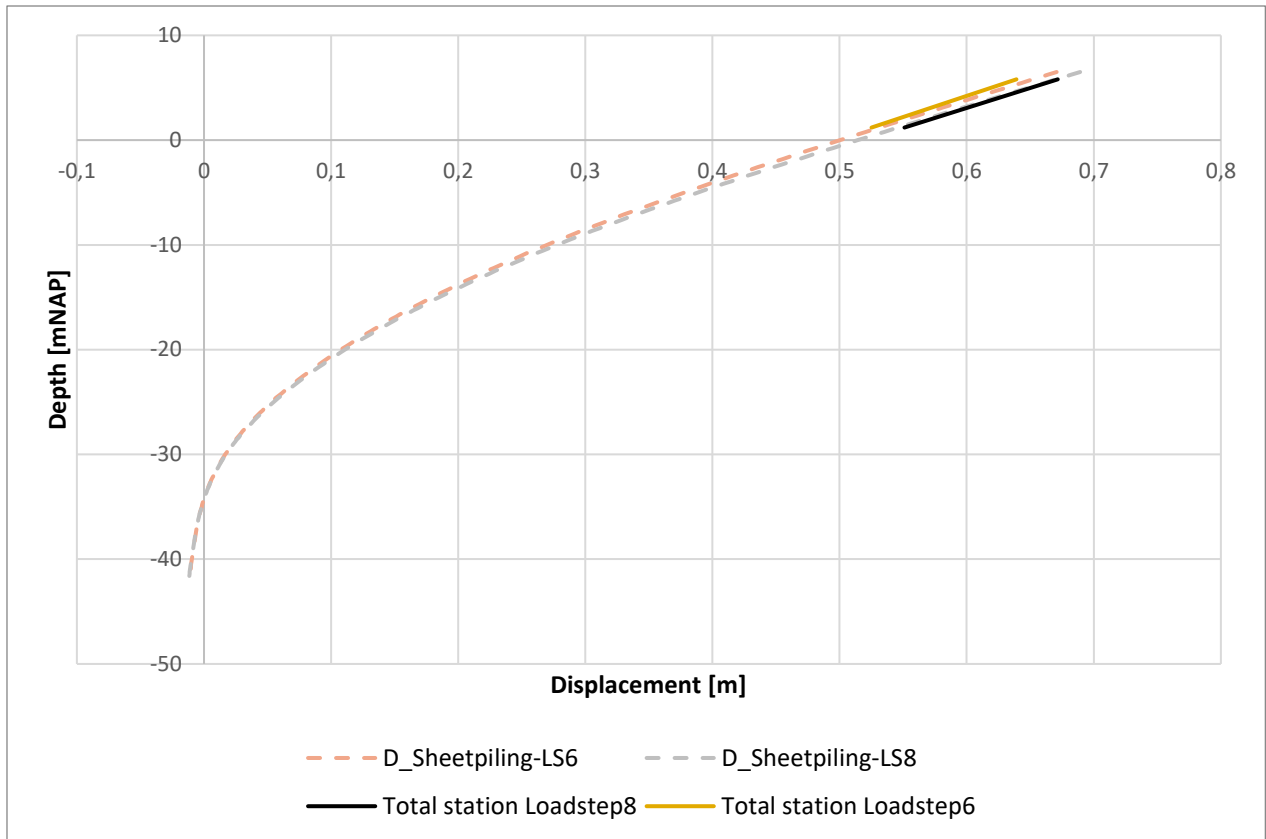
Figure 6.10: D-sheetpile calculated displacement compared with total station measurement.

The Blum model is used to calculate the displacement of the top of the pile. The model calculates the ultimate soil resistance. The input load in the model is one static load, it is not possible to do cyclic or repetitive calculations. The model is calculated twice, ones with the load of loadstep 6 (1357 kN) and once with the load of loadstep 9 (1391 kN). The displacement of the pile is shown in Figure 6.11. The displacement of the Blum model calculated at the height of the load (+6.5 mNAP).
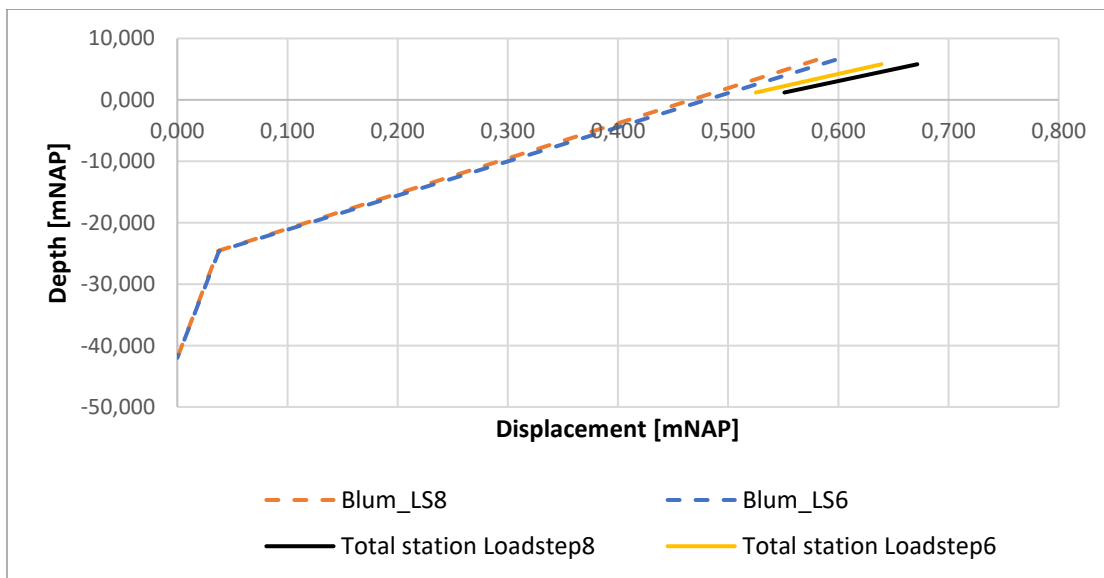

Figure 6.11: Blum calculated displacement compared with total station measurement.

The D-sheetpiling and D-pile group results are close to each other. The different models differ less than a millimetre at the top but increase to a few millimetres lower on the pile. Table 6.3 shows the results of both models..

Table 6.3: D-sheetpiling and D-pile group compared with Total station measurements

		D-pile group	D-sheetpiling	Total station
Loadstep6	1.2 mNAP	0.5289	0.5340	0.5252
	5.8 mNAP	0.6508	0.6501	0.6392
Loadstep8	1.2 mNAP	0.5440	0.5488	0.5511
	5.8 mNAP	0.6691	0.6680	0.6717

The D-sheetpiling and D-pile group models provide a displacements close to the actual measurements. The D-sheetpiling model calculates the ultimate resistance of the soil, while the D-pile group model calculates the displacement after a large number of load cycles. As each load step progresses, the pile's displacement increases, resulting in larger displacements over time. The measured displacements are already greater than the calculated displacements. If the test were extended and more load cycles were applied, the displacement would further increase and deviate more and more from the calculated results. The extent to which the pile would increase after the 8th load cycle is unknown. However, it appears that the models underestimate the displacement. Since both models yield comparable results, it is also possible that certain general input parameters of the test are incorrect.

The top displacements predicted by both models are close to each other, but the tip displacements differ significantly. The D-sheetpiling model calculates a tip displacement of -12 mm, while the D-pile group model predicts a tip displacement of -1.4 mm. This tenfold difference is substantial, especially considering the small magnitude of the displacement. The behaviour of the D-pile group model suggests that the pile behaves as a long and flexible pile, with minimal movement at the tip. On the other hand, the D-sheetpiling model represents more a shorter and stiffer pile, with the pile tip moving around a rotation point located higher up in the pile. The Plaxis tip displacement 4.5 mm, which is in between the two D-series models, but isn't clear about which model is right.

The Blum model has certain limitations when it comes to calculating the behaviour of a flexible dolphin. It is incapable of considering repetitive or cyclic loads. Instead, the model focuses on calculating the ultimate resistance of the soil, which does not align with the test performed and the resulting measurements. The displacements predicted by the Blum model are lower than expected, potentially due to uncertainties in the input values, as only one average wall thickness is utilized. Consequently, the Blum model employed in this thesis is not suitable for accurately simulating the behaviour of a flexible dolphin during the test.

6.5   Displacement overview

The adapted loads, using the strain data, ensures that the predictions made in chapter 3 are no longer applicable. The calculations need to be redone with the adapted loads from the strain-measurements. The other parameters and method-settings stays equal in the calculation. The calculation information is shown in chapter 3 and not repeated here. The results of the calculations with the adapted loads are shown in this section.

The calculations methods that are redone are: D-pile group, D-sheet piling and Plaxis calculation. The Plaxis results are already calculated in the section above. Figure 6.16.122 shows the results of the calculations. Next to the calculations, the total station measurement, optical fibre-displacements, and saaf-displacement are shown in the figure. The optical fibre and saaf displacement are corrected with the use of the total station data. The measurements are the maximum displacement of loadstep8. The calculation methods and the measurement results of the test are in the same order of magnitude. The displacement at the top of the pile differs only 2 or 3 centimetres. The calculation methods also show larger displacement, which makes the methods conservative compared to reality. The differences in tip displacement between the calculation methods is 1 cm. The tip displacement cannot be compared with the optical fibre measurement due to uncertainties. Since the top displacement of the models are in line with the measurements, the models can also be used to give a good guess about the tip displacement of the measurement. So, the measurement lines can be fitted to give the expected tip displacement.
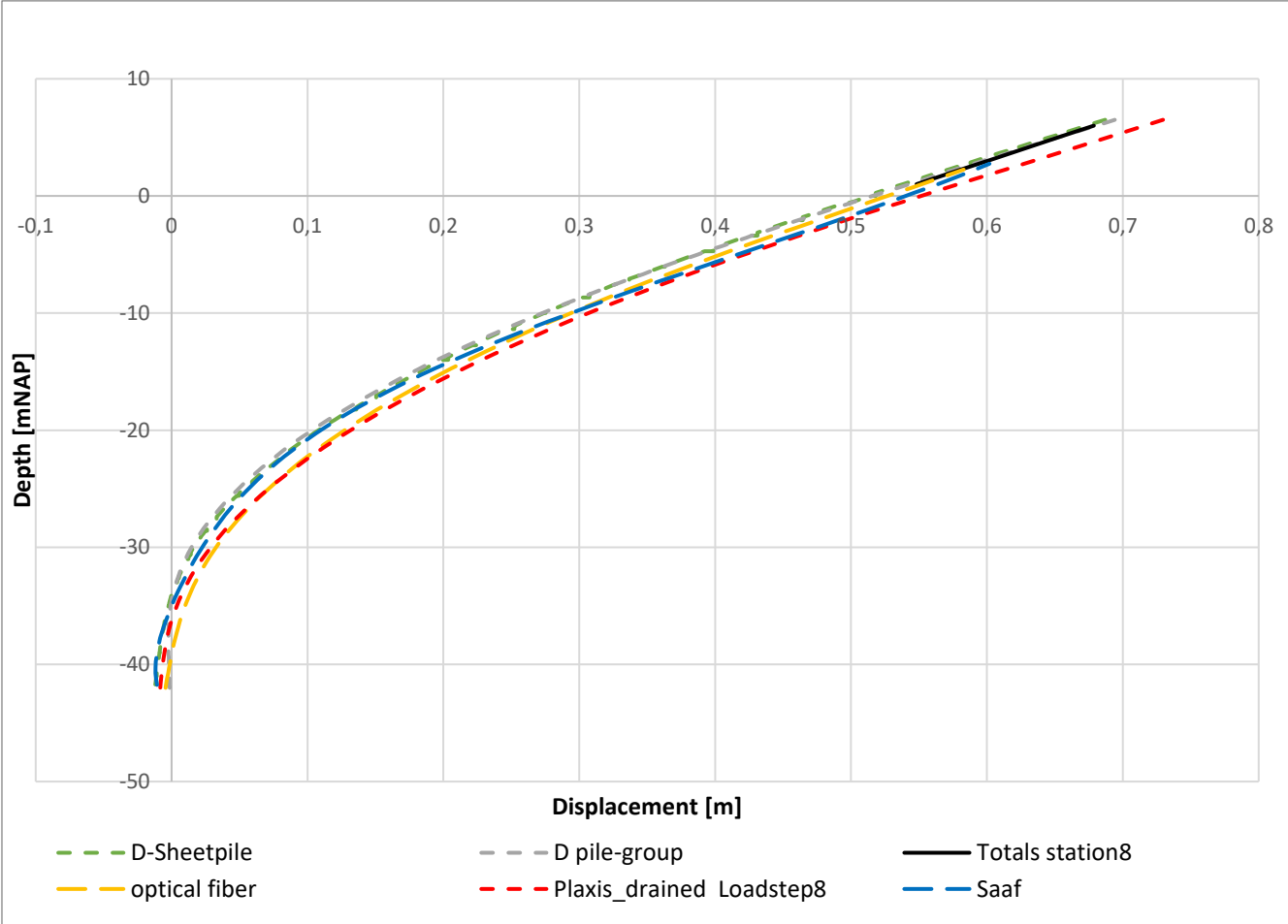

Figure 6.16.122: Comparison of measurements and calculations models

6.6   Sensitivity analyses

6.6.1   Young's modulus

A sensitivity analysis of the stiffness is conducted. The young's modulus of the steel changes throughout the entire analyses. The applied load of the optical fibre measurements changes with a different young's modulus. The sensitivity analysis is performed in Plaxis, since Plaxis calculates the most complete overview of the soil-pile behaviour. The adapted loads are used in the Plaxis model and the steel-plate properties of the pile are changed to the corresponding young's modulus.

The young's modulus of steel varies between roughly 190 GPa and 220 GPa. Most of the construction steels consists of a young's modulus of 210 GPa, which was also used in the calculations. Nevertheless, the stiffness of steel can deviate, therefor this analyses is done to have a further look into the sensitivity of the young's modulus of steel. The load determination is redone with young's moduli of 190, 200, 210 and 220 GPa. The bending moment determination is linear elastic with the young's modulus:

$$M = E * \left[\frac{\varepsilon * I}{z} \right]$$

The expected load is not linear elastic with the elastic modulus since the load application height is still decisive. The expected load deviates slightly from the linear elastic behaviour.

The adapted loads derived with the corresponding young's modulus are used as input parameters in Plaxis. In Plaxis, the young's moduli of the steel properties are adapted with the same young's modulus. The model is calculated with the 3 adapted young's moduli. A decreasing young's modulus in the load analyses, result in a decreasing expected load. Those loads are implemented in the model. The pile in the model contains of the same steel quality as used in the load analyses. A decreasing young's modulus in Plaxis results in larger displacement of the pile, since the pile becomes more flexible. The expectation is that the adaptation in young's modulus doesn't result in major differences in displacement. Since both adaptations balancing each other out since the same boundary conditions are used in both calculations.

The Plaxis models have small deviations in the models with different young's moduli. The models deviates a maximum deviation of 3 cm, with the original calculation. Table 6.4 shows the maximum displacements of each loadstep. The original calculation was done with a young's modulus of 210 GPa. The influence of the young's modulus is larger than expected.

Table 6.4: Results sensitivity analysis Young's modulus

Loadstep	Displacement using different Young's Modulus [m]			
	210 [GPa]	190 [GPa]	200 [GPa]	220 [GPa]
1	0,171	0,167	0,169	0,173
2	0,322	0,312	0,318	0,325
3	0,469	0,457	0,463	0,476
4	0,554	0,538	0,545	0,564
5	0,640	0,620	0,627	0,651
6	0,705	0,679	0,693	0,717
7	0,707	0,682	0,695	0,720
8	0,733	0,708	0,722	0,749
9	0,758	0,731	0,745	0,774

6.6.2   Soil parameters

The soils in the calculation models are approached with soil parameters. The soil parameters are derived before the test by others and written down in chapter 3.1 The cone resistance measured by the CPT is used to determine the soil parameters. The cone resistance is converted to a relative density. The soil parameters are determined with empirical formulas and the relative density. The empirical formulas that are used comes from the paper of Brinkgreve (Brinkgreve, 2010). The empirical formulas derive the input parameters for the hardening soil small strain model, those input parameters cover most of the input parameters used in this report. The report conclude that the empirical formulas provides a good first approach for the soil parameters, but doesn't replace soil investigation. The empirical formulas leads to conservative soil parameters. There is still uncertainty about the accuracy of the input data and further soil investigation is done to improve the input data. The extra soil investigation couldn't be included in this report, since the results were not determined on time.

To have a better understanding of the influence of the input parameters, a sensitivity analysis is done with the soil parameters in the Plaxis model. The analysis provides a general overview of the influence of the soil parameters. The relative density is increased, which will lead to a stronger soil The increase in the relative density leads to an increase of all the input parameters. It does not consider the sensitivity of a single parameter. Two extra calculations are done, the first model consist of a relative density of 110% and the second model uses a relative density of 120%. Since the empirical formulas are considered as conservative, only higher relative densities are used.

Table 6.5 illustrates the maximum displacements observed during each load cycle using the three Plaxis models and the total station measurements. These displacements are measured at a depth of 1.3mNAP. A comparison is made among the three models. The original model, featuring the weakest soil, exhibits the highest displacements at the top of the pile and on the soil bed. However, at the tip of the pile, the original model does not always exhibit the largest displacement. The magnitude of the largest tip displacement varies between the original model and the RD+10% model. The RD+20% model, characterized by the strongest soil, experiences relatively smaller pile movement over the entire pile length. The RD+10% model demonstrates lower displacement at the top of the pile, but similar displacement at the pile tip when compared to the original model.

Table 6.5: Sensitivity analysis of soil input parameters

Loadcycle	Top displacement [m]			
	Plaxis			Total station
	Original	RD+10%	RD+20%	
1	0,136	0,133	0,129	0,102
2	0,257	0,252	0,243	0,232
3	0,377	0,369	0,353	0,371
4	0,446	0,435	0,416	0,444
5	0,514	0,502	0,479	0,505
6	0,564	0,552	0,525	0,532
7	0,566	0,554	0,527	0,533
8	0,587	0,575	0,546	0,557
9	0,568	0,550	0,515	-

The Total station measurements are within the boundaries of the three models, but doesn't follow exactly the same trend as one of the models. From loadstep 6 on, the total station displacement are

most in line with the Plaxis RD+20% model. During the lower loadstep, the total station measurements are not in line with one of the Plaxis models, bur varies between the three Plaxis models.

The later load cycles exhibit higher accuracy compared to the earlier ones. This can be attributed to the larger loads present in the later cycles, which are derived from strain data with a higher margin of error. Additionally, small inaccuracies in displacement have less impact when larger displacements are involved. Throughout all load steps, the total station measurements indicate lower displacement than the original model. This could be attributed to conservative soil input parameters. The Plaxis models, employing with stronger soil input parameters, show displacements closer to the total station measurements. This suggests that the original input parameters are overly conservative. Notably, during the larger load steps 6, 7, and 8, the total station displacements closely align with those of the RD+20% model. It is important to note that the method employed in this analysis does not precisely reflect the actual soil parameters, but rather demonstrates the influence of a general increase in soil input parameters. It is also possible that only a few parameters in the original model need adjustment, as they may exert significant influence on soil resistance.

7 Repetitive behaviour

The full-scale test is conducted with the objective of enhancing the understanding of repetitive loading on flexible dolphins. Repetitive loading refers to the application of loads multiple times, although not in a consistent rhythm like in cyclic loading. Repetitive loading is also encountered during the operational phase of the pile, where ships periodically berth and generate loads on the pile. After a certain period, the ships depart, and the timing of the next ship's arrival can vary. In this chapter, the repetitive behaviour of the flexible is analysed, with the focus on the load-displacement behaviour.

7.1 Displacement analysis.

The total station measured the exact displacement of multiple points on the pile. Those point on different depth show the trend of the pile. The disadvantage of the total station is that it only has 3 measurement points per loadstep. The trend between loadstep can be shown, but the trend within the loadstep cannot be extracted from the total station. The advantage of the total station is that the measurements are very accurate. The total station measured 4 point per pile, each on different heights. The height varies between 5.8 and 1.3 m NAP. The maximal displacements of the loadcycles are lower than the ones from the hydraulic jack. The displacement during unloading are more in line with each other.

Table 7.1: Repetitive load analyse of Total station.

Loadsteps	Minimum displacement during unloading phase before the load [m]	Maximum displacement during entire loadstep [m]	Increase in Displacement [m]	Optical fibre maximum load [kN]
1	0,030	0,133	-	382
2	0,039	0,284	0,151	682
3	0,051	0,444	0,160	960
4	0,070	0,516	0,072	1109
5	0,086	0,583	0,067	1252
6	0,102	0,635	0,052	1357
7	0,113	0,647	0,012	1348
8	0,123	0,666	0,019	1391
9	0,129	0,670	0,004	1426

Table 7.1 shows the displacement of the pile during the loadcycles. The displacements increase with every increasing loadstep, during both loading and reloading. During repetitive loads with relatively constant maximum loads, the displacement increases every loadcycle. But the increase in maximum displacement during a loadcycle stagnate when the maximum load stays constant.

The maximum load is reached for the first time during the 5th loadstep according to the prescribed load scheme. The strain-measurement loads still increases in the load between loadcycle 5 and 6. The first maximum loadstep according the strain measurements, loadstep 6, reaches a new maximum load, which causes a relatively large displacement increase. The second maximum loadstep, loadstep 7, was the first repetitive loadcycle, with approximately the same amount of load. During loadstep 7, the displacement increases less than during initial maximum loadsteps, loadstep

6. The increase in displacement during the 7th, 8[th,] and 9th loadstep are relatively small, which is due to the relative constant unloading/reloading behaviour of the soil. Since the repetitive loadcycles ensures smaller load increasements compared to the initial maximum load, the stiffness of the soil during the repetitive loadcycles increases.

The displacement of the piletip can be divided in two parts, the cyclic displacement, and the plastic displacement. The cyclic displacement is the difference in displacement between unloading and loading of the pile, the changes in displacement are related to the amount of load. The plastic displacement is the permanent displacement when the pile is not loaded. The total displacement during unloading is increasing during every loadstep, which means that the permanent displacement increases.

Figure 7.1 displays the displacements of the pile as a result of repetitive load cycles, as measured by the total station. The displacements of the pile are shown with respect to the measured height. The pile experiences progressively larger displacements with each subsequent loadcycle. Loadcycle 9 has fewer measurement points. The measurements taken during load step 9 exhibit larger displacements compared to those of other load cycles, but the trend line of the pile appears different due to the reduced number of measurement points. Furthermore, the figure demonstrates a significant increase in displacement between load steps 5 and 6. This increase is consistent with the findings in Figure 7.1 and applies to all the total station data points. The cause of this increase may be attributed to the load increments that are anticipated between loadsteps 5 and 6, as indicated by the strain-measurement.

It can be inferred from these findings that the piles experience larger displacements with an increased number of load cycles, not only during loading but also during unloading. For every measurement point, the displacement of the pile increases with each subsequent load step. The pile was measured several days after the test, and the measurements demonstrate that the displacements decrease over time when the pile is not under load. The datapoints that are used in the figure are points from both piles. The assumption is made that those piles have identic displacements, but it can differ a little. Consequently, the data points during unloading does not have a clear trendline but contains some variations. It has been decided to utilize the displacement of both piles together in order to obtain a larger set of data points, particularly for load cycles where not all points have been measured
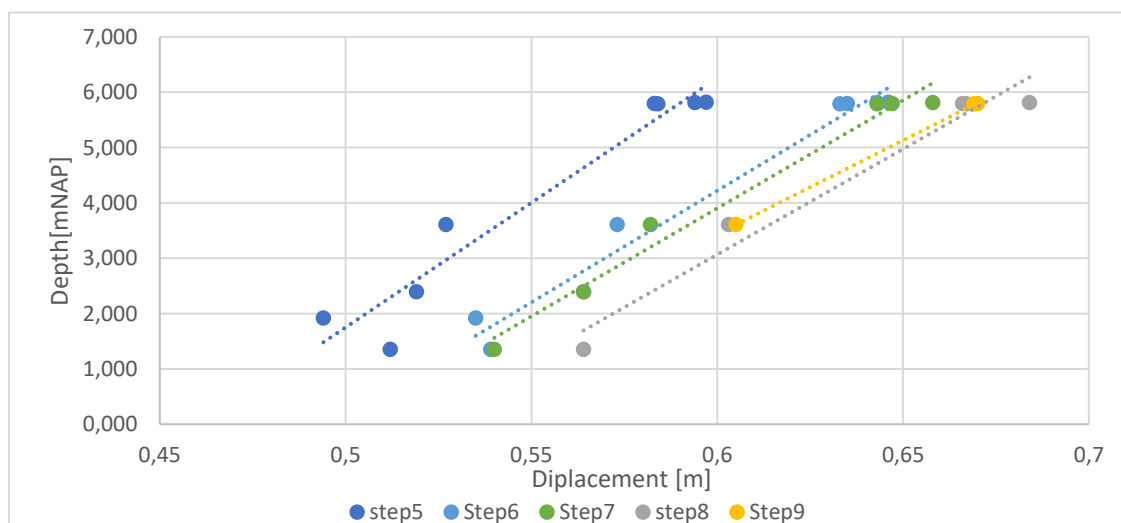

Figure 7.1: Displacement during different loadsteps measured with the total station, left during loading and right during unloading.

7.2   Load-displacement diagram

The load-displacement graph of the test is made using the optical fibre measurement. The load is determined as explained in chapter 5 and the displacement at the top of the optical fibre cable is calculated using the same measurement data. As a first approximation the displacement and angular displacement at the tip of the cable are zero during the entire test. Those loads and displacements leads to the f-u graph in Figure 7.2. The lines in the graph are mixed up, which makes the graph harder to interpret. The interpretation of the data is divided in smaller datasets to make it clearer. The three sub sections of the interpretation are:

- Hysteretic soil behaviour.
- Difference between initial load and repetitive loads.
- Energy absorption.

A small sidenote is that the added loads of the hydraulic jack are not fully reliable, which makes it difficult to calculate the real relative stiffnesses, but the trends of the loads can still be used. In chapter 5, the load analyses are done, the new loads are used in this chapter. The load and displacement response of the lateral loaded pile can be reviewed with the data from the total station, the hydraulic jack, and the Saaf.

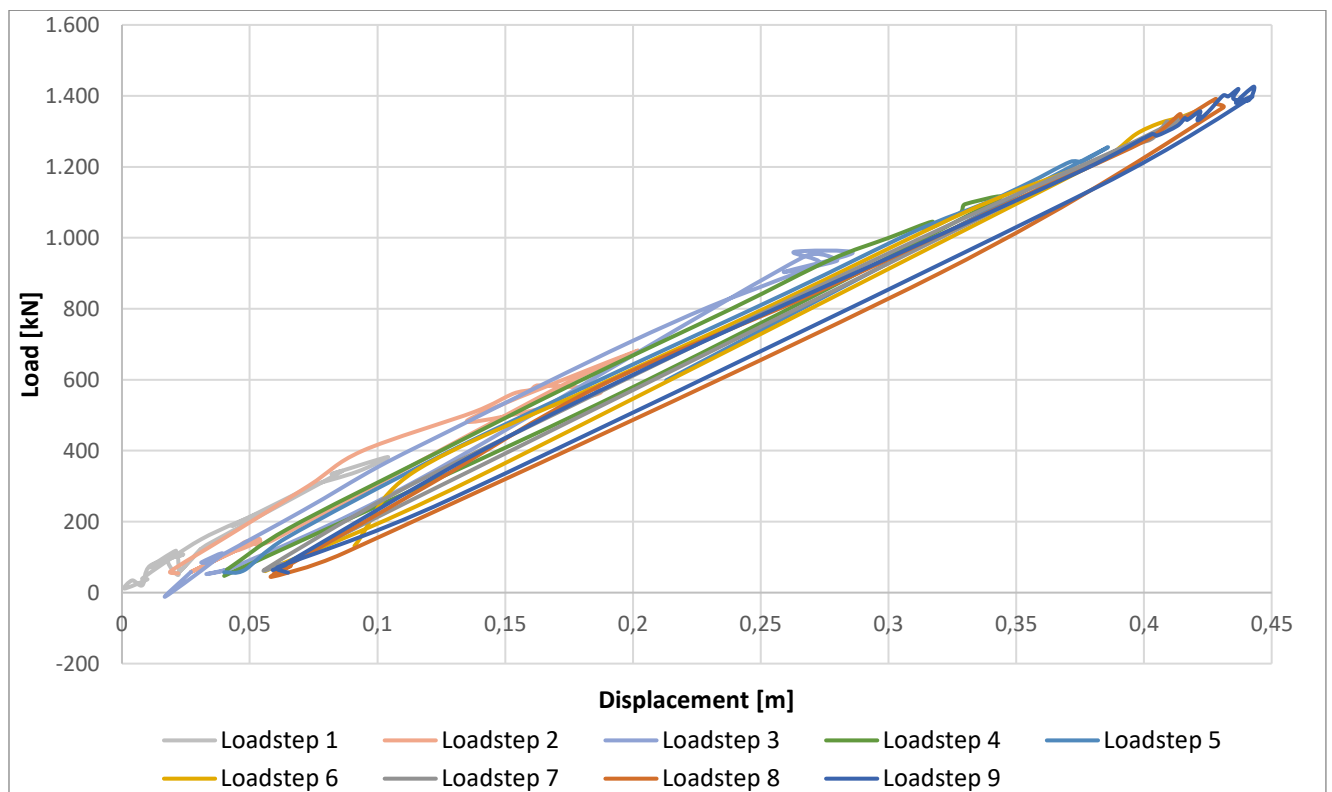*Figure 7.2: Load-displacement graph of optical fibre measurements at -2mNAP*

7.2.1   Hysteretic soil behaviour.

The f-u graph is constructed using two displacement measurements, the optical fibre displacement, and the Saaf displacement. Figure 7.3 illustrates the load-displacement behaviour of the soil during load step 6, which is representative of subsequent load steps. The optical fibre displacement exhibits

a hysteretic loadcycle in the graph, where the trend line during unloading is lower than the trend line during reloading. This phenomenon has been reported in literature.

The Saaf data is also used to calculate the load-displacement curve. At the time of each load calculation, the Saaf displacement at the same height as the top of the optical fibre cable is determined. However, since the measurements of both instruments are not taken simultaneously, the Saaf data used is the displacement at the last load step before the optical fibre measurement. The loadcycle with the Saaf data has the opposite direction compared to the loadcycle of the optical fibre measurements and literature. The reloading line of the optical fibre data is above the unloading line, while the reloading line of the Saaf data is below the unloading line, as indicated by arrows in the figure.

In the subsequent analyses presented in this report, the optical fibre displacement is used for load-displacement calculations. Given that the literature supports the optical fibre trend, it is expected that the optical fibre lines are more accurate. It is possible that inaccuracies occur in the Saaf analyses due to the difference in time between the load and displacement measurements.
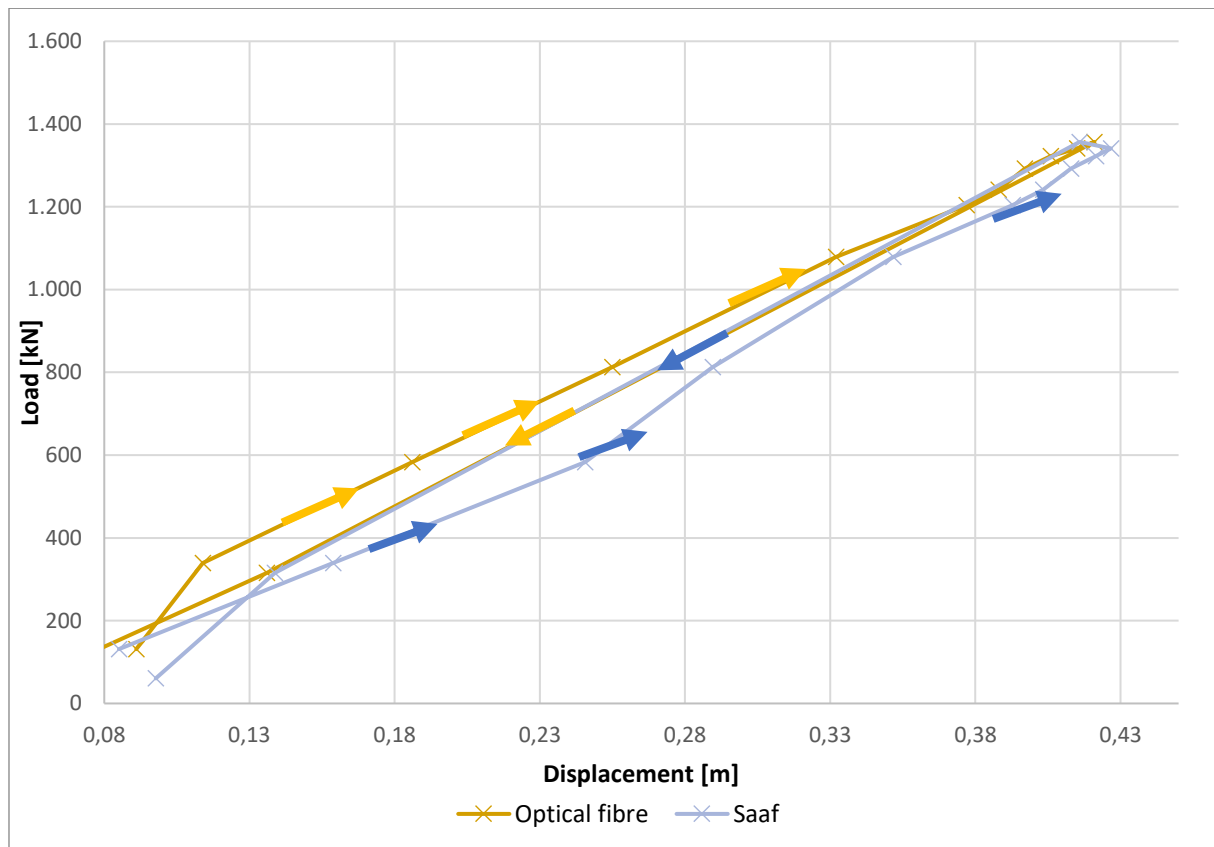
Figure 7.3: Load-displacement behaviour of loadstep 6 using optical fibre and saaf displacement.

7.2.2   Initial loading vs reloading.

The first 6 loadstep of the test are used to build up the load until its maximum load. At every loadstep, the load reached a new maximum. The parts of each loadstep where a new highest load is reached are taken separately. The combination of the first-time occurring loads of each loadstep create together the first fully loadstep. The initial loadcycle is a unique loadcycle in a load-displacement graph and differs from the subsequent cycles. During the initial load cycle, the soil experiences the force for the first time. During the subsequent cycles, the soil is already compacted

and has become stiffer. Next to that, the soil already experienced the amount of load. The combined first full load is plotted in Figure 7.4. The combined lines follow each other and form a fluent line. The trend of the initial loadcycle can be compared with the subsequent loadcycles.

Figure 7.4: initial maximum load using the combined data of the first 6 loadcycles.

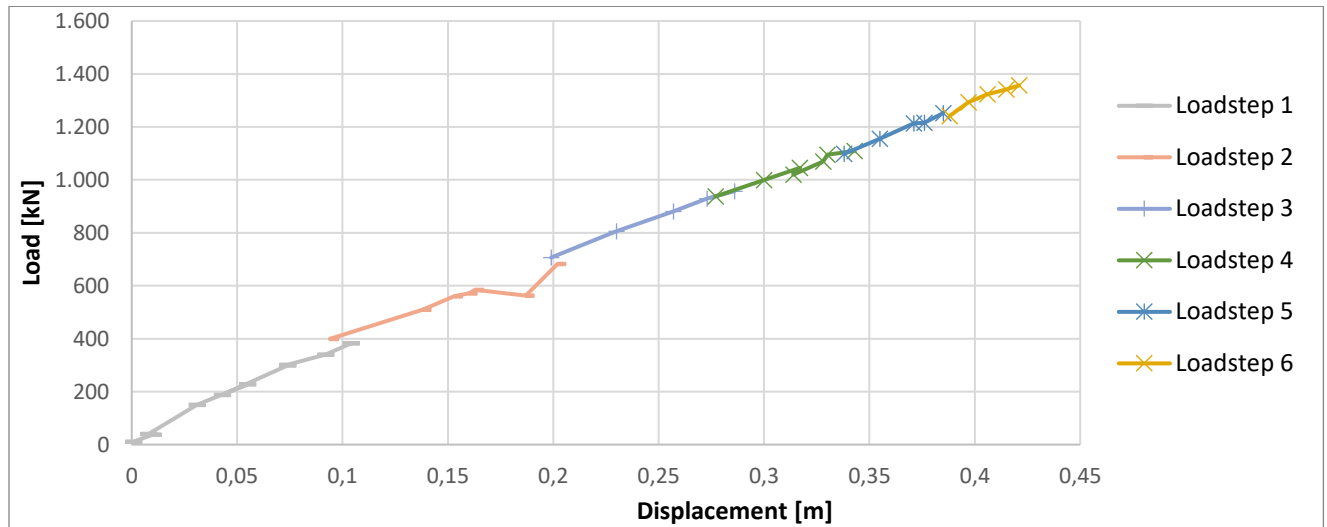After the combined initial load has reached its maximum value, subsequent load cycles reach about the same maximum load repeatedly, and these cycles are referred to as repetitive load cycles. The load-displacement behaviour of the repetitive load cycles differs from that of the initial load and is consistent with the theory of a separate unloading/reloading stiffness (E_{ur}) in addition to the initial stiffnesses (E_0, E_{50}). The unloading/reloading stiffness of the soil is assumed to remain constant over the repetitive load cycles.

The reloading/unloading stiffness-equivalent is determined for the repetitive load cycles using a trendline through the load cycle. The trendline goes through the hysteresis cycle, and no distinction is made between the unloading and reloading portions. The load-displacement lines of loadcycles 6, 7, 8 and 9 are constructed using loads from optical fibre measurements and displacements from the optical fibre too. The trendline is drawn using all the data points of the load step, both reloading and unloading. The expectation is that the reloading/unloading stiffness is steeper than the initial loading stiffness.

Figure 7.5 shows a load-displacement graph with the initial loadcycle and the repetitive loadcycles. The optical fibre displacements are used in this graph. The initial loadcycle differs from the repetitive loadcycles, while the repetitive loadcycles are almost equal. The load-displacement curve of the initial loadcycle is flatter than the repetitive loadcycles curves. The unique initial load in the cyclic/repetitive loading behaviour is a well-known behaviour in literature. The reloading cycles are close to each other. Due to the margin of inaccuracy is it not possible to have clear conclusion about the differences between the second, third and fourth maximum loading. But what stands out is the difference between the initial and the repetitive loadcycles.
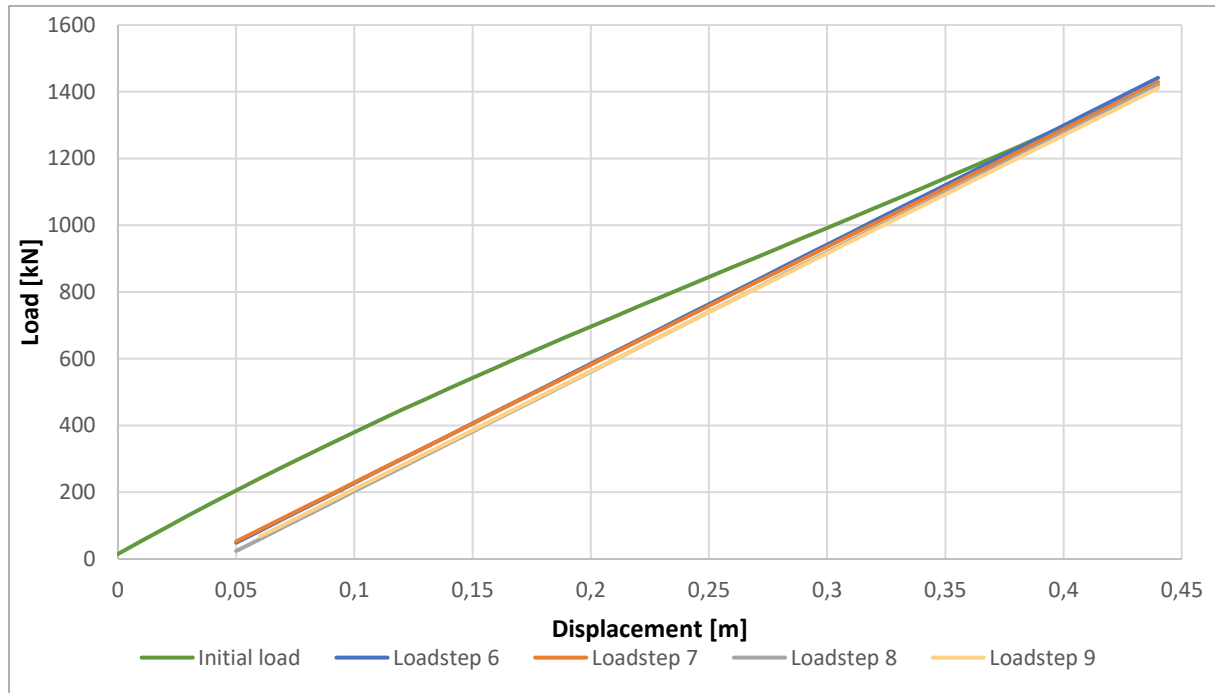
Figure 7.5: The initial maximum load and the repetitive loadcycles using optical fibre measurements.

7.3   Repetitive behaviour in Plaxis

The load-displacement can also be calculated using results of Plaxis. Plaxis calculated the displacement of the pile 10 times during each stage. Figure 7.6 displays the load-displacement behaviour of the last 5 loadsteps of the pile according to Plaxis. The maximum applied load for each loadstep is manually entered into the program using the strain-measurement data. The data points between zero load and the maximum load exhibit a linear relationship in time and load. The load-displacement graph shows a hysteretic trend in the loadcycle. This trend was also mentioned in the Plaxis manual for the hardening soil small strain model. The unloading part line is lying below the reloading part line. This is the trend that is mentioned in literature and what is shown with the optical fibre measurement. The hysteretic loadcycle trend is equal to the loadcycle trend with the optical fibre measurement data.

Figure 7.6: Load-displacement graph of the Plaxis calculation at +6.5mNAP

69

The trend between the initial load and the repetitive loads is analysed for the Plaxis results. The measurement data showed a less steep initial maximum load build up, compared to the repetitive load build ups. The same trend is visible in the Plaxis-results, shown in Figure 7.7. The initial load line is in the figure less steep, compared to the repetitive load lines. The repetitive load behaviour lines are about parallel to each other. So, the soil-pile behaviour during the test according to initial load and reloading is also seen in the Plaxis results. The flatter initial loading behaviour is related to the input parameter of the hardening soil model. In this model the first approximation for the E_{ur} is three times as large as the E_{50}. Which shows that the unloading/reloading cycles is steeper than the initial loading cycle (Plaxis, 2021).
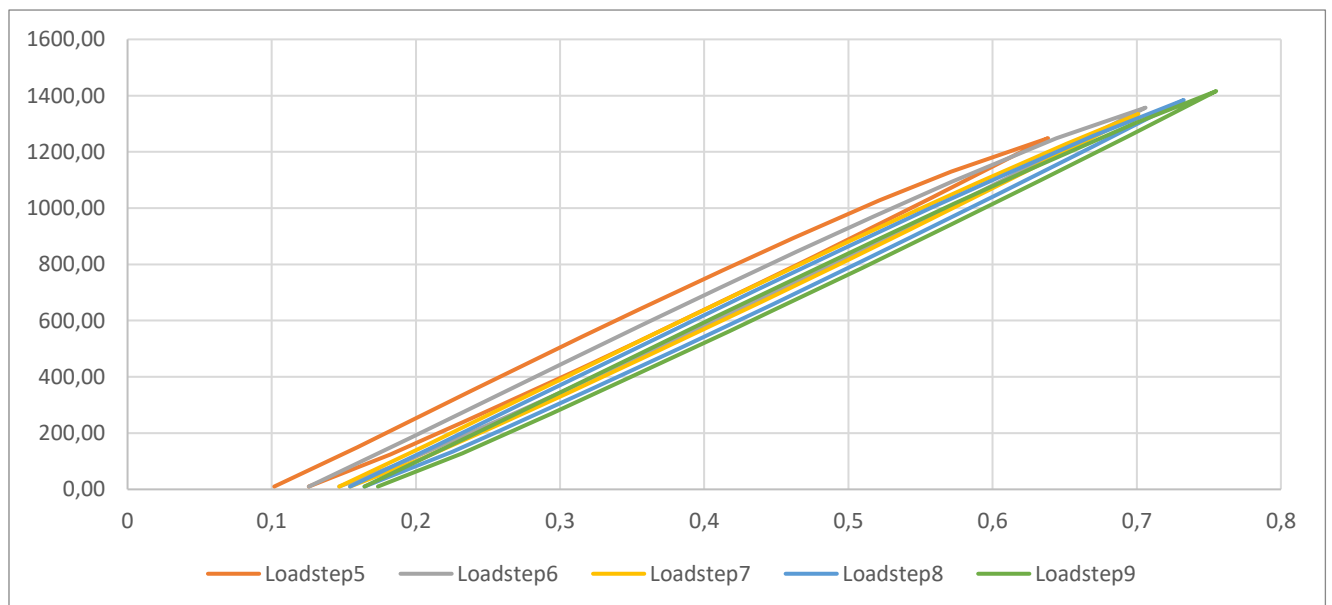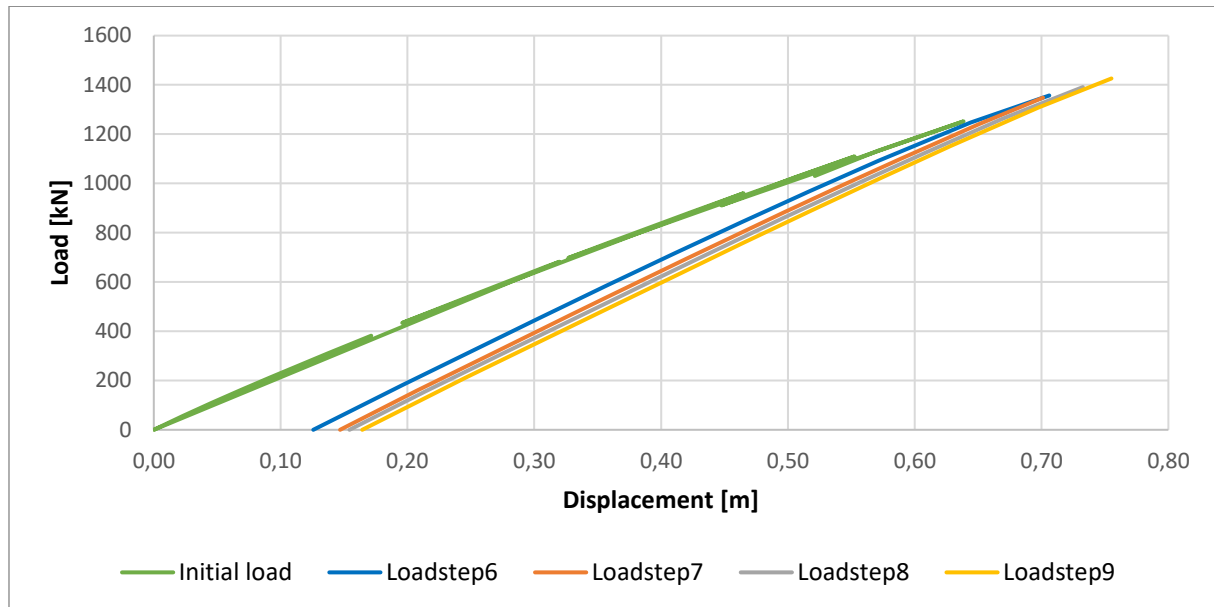

Figure 7.7: The initial maximum load and the repetitive loadcycles using Plaxis.

Figure 7.8 shows the combined f-u diagrams of Plaxis and the optical fibre measurements. Despite applying the same load, the two methods give different displacement values, which may be attributed to a discrepancy between a model and measurements, as discussed in chapter 6.3. Additionally, the optical fibre displacement and the displacement measurements of the total station also differ as shown in chapter 6.2. The total station measurements are not adequate to draw the load-displacement behaviour cycles, since only three measurements are done during every loadcycle. The slopes of both models in the f-u diagram are in the same order of magnitude, indicating that the unloading/reloading stiffness of the model is correct When the total station was compared with Plaxis, a different trend was observed, where the loading displacement differed while the unloading displacement was similar. Which suggests that the slope of the load-displacement behaviour varies between Plaxis and the total station. In the Plaxis model, Eur is the unloading/reloading stiffness, and its default value is three times that of E50, which is maintained as there is no better prediction of the unloading/reloading stiffness available.

The Plaxis calculation's displacement values differ slightly from the test measurements, which may be caused by the soil's input parameters, or the exact amount of load applied during the test. However, the repetitive trends in the Plaxis calculation, which are discussed in this section, are consistent with the test measurements. The loadcycles in the load-displacement graph follow the same trend as the measurements. The difference between the initial maximum loadcycles and the repetitive maximum loadcycles is another trend that is well shown in the Plaxis calculation, the test results, and the literature. This makes Plaxis a model that can be used to analyse the behaviour of a flexible dolphin. If a closer look is taken into the soil parameters, the expectation is that the

displacement of the soil can be determined even better. The only trend that is not consistent with the test results is the decrease in displacement for repetitive loadings with the same magnitude of load.
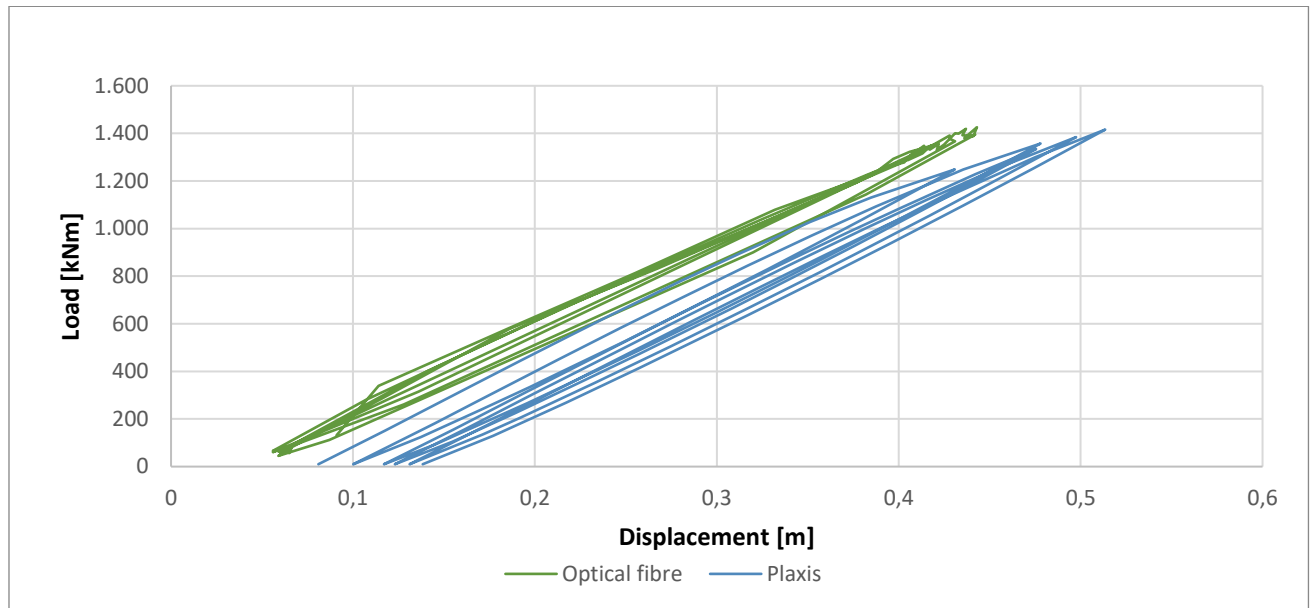

Figure 7.8: Load-displacement graphs of optical fibre and Plaxis.

The two methods have differences in the shape of their respective load cycles. The area enclosed by the load cycle is indicative of the soil's energy absorption capacity. A comparison is made between the areas of both models. The Plaxis results demonstrate smooth load cycles consisting of 20 evenly distributed measurement points per cycle. The displacement is measured after every 10% change in load. On the other hand, the optical fibre method exhibits a more erratic trend with 13 to 27 measurement points per load cycle. Displacement and load are measured every 3 minutes. The load build-up process spans approximately 10 to 15 minutes, while the load reduction process takes about 5 minutes. Multiple data points are collected during the load build-up phase, but only 1 or 2 data points are collected during the load reduction phase. The limited number of data points during unloading leads to less precise rounding of the load cycle. The rounding within the loadcycle significantly impacts the area of the load cycle, which serves as a representative measure of energy absorption during the load cycle. Therefore, the scarcity of data points during reloading and unloading must be carefully considered during the analysis of load cycles, as it can have a significant influence on the calculated area of the load cycle.

Table 7.2: Area of loadcycles according optical fibre measurements and Plaxis.

loadcycle	Maximum Load [kN]	Loadcycle area [kNm]	
		Optical fibre [kNm]	Plaxis [kNm]
5	1252	24,88	35,79
6	1357	18,64	37,47
7	1348	10,20	21,82
8	1391	32,87	26,13
9	1426	28,32	26,04

The areas of both methods for the last 5 load steps are presented in Table 7.2. Load steps 5 and 6 exhibit a substantial increase in virgin loads, resulting in relatively large energy absorption areas according to the Plaxis calculations, but the optical fibre measurements show smaller areas for these load steps. During Loadstep 7, the maximum load decreases in maximum load compared to the preceding load steps. Consequently, both methods indicate that load cycle 7 has the smallest loadcycle area and width. The smaller size of the repetitive load cycle appears to be associated with its lower load. Load steps 5, 6, and 7 exhibit significantly smaller areas in the optical fibre measurements compared to the Plaxis calculations. Load steps 8 and 9 experience minor increases in maximum load and behave as repetitive load cycles with smaller areas in the Plaxis calculations compared to loadsteps 5 and 6. However, the optical fibre measurements indicate that load steps 8 and 9 have larger areas than load steps 5 and 6, which contradicts the Plaxis calculations. Therefore, the proportion of areas across the load cycles does not align between the two methods.

Loadsteps 8 and 9 consist of more developed loadcycles with a measurement point during unloading. The measurement point during unloading ensures a rounder loadcycle, with a larger area. The optical fibre areas are also larger than the Plaxis areas in this loadsteps. However, it is important to consider the inaccuracy resulting from the limited number of data points during unloading and reloading. The lower amount of measurement data provides a underprediction of the area, since more data points will give the loadcycle a more round shape instead of the angular shape it currently has.

Plaxis overpredict the pile displacement compared to the total station measurements , the overpredictions are probably caused by the uncertainties in the input parameters. The expectation is that the input parameters were too conservative, which resulted in a too weak soil and larger displacements. The displacement are overpredicted and smaller displacements are expected. The smaller displacement ensures smaller loadcycle areas. This makes the current Plaxis energy absorption too optimistic compared to reality.

The differences in areas vary across the load cycles. Load steps 5, 6, and 7 exhibit significantly smaller areas, which may partly be attributed to the absence of a measurement point during unloading. Load steps 8 and 9, on the other hand, have larger areas compared to Plaxis, and these steps do have a optical fibre measurement point during unloading. This suggests that the last two load cycles are more comprehensive in terms of the optical fibre measurements. If we consider these last two load steps, it will imply that Plaxis underestimates the energy absorption of the soil. Next to that, the optical fibre measurements underpredict the area, while Plaxis overpredict the displacement and hence the loadcycle area. However, caution should be exercised when drawing this conclusion, as not all load steps demonstrate the same pattern.

7.3.1 Embedded pile depth

The research of Flexible dolphins is focused on the knowledge about the behaviour of the pile. An increase in the knowledge of the soil-pile behaviour results in more perfectly fitted piles. Flexible dolphins roughly costs between the €60.000 and €300.00 (Roubos, 2022). The costs of the piles depend on the amount of steel that is used and the length of the pile. The knowledge about the flexible dolphin will be used to have a better look into the pile-soil behaviour. Better understanding of the pile-soil behaviour may lead to a decrease the length of the pile, which will decrease the costs. The lower amount of steel is also beneficial for the CO_2 footprint of the pile. The carbon emissions of steel production are 1.39 ton CO_2 per ton steel (IEA, 2021). The total weight of the current pile is 105 ton, which result in a carbon footprint of 146 ton CO_2, for only the steel production.

Plaxis is used for a sensitivity analysis of the embedded pile depth. The first calculation contains an infinitely long pile, which is modelled with a pile length of five times the diameter below the current pile. The infinite pile goes down to -54 mNAP. In the infinite pile model, the minimum available

displacement of the pile will be reached, with the current pile specifications like the wall-thickness and the diameter. After that, four more models are made with embedded depths of -40, -41, -43 and 50 mNAP. The pile depths close to the current pile depth gives a good first insight in the sensitivity of the pile depth. The results of the models are shown in Table 7.3.

Table 7.3: Maximum pile displacement of Plaxis models using different embedded pile depths.

	Maximum pile displacement [m]					
	-40mNAP	-41mNAP	-42mNAP	-43mNAP	-50mNAP	-54mNAP
Loadcycle 1	0,175	0,172	0,171	0,171	0,171	0,170
Loadcycle 2	0,335	0,327	0,323	0,321	0,320	0,319
Loadcycle 3	0,500	0,482	0,471	0,467	0,464	0,463
Loadcycle 4	0,598	0,573	0,556	0,549	0,545	0,544
Loadcycle 5	0,699	0,665	0,640	0,632	0,624	0,624
Loadcycle 6	0,778	0,735	0,702	0,694	0,683	0,683
Loadcycle 7	0,783	0,738	0,703	0,694	0,684	0,684
Loadcycle 8	0,816	0,768	0,729	0,720	0,708	0,708
Loadcycle 9	0,846	0,795	0,753	0,743	0,730	0,730

The new method in CROW guidelines is that the displacement of the top of the pile may not deviate more than 2% compared to an infinite long pile. The infinite long pile is determined at 5 times the diameter longer than the current pile, which results in a embedded pile depth of -54mNAP. The current pile deviates 3% of the infinite long pile, which is not within the guidelines of CROW. This can be caused by differences in soil parameters, this research uses the expectation values instead of characteristic values with safety factors. Furthermore, the pile is designed with a higher load than which is used during the test, which was concluded in chapter 5. And the Plaxis results doesn't completely match with the test measurements, explained in chapter 6.

The displacement increases significant with an decreasing pile depth. When the pile is shortened by a meter, the displacement increases maximum with 4 cm. When the pile is largened with a meter compared to the original pile depth, the displacement decreases by 1 cm. The pile with the embedded depth of -43mNAP meets the 2% requirements. The ideal pile depth with an deviation of 2% to the infinite long pile is a little bit shorter than -43mNAP, according this data. But the inaccuracies in the data needs to be taken into account. Those inaccuracies will have influence on the displacements and the corresponding deviation. The pile embedded at -41mNAP deviates up to 9% from the infinite long pile.

A shorter pile length will result in more energy absorption during loading. Therefore a shorter pile can also be beneficial. The areas of the loadcycles of the shorter piles are determined using the Plaxis results. The areas of the energy absorption will give an better inside in the benefits of a shorter pile. Table 7.4 shows the areas of the loadcycles of the Plaxis models with different embedded pile depths.

Table 7.4: Loadcycle areas with different embedded pile depths using Plaxis.

	Loadcycle Area's [kNm]		
	-40mNAP	-41mNAP	-42mNAP
Loadcycle 5	48,4	41,1	35,8
Loadcycle 6	48,4	42,0	37,5
Loadcycle 7	24,9	24,8	21,8

| Loadcycle 8 | 30,8 | 28,8 | 26,1 |
| Loadcycle 9 | 31,8 | 29,7 | 26,0 |

The decision according the required depth of the pile depends on the displacement of the pile and the energy absorption on the soil. A shorter pile moves more through the soil and absorbs more energy. But larger displacement will lead to plastic deformation of the soil. Plastic deformation of the soil leads to misalignment of the pile. The plastic deformation are distinguished during unloading, while the cyclic displacement is neglectable during unloading. The displacement of the soil are more important than the top displacement, because during unloading the top displacement comes from the misalignment of the pile in the soil. The top displacement only becomes a problem when the functional requirements of the flexible dolphin becomes no longer possible. But the expected failure of the pile is when the pile moves to much through the soil and the soil will fail. The steel pile can also fail itself, due to local buckling.

The misalignment of the pile the most critical at the tip of the pile. If the tip of the pile moves, a rotation point in pile is created. The rotation point in the pile indicates a short pile behaviour. Short piles will have more permanent displacement, since, the whole pile is moved. The displacement of a long pile is due to bending of the pile, when the pile is unloaded, the pile tends to move back to the straight position. But a short pile moves as a straight pile, so the permanent displacements are really permanent and wouldn't decrease during unloading. This makes the tip displacement an important parameter in the determination when the pile will be still safe. The displacement of the different models at -40mNAP during unloading are shown in table 7.5. The displacements of a specific depth is chosen instead of the different tip displacements. A constant enables analysing the different deep soil pile behaviour.

Table 7.5: Pile displacement at -40mNAP for piles with different embedded pile depths

	Pile displacement at -40mNAP [m]				
	-40mNAP	-41mNAP	-42mNAP	-43mNAP	-54mNAP
Loadcycle 1	-0,0010	-0,0009	-0,0007	-0,0006	-0,0003
Loadcycle 2	-0,0026	-0,0021	-0,0014	-0,0010	-0,0006
Loadcycle 3	-0,0058	-0,0040	-0,0025	-0,0016	-0,0009
Loadcycle 4	-0,0083	-0,0055	-0,0033	-0,0020	-0,0010
Loadcycle 5	-0,0113	-0,0074	-0,0041	-0,0025	-0,0011
Loadcycle 6	-0,0140	-0,0090	-0,0042	-0,0028	-0,0011
Loadcycle 7	-0,0145	-0,0094	-0,0044	-0,0029	-0,0012
Loadcycle 8	-0,0157	-0,0101	-0,0045	-0,0031	-0,0012
Loadcycle 9	-0,0169	-0,0108	-0,0047	-0,0033	-0,0013

The current pile, embedded depth of -42mNAP, has a maximum tip displacement during unloading of only 4.7 mm, while the pile with an embedded depth of -40 mNAP has an tip displacement of 16.9 mm. The displacement of a 2 meter shorter pile is nearly 4 times larger. The tip displacement of the shorter pile 40mNAP still increases with a millimetre every new loadcycle. A choice has to be made what order of tip displacement is allowed to have a safe pile. Further research is needed for a good overview of the acceptable pile depth and tip displacement.

8   Conclusion & Recommendations

8.1   Conclusion

In this research, an answer is found to the research questions: "How can the behaviour of a flexible dolphin subject to repetitive berthing loads be determined, using the data from a full-scale test?". The measurements from a full-scale test in the Calandkanaal and existing calculation models are used to answer the question. The research includes the Blum model, Brinch Hansen model, P-y curves and Plaxis models.

This research contributes to closing the gap between the theoretical and practical behaviour of a flexible dolphins. The research uses the measurement results of a full-scale test in the Port of Rotterdam. Flexible dolphins experience repetitive lateral loads causes by the vessels. But there is no clear evidence of the behaviour of a flexible dolphin during repetitive lateral loading. This research contributes to understanding the behaviour of a flexible dolphin under repetitive loading, using the test results. The extensive measurements of the test give a clear understanding of the flexible dolphin behaviour. The measurement results have been compared with the calculation models where the models predict the behaviour of the flexible dolphin. The test involves 9 loadcycles, the load cycles are one way loadcycles. The test uses a prescribed load scheme, with 5 loadcycles where the maximum load is built up and then 4 repetitive load cycles with the same amount of load. The research discusses the repetitive behaviour of the pile and the models.

The predictions of the pile behaviour from the calculation models did not align with test results. The majority of the models predicted a top displacement close to 0.90 m, when the maximum load was applied, but two models had divergent results. The Plaxis model with drained soil layers calculated a top displacement of 1.05 meter, while the Blum model predicted a top displacement of 0.8 m. The total station measured the displacement of the pile during the test, with a maximum displacement of 0.68 meter. The predictions deviate from the measurements by more 20 cm, expect of the Blum model.

The measurement yielded redundant results, as most parameters are measured twice. The hydraulic jack measured the applied load during the test and the optical fibre strain measurements checked the load determination. The loads from the stain-data are hundreds of kilonewtons lower compared to the hydraulic jack measurements. The reliability of the strain-measurements is higher than the hydraulic jack measurements. Therefore, the expected applied load by the hydraulic jack was not met and the predictions needs to be redone with the optical fibre-based applied load.

Three measurement instruments determine the displacement of the pile during the test. The SAAF and optical fibre measure the curvature of the pile, while the total station measured the exact displacement of 8 specific point on the pile. The two curvature measurements match well with each other. But the strain-measurements do not match with the total station when a fixed pile-tip is considered. The curvature needs two boundary conditions to have the real displacement. The total station provides the first boundary condition. The measurements do not include a second boundary conditions, and an assumption is needed to determine the displacement of the entire pile.

The p-y curve model, Brinch Hansen and Blum model calculations with the loads from the strain-measurements provides displacements within 2 centimetres of the total station measurements. But both models are not able to determine the behaviour of every single loadstep of a flexible dolphin

test, which makes it more difficult to compare the calculation with the test-measurements. The three models can be used as first assumption, but are not able to determine the detailed soil behaviour.

The load-displacement curves using the strain-measurements shows a difference in stiffness behaviour between the virgin maximum load and the repetitive maximum loads measurements. The soil behaves stiffer during reloading than during the virgin load. The hysteretic loadcycles are visible in the literature, optical fibre measurements and in the Plaxis calculation. The Plaxis model show matching properties with the measurements according the hysteretic loadcycles and the difference in stiffness between virgin loading and repetitive loading.

The energy absorption of the soil during unloading and reloading of the pile is compared between the measurements and the Plaxis model. Due to a low amount of measurements point during the test, the optical fibre areas are conservative. But the most complete loadcycles point to the fact that Plaxis underpredict the energy absorption of a loadcycle. However, the uncertainties in the report needs to be taken into account regarding the soil parameter and the applied load and the amount of measurements points.

The Plaxis predictions with the loads from the strain-measurements are slightly larger than the test-measurements. The Plaxis model is capable to approach the test behaviour. Plaxis calculates similar displacement, load-displacement cycles and energy absorption capacity as the measurements during the test. Which makes Plaxis with the Hardening soil small strain model the best method to determine the behaviour of a flexible dolphin.

8.2   Recommendations

A shorter pile results in larger displacements of the pile and soil, but ensures larger energy absorption capacity of the soil. The amount of permanent pile tip displacements is determinative of the maximum length to which the pole can be reduced. The Plaxis model couldn't be checked regarding the tip displacement, since the tip displacement cannot be derived with the measurements results. Further investigation into the actual displacement of the pile tip is required, regarding the maximum allowable tip displacement and the amount of tip displacement during the test.

Plaxis is the most complete tool to determine the exact behaviour of a flexible dolphin. The model can determine the displacements, hysteretic loadcycles, initial and repetitive loadcycles and energy absorption capacity with close results to the measurements. Extra soil investigation will probably lead to even more comparable results.

The research about flexible dolphins needs to be continued for the best possible understanding about the behaviour of the pile and soil. During this research, some uncertainties came to light. Those uncertainties can be starting point for new research. In addition, there are recommendations for a further test which could help to improve the data gained from the test. The following topics are suggested for further research.

8.2.1   Further research
1. Examination of the calculation models, in particular Plaxis, using the soil investigation data.
2. The amount of permanent pile/soil displacements that is allowed for a flexible dolphin.
3. The repetitive behaviour in Plaxis using equal or slightly lower loads.
4. The energy absorption of the soil, during repetitive loading.
5. The tip displacement of the pile by making sure that the saaf-measurements can be fitted with total station measurements to get the displacement of the entire pile.
6. The hydraulic jack load determination.

References

Abspoel, A. D. (2014). *Dictaat CTB2220 staalconstructies.*

Anderson, K. (2015). *Cyclic soil parameters for offshore foundation design.* Oslo: NRC Reserach Press.

API. (2000). *Recommended Practice for planning, Desinging and constructing fixed offshore platforms-working stress design.*

Blum, H. (1932, January 29). Wirtschaftliche Dalbenformen und dereń Berechnung. *DIE BAUTECHNIK*, p. Heft 5.

Brinch Hansen, J. (1961). *The ultimate resistance of rigid piles against transversal forces.* Copenhagen: Geoteknisk institut.

Brinkgreve. (2010). *Validation of empirical formulas to derive model parameters for sands.*

Davidovits, P. (2013). *Physics in Biology and Medicine.* Elsevier.

De Klerk. (2022, July 5). *Facebook.* Retrieved from De Klerk Werkendam: https://www.facebook.com/deklerkwerkendam/posts/pfbid02SePaFB4aawFtabKaHMsqJow T8CiChdRyUCKPaMHbfJp8V28sSWCtzNcUKoAtmPyNl?locale=nl_NL

Deltares. (2020). *D-PILE GROUP .* Delft: Deltares.

Deltares. (2021). *D-Sheet piling user manual.* Delft: Deltares.

Doherty, J. (2020). *Lateral analysis of piles.*

EA-Pfähle. (2012). *Empfehlungen des Arbeitskreises 'Pfähle'.* Berlin: Ernst & Sohn.

Fleming, A. (1985). *Pile Engineering.* New York: Kluwer Academic Publishers.

Griffioen, P. (2021). *Paalproef Callandkanaal Predicties.*

Hardin, B. D. (1972). *Shear Modulus and Damping in Soils: Design Equations and Curves.* ASCE; Journal of the soil mechanics and foundations division.

Hartsuijker, C. (2021). *Mechanica.* Nootdorp: Academic service.

Hetenyi, M. (1946). *Beams on elastic Foundation.* Michigan: Ann Arbor: The University of Michigan Press.

IEA. (2021). *IEA.org*. Retrieved from Iron and steel: https://www.iea.org/reports/iron-and-steel

Inventec. (s.d.). *Inventec.* Retrieved from Products: https://www.inventec.nl/Portals/0/ProductsheetsUK/SAAF%20engels.pdf

Krupp, T. (2007). *Spundwandhandbuch berechnung.* Hamburg.

Masing, G. (1926). *Eigenspannungen und verfestigung beim messing.* Zurich.

Meetconsult. (n.d.). *Meetconsult*. Retrieved from Total statoin GeoMax Zoom95: https://www.meetconsult.nl/onze-meetapparatuur/total-stations/geomax-zoom95/a-1522-10000110

Mohamad1, H. e. (2019). *Instrumented Laterally Loaded Pile Test using Distributed Fibre Optic Sensor .*

OZ-optics. (2015). Fiber Optic Distributed Strain. Ottowa.

Peters, D. J. (2017). *Ontwerpmethodiek flexible dolphins.*

Plaxis. (2021). *Plaxis 3D: Material models manual.* Bentley.

Port of Rotterdam. (n.d.). *portofrotterdam*. Retrieved from weather-tide: https://weather-tide.portofrotterdam.com/desktop/

Reese, L. &. (2011). *Single piles and pile groups under lateral loading.* London: CRC Press/Balkema.

Roubos, A. (2022). *PAO Cursus: Dolphins & Jetties.* PAO.

Ruigrok, J. (2010). *Leterally loaded piles.* Delft: TU Delft.

SBRCURnet. (2018). *Flexible Dolphins.* Delft.

Suryasentana, S. L. (2014). *Numerical derivation of CPT-based p-y curves for piles in sand.* GEotechnique.

Verruijt, A. (2001). *Grondmechanica.* Delft: Tu Delft.

Xue, J. M. (2016). *An optimization technique to determine the p-y curves of laterally loaded stiff piles in.* Geotechnical Testing Journal .

Appendix

A. Test comments

The set-up and the load schemes are already shown in chapter 3, but during the test some things does not go exactly as predicted. This can have influence on the test-results. The differences between the prescribed scheme and the test are summed up in this section.

- The optical fibres were reconnected, causing different strain paths and measurement that were not one on one comparable between different days.

- The first loading step is not the first time the test is loaded. The day before the test the installation is set up and tested, part of this test was loading the pile. So, during the first loadstep, the soil around the pile is already disturbed due to the installation and the loads of the day before.

- During the first loading step, the bars of the hydraulic jack started spinning. This could influence the load applied on the piles. The load has reached a load of approximately 600 kN, before it was unloading to stabilize the bars. After the intervention, the bars hung more stable, and the load could be distributed better through the bars. Loadstep 1 started over again.

- The unloading phase after the 8th loadstep was extended due to diner. This longer unloading phase can cause some smaller displacement at the end of the phase. The expectation is that these differences are small and does not influencing the test, but it can be considered when there are differences in the measurements.

- After diner, unloading phase 8, the saaf is taken of the tube and an inclinometer is placed in the same tube. The inclinometer could not go the bottom of the tube for one pile since there was a disruption in the tube due to a welding line. For the second pile, the inclinometer could go to the bottom, but could not go up anymore, due to the same type of welding. The inclinometer could only measure half of both piles.

B.   load analyse

B.1   Python code

In this section, the python code which is used to determine the applied load using the strain-measurement is shown. Parts of the code are shown, with the explanation.

Upload the text file and drop the datapoints that are not attached to the north side of the pile. Next to that, the parameters that are not used in this calculation are dropped.

```python
def load_calculation(a):
    df=pd.read_csv(a, sep = '\t', skiprows=32, header=1 )
    base = pd.read_csv('2022_06_30_09_03_21_761.txt', sep = '\t', skiprows=32, header=1 )
    df = df.drop(['Width(MHz)', 'Temperature(deg.C)', 'Frequency(GHz)', 'Gain(%)' ], axis=1)
    df = df.drop(df.index[:470])
    df = df.drop(df.index[315:])
```

Pick the time out of the uploaded filename.

```
hour = a[11:13]
minute = a[14:16]
second = a[17:19]
time = f'{hour}:{minute}:{second}'
date_time_str = f'{time}'
date_time_obj = datetime.strptime(date_time_str, '%H:%M:%S').time()
```

Determine the distance to the cable tip. The cable tip is between 160 and 160.5 meter on the cable. And determine the wall-thickness using the distance to the tip.

```
con = [
    df['Distance(m)']<160,
    df['Distance(m)']>160]
op = [np.abs(df['Distance(m)']-160), np.abs(df['Distance(m)']-160)-0.5]

df['Distip'] = np.select(con, op)

conditions = [
    df['Distip']<5,
    df['Distip']<8,
    df['Distip']<19,
    df['Distip']<23.75,
    df['Distip']<26.75,
    df['Distip']<29.25,
    df['Distip']<32,
    df['Distip']<42,
    ]
output=[0.03, 0.04, 0.055, 0.05, 0.04, 0.035, 0.03, 0.025]
df['wall'] = np.select(conditions, output)
```

Determine the other parameters that will be used during the calculation.

```
E = 210000000
df['I'] = np.pi/64*(2.4**4-(2.4-2*df['wall'])**4)
df['base_strain'] = base['Strain(micro-strain)']
df['real_Strain'] = df['Strain(micro-strain)'] -df['base_strain']
df['BM'] = E * df['real_Strain']/10**6 * df['I']  /1.2
df['curvature'] = df['real_Strain']/(1.2*10**6)
df['exp-load'] = df['BM']/(48.5-df['Distip'])
```

Make a new data frame with the datapoint above the soil bottom.

```
df1 = [df[0:72], df[242:315]]
df1 = pd.concat(df1)
```

Determine the bending moment of the point around a specific height on the pile. The average is taken from these multiple bending moments.

```
num = 4
start = 20
re = np.zeros(num)
ss = 0
df1 = [df[0:72], df[242:315]]
df1 = pd.concat(df1)
plt.plot(df1['Distip'], df1['BM'])
for i in range(num):
    srs = start+i

    id1 = bisect_left(df['Distance(m)'].values, 160-srs)
    id2 = bisect_right(df['Distance(m)'].values, 160.5 + srs)

    bm1 = df.at[470+id1,'BM']
    bm2 = df.at[469+id1,'BM']
    bm3 = df.at[469+id2,'BM']
    bm4 = df.at[470+id2,'BM']


    exp_bm = (bm1+bm2+bm3+bm4)/4
    plt.plot(( srs+i, 48.5), (exp_bm, 0), color = 'red')
    print(bm1-160, bm2-160, bm3-160.5, bm4-160.5)
    #exp_bm = (bm1+bm3)/2
    load = exp_bm/(48.5-srs)
    re[ss] = load

    ss +=1
Load = (np.average(re))
```

Calculate the mean value of the expected loads of this data frame.

```
load = df1['exp-load'].mean()
```

Calculating the least squared error of multiple different loads with the bending moment measurements. Determine the optimal least squared error of the different loads, that load is the expected load using this method.
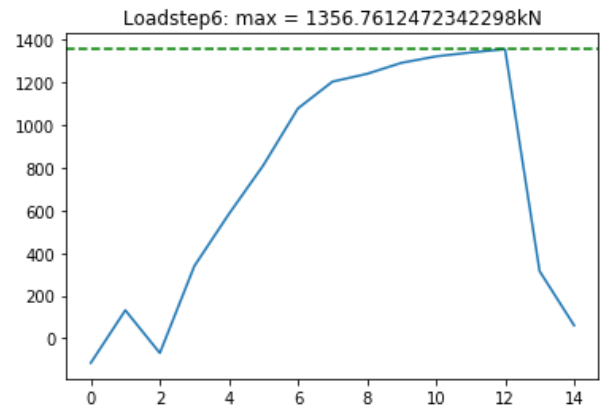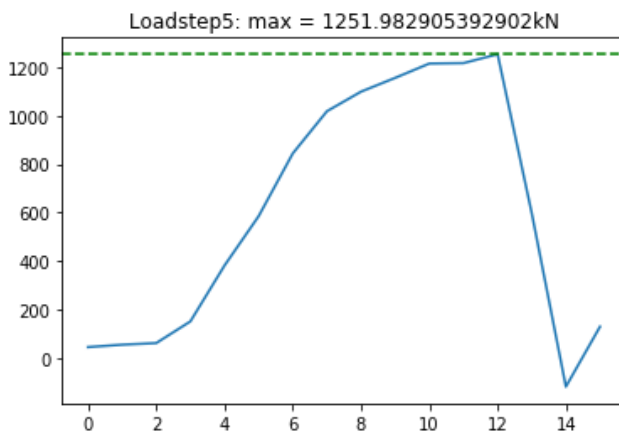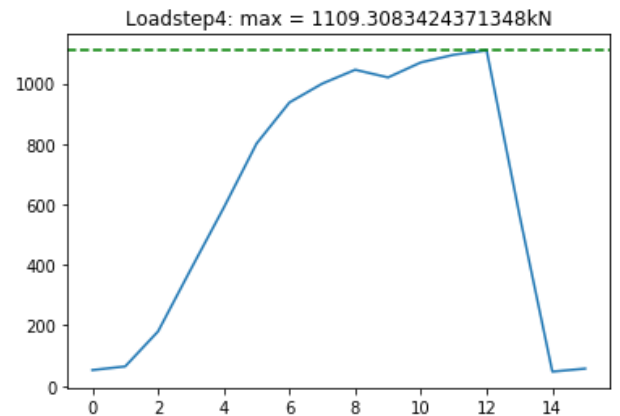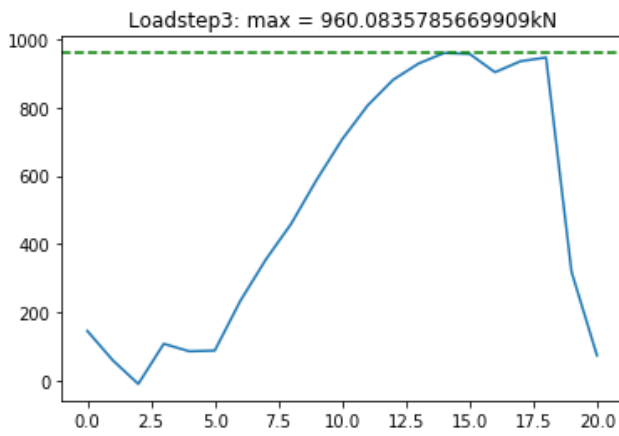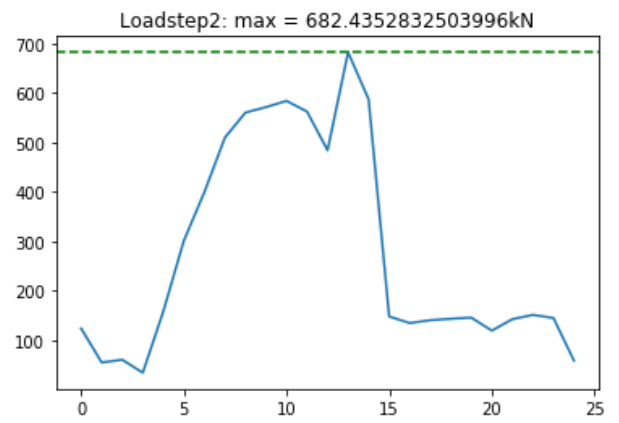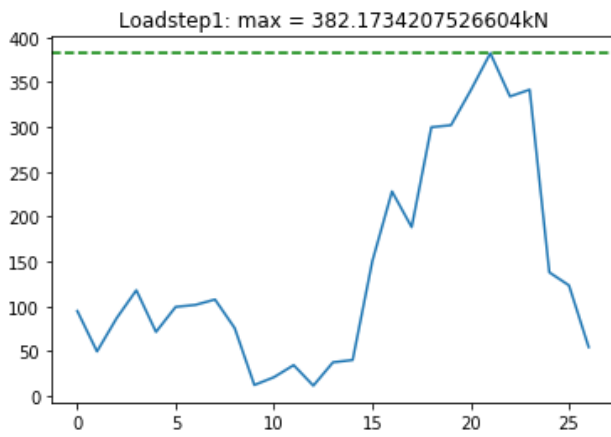
```
step = 1
Load2 =  np.arange(Load-50, Load+50, step)
dd = np.zeros((2, len(Load2)))
sss = 0
plt.figure(figsize=(16, 8))
plt.plot(df1['Distip'], df1['BM'])
plt.grid()

for i in Load2:
    #plt.plot((48.5, 39.9), (0, 8.6*i))
    plt.plot(df1['Distip'], (48.5-df1['Distip'])*i,  color='red')
    r2 = r2_score(df1['BM'], (48.5-df1['Distip'])*i)
    dd[0, sss] = i
    dd[1,sss] = r2
    sss +=1
arg = (np.argmax(dd[1, :]))
ll = (dd[0, arg])
```
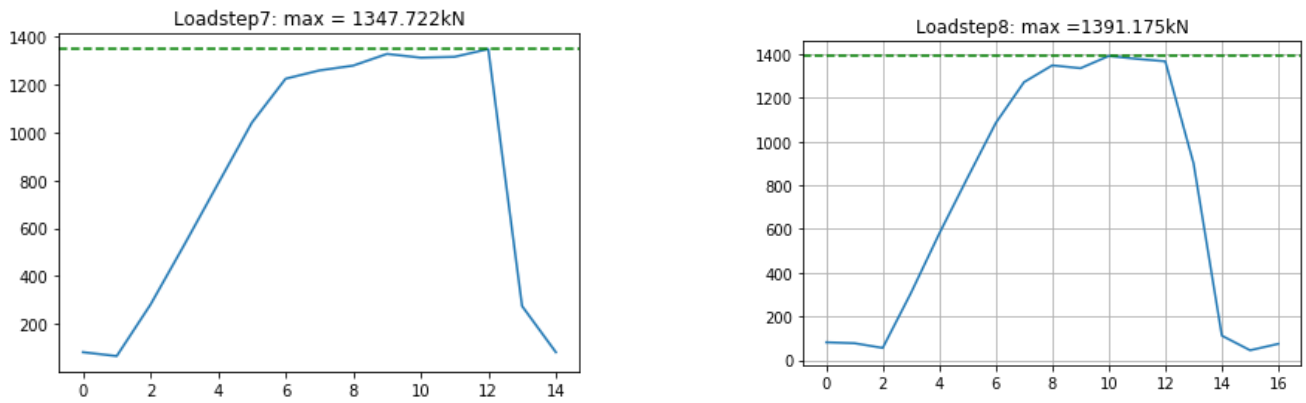
B.2   Loadcycle courses

Loadstep1: max = 382.1734207526604kN

Loadstep2: max = 682.4352832503996kN

Loadstep3: max = 960.0835785669909kN

Loadstep4: max = 1109.3083424371348kN

Loadstep5: max = 1251.982905392902kN

Loadstep6: max = 1356.7612472342298kN

Figure B.1: The loadcycles measured with the optical fibre strain data

C. Measurement data

C.1   Strain measurements

D01-Z

The strain data that is shown in the graph, is the strain data of the cable that was connected to the south side of pile D01. The strain measurements are shown in figure C.1. The grey line represents the base-measurement, which is taken before any load was added on the pile, at 09:01 on the testday. The orange line represents the strain at the end of the eighth loadstep. The green line represents the difference in strain between the blue and grey line, which is the added strain due to the load.

The first 110 meter of the cable is not printed in the data file, the expectation is that this part of the cable was the extra length, which was not attached to the pile. The data shows a clear trend with two symmetric parts. In the middle of the data, there is a peak. This peak in the middle of the trend means the tip of the cable.

The 40 meters before the peak, the cable is going down alongside the north side the pile and the 40 meters after the peak the cable is going up again. The data has some symmetric peaks, they ensure a less nice and clear trend. The peaks must be considered when the data is used for calculations.

The strains are negative, which means that the cable length decreases. This is also expected, since the south side of the pile is on the compression side when the pile is loaded like it is.
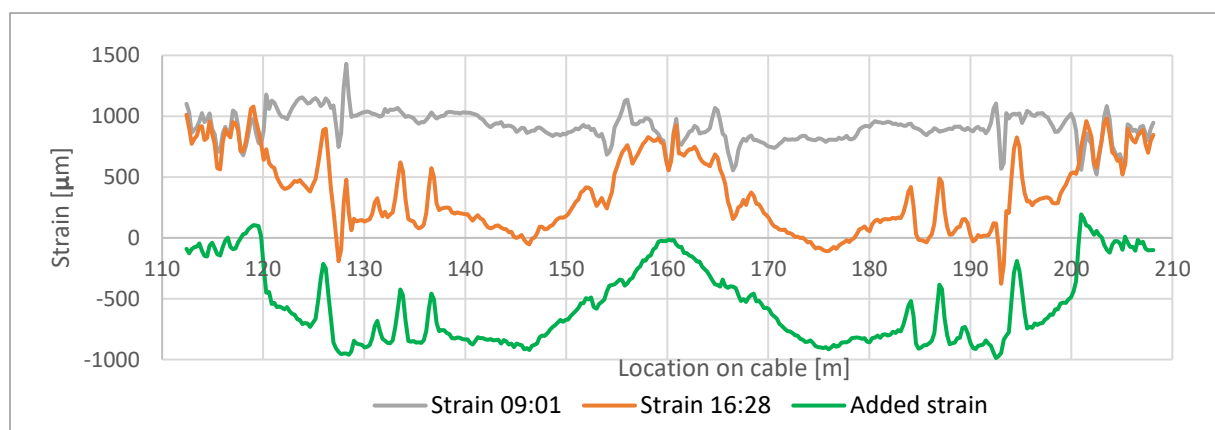

Figure C.2: Strain-measurement of cable D01-Z

D04-N

The strain data that is shown in the graph, is the strain data of the cable that was connected to the north part of pile D04. The strain measurements are shown in figure C.2. The grey line represents the base-measurement, which is taken before any load was added on the pile, at 09:01 on the testday. The orange line represents the strain at the end of the eighth loadstep. The blue line represents the difference in strain between the blue and grey line, which is the added strain due to the load.

The first 100 meter of the cable is extra cable length that is not connected to the pile, so this data can be filtered out. The second part, between roughly 100 and 160 meters, shows a trend. The last +-150 meter is very noisy and there is no trend visible in the data, which makes this data unusable. After 161 meters on the cable, the data in the file changes in trend. The gains become zero and the other data becomes less accurate. It looks like the cable is stuck on that location and the radiation thought the cable becomes unstable. Due to the trend before the 161 meter and the fact that the cables are more likely to break at the location of a sharp bend, it is assumed that the cable is broken at the tip of the pile. So, the 40 meters before the fracture, the cable was connected to the pile.

There is a little trend visible between 120 and 160 meters, but since there is only 1 measurement, the data cannot be checked with each other.
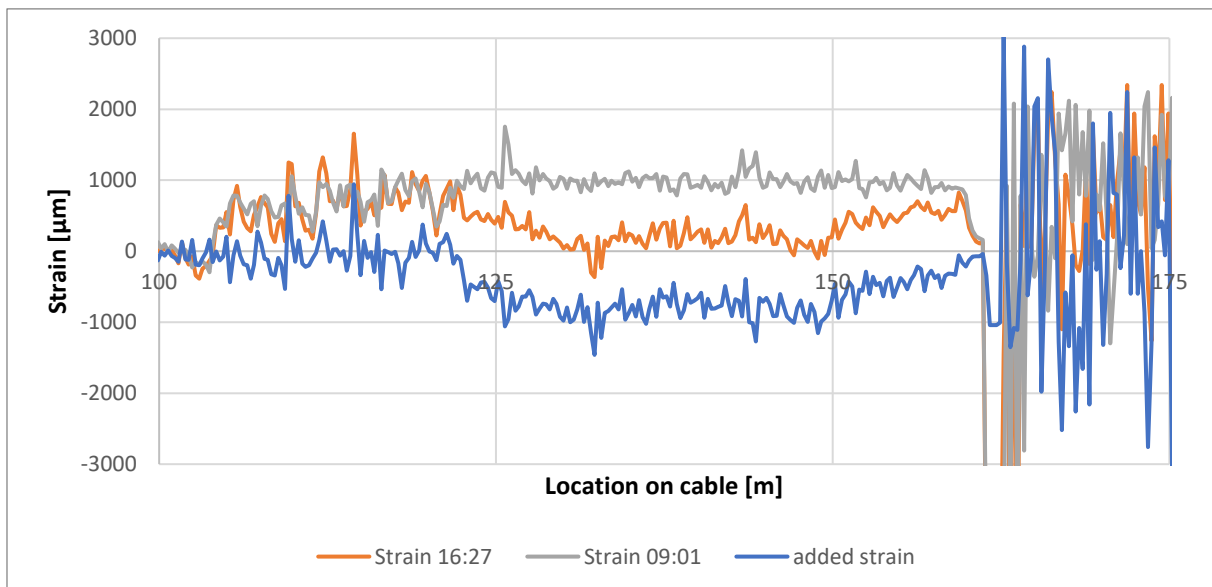

Figure C.3 Strain-measurement of cable D04-N

D04-WZ

The strain data that is shown in the graph, is the strain data of the cable that was connected to the west and south part of pile D04. The strain measurements are shown in figure C.3. The grey line represents the base-measurement, which is taken before any load was added on the pile, at 09:02 on the testday. The grey line represents the strain at the end of the eighth loadstep. The orange line represents the difference in strain between the blue and grey line, which is the added strain due to the load.

The first 100 meter of the cable is extra cable length that is not connected to the pile, so this data can be filtered out. The middle part, between roughly 100 and 220 meters, shows a clear trend with two bows. This part is connected to the North side of the pile. The last +-100 meter is connected to the east part of the pile. The third part, between roughly 220 and 330 meters, shows a trend too.

The middle part shown a clear trend, with a sharp peak in the measured strains around 160 meters. This peak in the middle of the trend means the tip of the cable. In the 40 meters before the peak, the cable is going down alongside the west side the pile and the 40 meters after the peak the cable is going up again. The two parts looks quite symmetric.

The middle part shown a trend, despite the noise data. There is a peak in the lines around 270 meters. In the 40 meters before the peak, the cable is going down alongside the south side the pile and the 40 meters after the peak the cable is going up again.
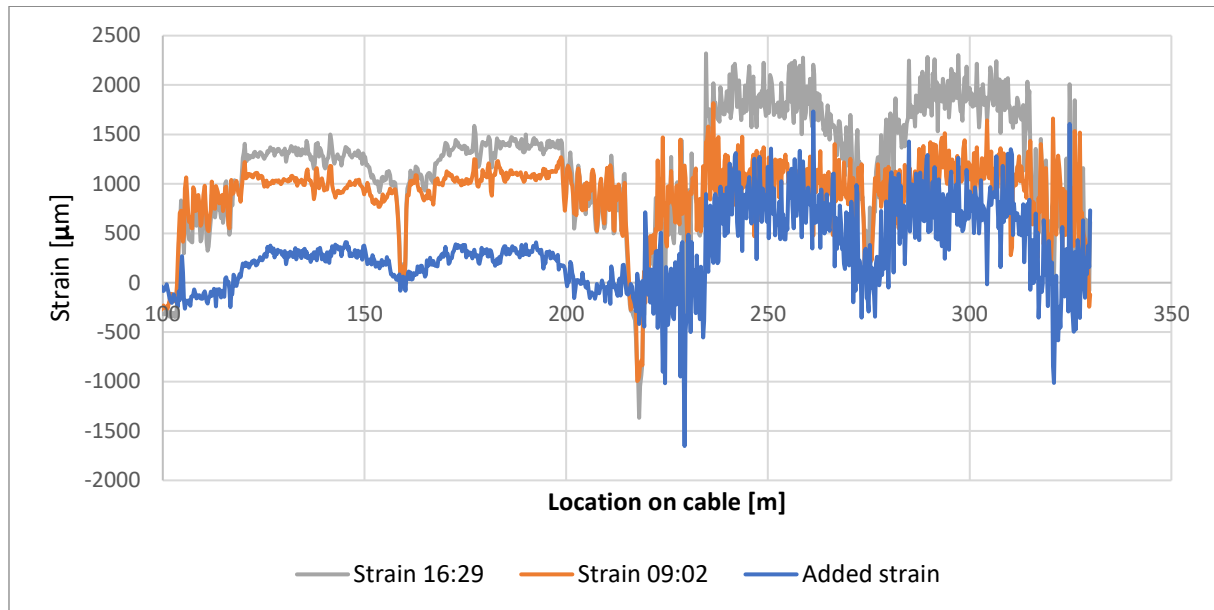

Figure C.4 Strain-measurement of cable D04-N

C.2 Inclinometer

The inclinometer is a displacement measurement tool, which measures the displacement in two horizontal directions every 0.5 meter of depth. The inclinometer has measured the displacement in the pile three times, the first time after unloading loadstep 8, the second time at the maximum load of loadstep 9 is reached and the third time after unloading loadstep 9. The inclinometer gives as output the differences between the loading and unloading measurements. The inclinometer is placed in the same pipe as the saaf-tube. The data of the inclinometer is sent in an excel file, with the displacements in both horizontal directions, x- and y-direction, for the corresponding depth, z-coordinate.

The inclinometer on pile D01 got stuck at the weld between two parts of the pipe. This weld was on -17.4 mNAP. The measurement could only be done above this level, until the top of the inclinometer tube at 3.1 mNAP. The inclinometer in pile D04 also had problems with the weld. But now the inclinometer went to the bottom of the pipe but could not pass the weld when the tube went up again. So only the lower part of the pile could be measured, from -41.1 m to -18.1m. The results of the inclinometer are shown in figure C.4. The inclinometer D01 measured the unloaded phase before loadstep 9 and the loaded phase during loadstep 9, while D04 measures the loaded phase during loadstep 9 and the unloading step after loadstep 9.

The displacement in y-direction has a lot of noise and no trend or pile behaviour is visible. Therefore, the displacement in y-direction is not usable.

Since both inclinometers only measure half of the pile, the two measurements can be combined to have a better overview of the entire pile. A few comments about the combination of the two measurements:

- It looks like a smooth transition between the two data-trend.
- It is assumed that both piles behave the same.
- The measuring moments of both piles differ from each other.

The displacement in x-directions have a smooth transition zone. It looks like the two parts follow the same trend around the transition zone. The combined data can be used in the future, but with extra attention.
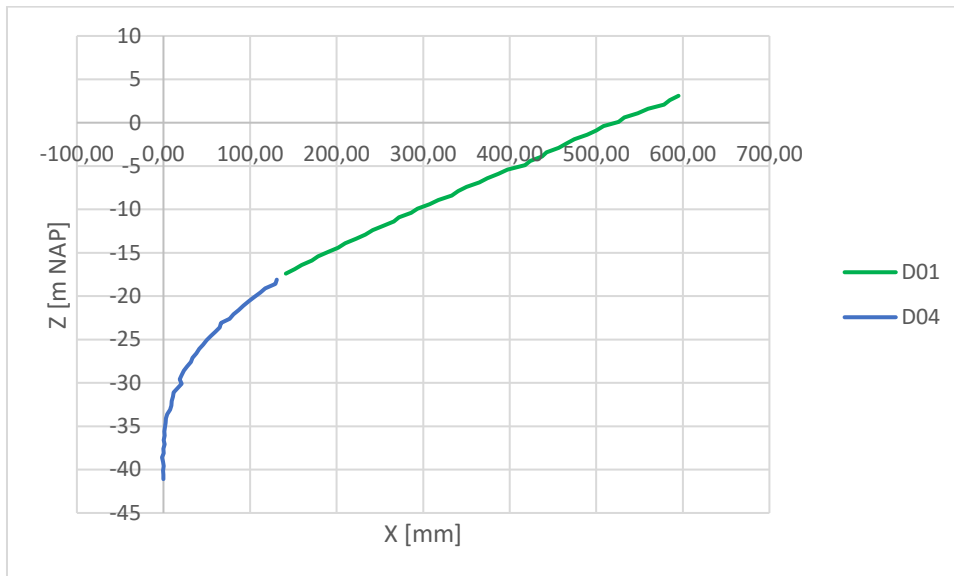

FigureC.5 Horizontal displacement of inclinometers

C.3 Preparation-day measurements
Both measurement types have some limitations and inaccuracies in their measurements. Most of the times the hydraulic jack is used together with a loadcell, the loadcell measures the load with a high accuracy and checks the hydraulic jack. The loadcell is not used during this test and the hydraulic jack data is not checked during the test and therefor there can be some errors in the data. The day before the testday, the set-up was tested. Everything was checked and the pile was loaded for the first time. The displacements of that loadstep were more in line with the expectations. At the start of the testday, the hydraulic jack setup was adapted, and the jacks were reinstalled. The reinstallation of the set-up can have cause an error in the measurement.

The day before the test, the system was tested with a similar load to the first loadstep. During this loading, the displacement of the pile with the corresponding load are measured. The measurements were done with the hydraulic jack and the optical fibre cables. Those tools gave different answers load measurements during the testday, but it may be due to some chances in the setup between the preparations and the test. The bars were corrected, and the optical fibre cables were reconnected. During the preparation day, the optical fibre cables were installed in another system. The cables were connected differently to each other and in different orders. The strain-measurements from this test are shown in **Error! Reference source not found.**. The figure shows the strain-data from the construction day (28-6), the preparation day (29-6) and the test day (30-6). What stands out from the data is the noisy strain-data during the preparation day (29-6) compared to the test day (30-6). The

noise in the strain-data of the preparation day is much larger than the noise in the data during the test. The differences between the two measurements are also minor compared to the amount of noise. The bending moment results of the two measurements on 29-6 is shown in **Error! Reference source not found.**. There is no clear trend in this data and therefor it is not possible to determine the expected load. Especially on the depth, which is used for the load determination, between 20 and 40, there is no trend visible. The results are both positive and negative, which is unexpected. Two measurements that are used to calculate the bending moment, one measurement before the preparation load (10:20) and a time during the load on the pile (12:19). The data from the preparation day is not dependable to use for the load determination of the preparation day.
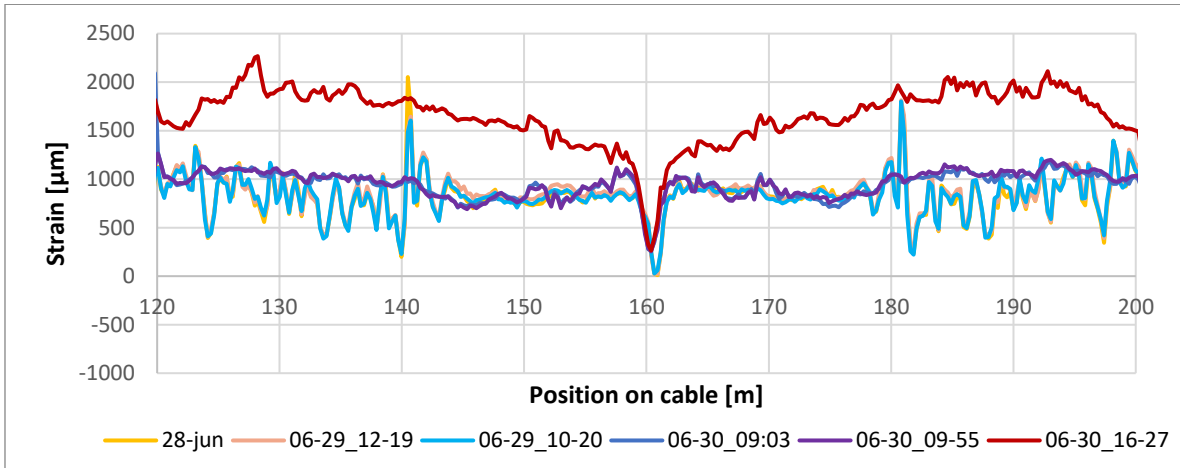

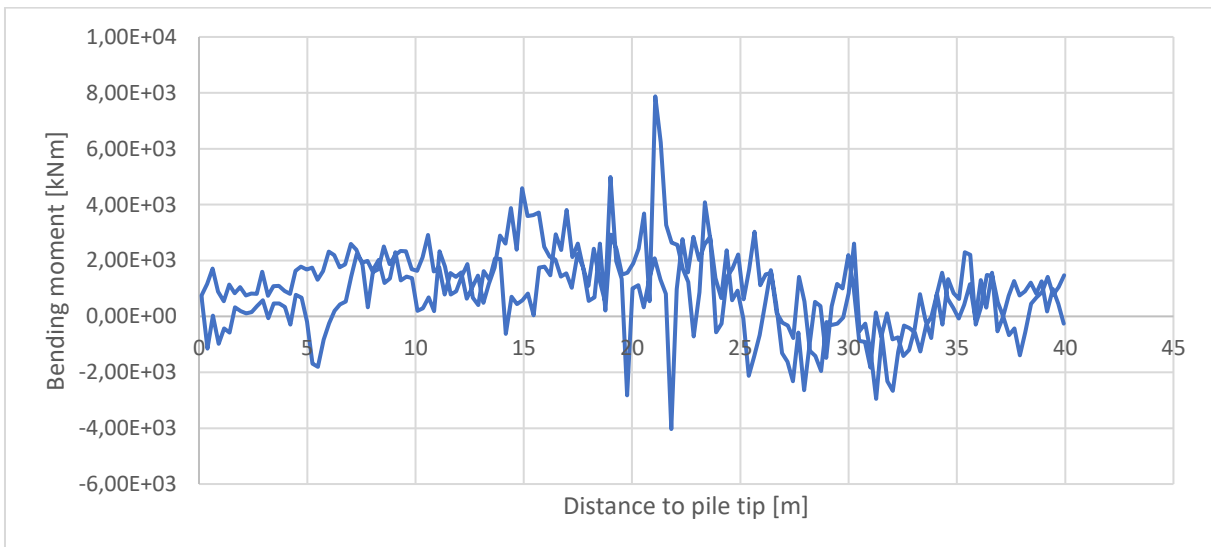*Figure C.6: strain measurements of three different days*

Figure C.7 Bending moment of the pile on 29-6

D Cyclic models

The literature prescribes models to determine the displacement of a flexible dolphin after cyclic loadings. The two models that are reviewed in this section, are the models that determines the displacement of the pile tip during every loadcycle. The models are mentioned in literature (EA-Pfähle, 2012). The boundaries of the logarithmic equation and the exponential equation are shown in figure D.1. The exponential equation uses the long and flexible pile. The test-pile was flexible, and the expectation is that the pile behaves as a long pile. The expectation is that the pile is longer than needed, which result in a practically fixed pile tip and a plastic hinge in the pile.

The total station displacement is added in the graph. The data of D01-trap is used for the calculation. The results are verified with other measurement points. The total station trend is calculated in two separate ways. The first method uses the 5th loadcycle as base measurement, which is the first maximum load in the prescribed load scheme. The second method uses the 6th loadcycle as base measurement, since the load increasement becomes smaller after the 6th loadcycle.

The first total station method is within the range of the exponential approach. The α-value can be fitted to the data, which result in a similar trend. The load built-up loadcycles are not considered. Those loadcycles will have influence on the first few loadcycles. The influence will become limited after increasingly loadcycles. The test only had 5 loadcycles, whereby the influence cannot be analysed. It is assumed that the influence is limited in this loadcycles, so that the models can be used in this report.

The approaches that are used in **Error! Reference source not found.** are methods with one load m agnitude. More load magnitudes are used during the test, which are not considered in these formulas. There is another approach in the literature that take different loads into account. This method uses equivalent loadcycles for different loads. The method uses the nearly the same formula as the logarithmic formula, but the number of cycles is changed to a total equivalent number of cycles. The equivalent number of cycles per load magnitude is relative to a chosen load magnitude. The equivalent load cycle determination needs the static horizontal pile deformation under the load. The static horizontal pile deformation under the loads is not measured during the test. The test loaded the same pile in series, so the static deformation of a specific load is not known (only for the first load). The different load magnitude calculation is not considered in this report.
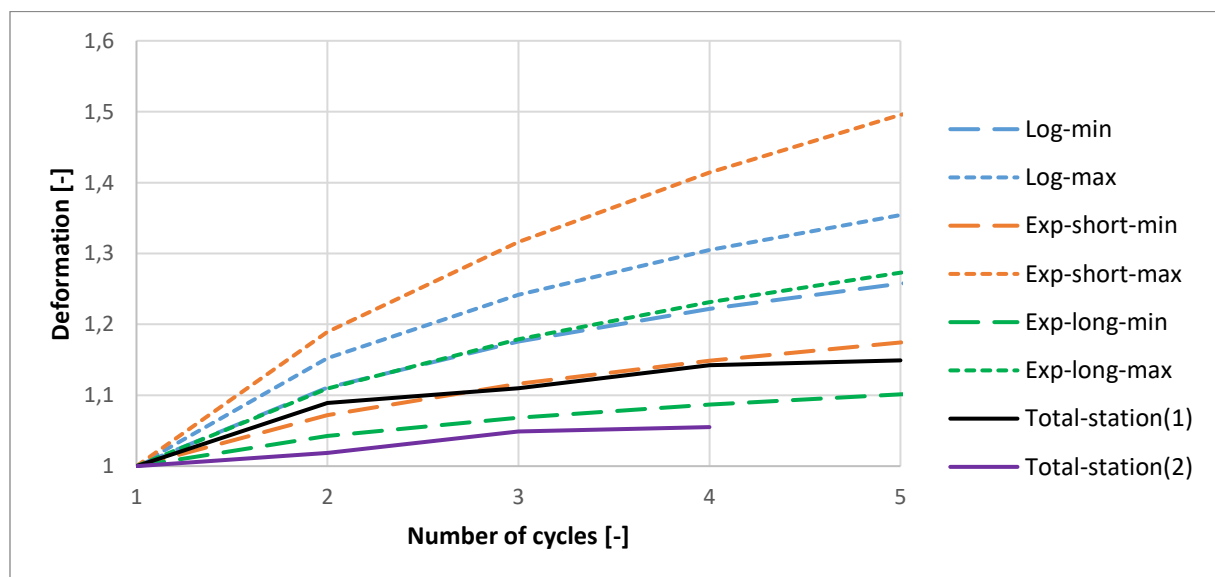

Figure D.8 Calculation methods of displacement course during repetitive loadsteps